4-2021

NUMERICAL INVESTIGATION OF MESH-BASED ENHANCEMENT OF VAPOR BUBBLE CONDENSATION

Omar Darwish Ali Alqadi Alhammadi

United Arab Emirates University

College of Engineering

Department of Mechanical Engineering

NUMERICAL INVESTIGATION OF MESH-BASED ENHANCEMENT
OF VAPOR BUBBLE CONDENSATION

Omar Darwish Ali Alqadi Alhammadi

This thesis is submitted in partial fulfilment of the requirements for the degree of Master
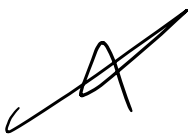of Science in Mechanical Engineering

Under the Supervision of Dr. Fadi Alnaimat

April 2021

Declaration of Original Work

I, Omar Darwish Ali Alhammadi, the undersigned, a graduate student at the United Arab Emirates University (UAEU), and the author of this thesis entitled "*Numerical Investigation of Mesh-Based Enhancement of Vapor Bubble Condensation*", hereby, solemnly declare that this thesis is my own original research work that has been done and prepared by me under the supervision of Dr. Fadi Alnaimat, in the College of Engineering at UAEU. This work has not previously been presented or published, or formed the basis for the award of any academic degree, diploma or a similar title at this or any other university. Any materials borrowed from other sources (whether published or unpublished) and relied upon or included in my thesis have been properly cited and acknowledged in accordance with appropriate academic conventions. I further declare that there is no potential conflict of interest with respect to the research, data collection, authorship, presentation and/or publication of this thesis.

Student's Signature: _____ Date: 19/05/2021

Advisory Committee

1) Advisor: Dr. Fadi Alnaimat

Title: Assistant Professor

Department of Mechanical Engineering

College of Engineering

2) Co-advisor: Dr. Bobby Mathew

Title: Assistant Professor

Department of Mechanical Engineering

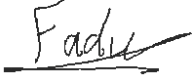College of Engineering

Approval of the Master Thesis

This Master Thesis is approved by the following Examining Committee Members:

1) Advisor (Committee Chair): Dr. Fadi Alnaimat

   Title: Assistant Professor

   Department of Mechanical Engineering

   College of Engineering

   Signature _____*Fadi*_____   Date 28/04/2021

2) Member: Emad Elnajjar

   Title: Associate Professor

   Department of Mechanical Engineering

   College of Engineering

   Signature __*Emad Elnajjar*_____   Date *April 28, 2021*

3) Member (External Examiner): Andre Benard

   Title: Associate Professor

   Department: Mechanical Engineering

   Institution: Michigan States University, East Lansing, MI, USA

   Signature _____*Tariq Darabseh*_____   Date 28/4/2021_____

This Master Thesis is accepted by:

Dean of the College of Engineering: Professor James Klausner

Signature _James F. Klausner_   Date _19/5/2021_

Dean of the College of Graduate Studies: Professor Ali Al-Marzouqi

Signature _Ali Hassan_   Date _19/5/2021_

Copy ____ of ____

Abstract

The aim of this work is to study the vapor bubble condensation process and the enhancement technique via affecting bubbles dynamic using a mesh-based structure. The bubble dynamics and thermal behavior are studied by considering the heat and mass transfer through the bubble's interface area between the vapor and liquid regions and the resulting condensation effects. The thermal characteristics of bubbles are observed considering the initial and final liquid temperatures. Additionally, the bubble dynamics are studied in terms of several parameters including the relative velocity of the bubble, bubble deformation, interfacial area, and the bubble diameters. The relation between the thermal and dynamic parameters of bubble condensation is analyzed under different operating conditions. A Semi-Empirical simulation is developed to analyze the heat transfer and condensation of a spherical rising bubble. The model includes bubble shrinkage during condensation, and can be used to analyze the total energy loss of the bubble, raising velocity and bubble condensation rate of a single bubble compared to multiple bubbles with the same total thermal energy. A MATLAB code is developed in order to calculate the instantaneous velocity, the radius, and the mass loss of the vapor bubble in each time step. Moreover, the fundamental behavior for a single bubble and multiple bubbles was investigated in various initial conditions under the same total thermal energy. The effects of the initial bubble radius and the temperature difference between the liquid and vapor phases were analyzed for both scenarios in order to examine the condensation rate. To overcome the complexity of the interface between the multi-phases in the flow field, a computational fluid dynamics (CFD) simulation is carried out and adapted using interface capturing methods (Volume of Fluid) with durable time-stepping schemes in ANSYS FLUENT. This study proposes to enhance the bubble condensation by designing a mesh-based structure to be placed in the flow direction so the bubbles will enter the domain through many small holes of the mesh structure, which will force bubble deformation and redirect the bubbles through the liquid domain. The mesh-based structure enhancement method is based on breaking the bubbles into several smaller bubbles realizing a very high surface contact area between the bubble and the liquid. This design arrangement showed an improvement in the condensation and heat transfer.

Furthermore, the obtained results from the semi-empirical model of bubbles condensation are examined and compared with experimental data from previous investigations in the literature.

Keywords: Bubble Condensation, Condensation Enhancement, Bubble Dynamics, Bubble Collapsing Rate, CFD.

Title and Abstract (in Arabic)

دراسة تحليلية في تحسين عمليات تكثيف فقاعات البخار عن طريق الهياكل الشبكية

الملخص

الهدف من هذا العمل هو دراسة عملية لتكثيف فقاعات البخار وتقنية التعزيز من خلال التأثير على ديناميكية الفقاعات باستخدام بنية شبكية. تمت دراسة ديناميكيات الفقاعة والسلوك الحراري من خلال النظر في انتقال الحرارة والكتلة عبر منطقة واجهة الفقاعة وبين منطقتي البخار والسائل وتأثيرات التكثيف الناتجة. يتم ملاحظة الخصائص الحرارية للفقاعات مع الأخذ في الاعتبار درجات حرارة السائل الأولية والنهائية. بالإضافة إلى ذلك، تمت دراسة ديناميكيات الفقاعة من حيث العديد من المعايير بما في ذلك السرعة النسبية للفقاعة وتشوه الفقاعة والمنطقة البينية وأقطار الفقاعة. يتم تحليل العلاقة بين المعايير الحرارية والديناميكية لتكثيف الفقاعات في ظل ظروف تشغيل مختلفة. تم تطوير محاكاة شبه تجريبية لتحليل انتقال الحرارة وتكثيف فقاعة كروية صاعدة. يشتمل النموذج على انكماش الفقاعة أثناء التكثيف، ويمكن استخدامه لتحليل إجمالي فقد الطاقة للفقاعة، وزيادة السرعة ومعدل تكثيف الفقاعات لفقاعة واحدة مقارنة بالفقاعات المتعددة بنفس الطاقة الحرارية الإجمالية. تم تطوير برمجية MATLAB لحساب السرعة اللحظية ونصف القطر وفقدان كتلة فقاعة البخار في كل خطوة زمنية. علاوة على ذلك، تم فحص السلوك الأساسي للفقاعة الواحدة والفقاعات المتعددة في ظروف أولية مختلفة تحت نفس الطاقة الحرارية الكلية. تم تحليل تأثيرات نصف قطر الفقاعة الأولي وفرق درجة الحرارة بين مرحلتي السائل والبخار لكلا السيناريوهات من أجل فحص معدل التكثيف. للتغلب على التعقيد بين المراحل المتعددة في مجال التدفق، يتم إجراء محاكاة ديناميكيات الموائع الحسابية (CFD) وتكييفها باستخدام طرق التقاط الواجهة (حجم السائل) مع مخططات متينة للخطوات الزمنية في ANSYS FLUENT تقترح هذه الدراسة تعزيز تكثيف الفقاعات من خلال تصميم هيكل شبكي يتم وضعه في اتجاه التدفق بحيث تدخل الفقاعات إلى المجال من خلال العديد من الثقوب الصغيرة في البنية الشبكية، مما يؤدي إلى تشوه الفقاعات وإعادة توجيه الفقاعات عبر السائل. نطاق تعتمد طريقة تحسين البنية الشبكية على تقسيم الفقاعات إلى عدة فقاعات أصغر لتحقيق مساحة تلامس سطحية عالية جدًا بين الفقاعة والسائل. أظهر ترتيب التصميم هذا تحسنًا في التكثيف وانتقال الحرارة.

علاوة على ذلك، تم فحص النتائج التي تم الحصول عليها لتكثيف الفقاعات ومقارنتها مع البيانات التجريبية في الدراسات السابقة.

مفاهيم البحث الرئيسية: فقاعات التكثيف. تعزيز تكثيف ديناميكيات الفقاعة معدل انهيار الفقاعة CFD.

Acknowledgements

I would like to express my appreciation to all of whom supported me in completing this master thesis. A special thanks and gratitude go to my main advisor Dr. Fadi Alnaimat, and co-advisor Dr. Bobby Mathew from Mechanical Engineering Department for their valuable guidance, encouragement, and unlimited support. Without their knowledge, experience, and endless ideas, this work would not have been possible. It was a great honor to work under their supervision.

My sincere thanks to all my family members and friends for their continued encouragement and advice. Special thanks go to my parents, for their consistent support, understanding, and motivation. Their passionate encouragement was a great help during this work.

Dedication

To my beloved parents. and advisers.

Table of Contents

List of Tables

List of Figures

List of Abbreviations

A	Area (m^2)
C$_d$	Drag Coefficient
CFD	Computational Fluid Dynamic
CIP	Constrained Interpolation Profile
CLSVOF	Coupled Level-Set/Volume of Fluid Method
CSF	Continuous Surface Force
F	Force (N)
FT	Interface Front-Tracking
h	Heat Transfer Coefficient (W/(m2k))
h$_{fg}$	Latent Heat of Evaporation (kj)
HVAC	Ventilation and Air Conditioning
Ja	Jakob Number
L	Liquid
LS	Level-Set Method
m	Mass (kg)
Nu	Nusselt Number
PF	Phase Field
Pr	Prandtl Number
Q	Watt
Re	Reynolds Number
T	Temperature (K)
v	Vapor

V	Velocity (m/s)
VOF	Volume of Fluid
2D	Two Dimensional
3D	Three Dimensional

Greek Alphabets

μ	Viscosity (Pa.s)
π	Pi
ρ	Density (kg/m3)

Subscript

b	Buoyancy
d	Drag
g	Gravity
x	X-Direction
y	Y-Direction
z	Z-Direction
Δt	Time Step (s)
ΔT	Temperature Differences

Chapter 1: Introduction

1.1 Motivation

Industries involved in power generation, electronics thermal management, air-conditioning, and distillation, depend extensively on boiling and condensation processes. The steam Rankine cycle is one of the most widely employed power cycles, where the working fluid goes through cyclic evaporation and condensation processes. Coolants that often reached boiling conditions often cool electronic devices; then after, the evaporated fluid is condensed back to liquid. In the distillation of oil and gas industry, the evaporated chemicals must be condensed back into liquid phase at different temperatures to separate the different chemicals and also remove undesirable impurities. Thus, condensation has an essential role in numerous industries; however, it has not been extensively studied as boiling and evaporation. In-depth understanding and enhancement of the condensation will benefit a wide range of industries, and this thesis is dedicated to the task of understanding condensation.

Bubble condensation is a highly complex phenomenon, which is encountered in many industrial applications, especially electronics cooling and nuclear reactors. Condensation can occur over a different range of configurations and operation conditions including internal flow condensation, external condensation over surfaces, and bubble condensation in a pool of liquid. In bubble condensation in liquid, the investigation of the phase change process and the dynamic phenomena with the occurrence of evaporation, break-up, coalescence, and bubbles behavior has crucial importance in understanding the

condensation heat transfer. In particular, bubble condensation is a fundamental parameter to describe the heat dissipation process. Since it is difficult to model or represent the bubble condensation theoretically, various experimental works have been conducted in vapor bubble condensation. These experiments evaluate the interfacial heat transfer coefficient, surrounding liquid temperature and the flow rate, bubble condensation rate, bubble's volume, and the interfacial area between the vapor and liquid phases.

1.2 Objectives

This work aims to analyze and develop a bubble condensation enhancement technique. by designing a mesh-based structure to be placed in the flow direction, such the bubbles enter the domain through many small holes of the mesh structure. To achieve these objectives, a Semi-Empirical mathematical model describing the heat and mass transfer between the interface regions through the condensation phenomena is developed. The mathematical model is solved numerically using MATLAB to describe the heat transfer and bubbles condensation under different operating conditions. In addition, the bubble's dynamic behavior during the bubbles' creation and levitation are simulated and observed using the computational fluid dynamic (CFD) in FLUENT module of ANSYS workbench. Through the simulation, the different types of numerical schemes on time-stepping schemes are studied and compared in terms of computational speed and the feasibility of the results. Thereafter, the enhancement technique (mesh structure) is applied to the simulation. The investigation is extended to study the influence of different bubble dynamic parameters like the relative velocity of the bubble, bubble deformation, interfacial area, and the bubble diameters, as well as various thermal characteristics from

initial and final liquid temperatures and bubble inlet temperatures. Additionally, a comparative study between different numerical results (before and after the enhancement) was carried out and compared the obtained results with other experimental results available in the literature.

1.3 Thesis Methodology

This work consists of a semi-empirical mathematical model describing the heat and mass transfer between the interface regions and computational fluid dynamics (CFD) simulations followed by a comparison study between the numerical results. The study covered the size of the bubble from the departure to collapse stages, the lifetime of the bubbles during the condensation process, the deformation that accrued on the bubbles, and the bubble dynamics. Furthermore, the flow field characteristics, bubbles surrounded temperature, velocity, and the volume history have been measured. During the study, an analysis is conducted to evaluate the different types of geometrical modifications taking into consideration the changes that will be occurred on the bubble dynamics and flow behavior during the rising and collapsing of the bubble. Based on the obtained results, the changes in the flow field were studied with the enhancement of the condensation process. The development included adding a mesh-based structure in the flow direction so that the bubbles will enter the liquid domain through the gaps of the mesh.

Moreover, to evaluate the enhancement on the bubble condensation, a validation study with available experimental data from previous research in the literature, such as Kamei and Hirata [42], was conducted to examine the semi-empirical model bubble behavior in terms of the bubble's deformation phenomena under a variety of bubble

diameters, temperature differences, surface area and bubble lifetime. Furthermore, the obtained results have been examined and compared with the bubble and flow field parameters obtained without the enhancement condition.

1.4 Thesis Structure

The thesis is divided into six chapters, including this introduction with its motivation, objectives, methodology, and thesis structure (Chapter 1).

The literature of different theoretical models and experimental works describing the bubble dynamics and the condensation, as well as a state of art review of multiphase heat and mass transfers through the interface region between the bubble and surrounded liquid are discussed in Chapter 2.

In Chapter 3, a detailed mathematical derivation of semi-empirical mathematical model and the numerical governing equations used in the simulation with time-dependent heat transfer coefficient of vapor–liquid interface and the source terms of the mass and energy models.

Chapter 4, introduce the results of the Semi-Empirical mathematical model using MATLAB code. The code has examined with the available data from the literatures. A parametric study is conducted to evaluate the bubble behavior under various fluid and bubble initial conditions. In this chapter the condensation rate is evaluated by breaking up a single large bubble into smellier bubbles under several scenarios.

The mesh-based structure was introduced in Chapter 5, this chapter illustrates the bubble's behavior through the mesh structure using ANSYS fluent. Additionally, the bubble separation is introduced and examined under various structure parameters.

Finally, the findings obtained from this study, along with some recommendations proposed for the future are dedicated in Chapter 6.

Chapter 2: Literature Review

2.1 Background

In the past decades the thermal management system has played a massive role in many applications which employ the single-phase methods to meet the cooling requirements. However, the modern application required very high rate of heat dissipation in addition to decrease the overall volume of any cooling systems. However, the requirements have rapidly raised the rate of the required heat dissipation in many applications, which also raised the need to decrease the overall volume of any cooling systems. Therefore, the single-phase systems show incapability to meet the dramatic increase of cooling requirements. These changes include cooling the electronics in super computers and data centers, for the medical application such as X-ray equipment, also the hybrid vehicle power electronics and heat exchangers for hydrogen storage in automobiles [1-3]. The transition to the phase change heat transfer systems has increased rapidly due to the need for higher heat transfer coefficients in both boiling and condensation which can overcome the lower effectiveness of single-phase heat transfer systems.

In the early implementation of heat pipes wick structure, two-phase heat transfer occurs and assisted by capillary forces to move the cooling fluid between heat acquisition section (evaporator) to heat rejection section (condenser) in a close loop pipe system as shown in Figure 1 [4]. But this system has shown several fundamental limitations, particularly the low flow rate of the coolant in the system, which is typically lower than the cooling requirements of many evolving technologies [1]. This lack of effectiveness in heat pipe wick system has shifted the interest to passive schemes, such as pool-boiling

thermosyphons, which utilizes the buoyancy affect to let the cooling fluid circulate between the lower part of the heat acquisition section and the upper part the heat rejection section in a closed vessel [5-6]. The limited cooling performance also motivated the interest in passive cooling; for instance pumpless loop system consists of a liquid reservoir and a condenser with two vertical tubes connected between both of them [7]. In semi passive falling film cooling systems, the cooling fluid flows downward due to gravitational force as a thin film in the heat dissipating section [8]. In this system the working fluid is recollected passively by the condensation in the reservoir [9].
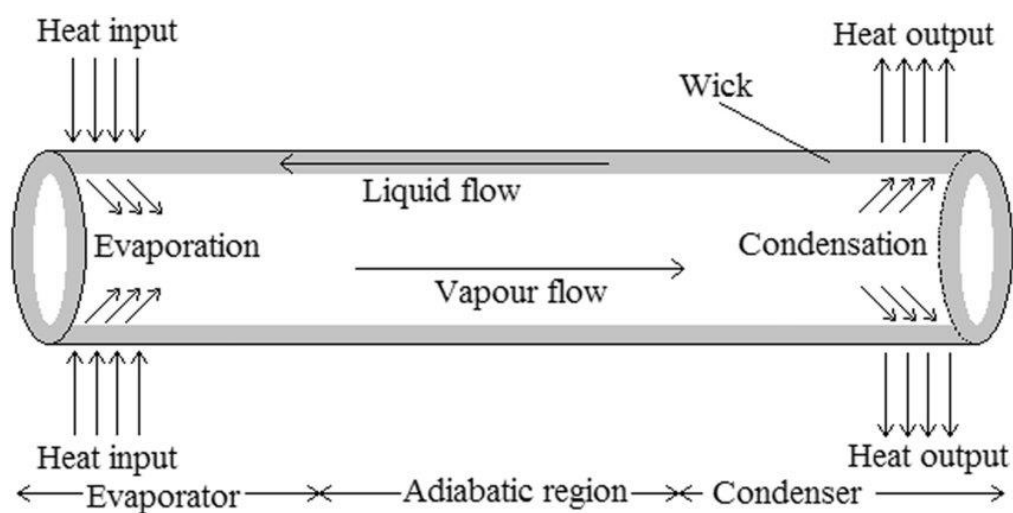
Figure 1: Heat pipe wick structure [4].

The cooling efficiency can be enhanced by increasing the cooling fluid velocity along the heat dissipating section. Therefore an additional development was achieved by using a mechanically driven pumped loop systems; this can be done by implementing a simple cooling system that consist of loop pump configuration that depends on flow

boiling concept in a channel [10]. These systems configuration have advanced during the last decade by implementing the same concept in mini and micro channels, which can provide a significant small cooling fluid compartment, a lightweight system's hardware, and enhanced heat transfer coefficient [11, 12]. In addition, to the cooling configurations that are powered by mechanical pumps, there are farther improvements achieved in jet and spray cooling systems. The two systems increase the heat transfer rate by increasing the surface area of the cooling. In jet cooling system, the cooling fluid is applied on the heat dissipation surface as a bulk liquid and in the spray system, the nozzle spray the coolant in droplets [13, 14]. A combined configuration between pump driven system and jet / spray cooling system was introduced in order to utilize the advantages of both systems which leaded to enhanced cooling performance [15].

2.2 Predictive Methods for Two-Phase Flow and Heat Transfer

Many theoretical models have been intensively utilized to predict the fluid and heat transfer behavior of two-phase interactions such as the model for basic flow configurations like falling films, annular flow for boiling and condensation [16, 17]. The utilization of empirical or semi-empirical correlations can be considered as the most famous methodology in predicting the boiling and condensation phenomenon. Accurate correlations are limited to few ranges of flow variables and small range of geometrical parameters. In many modern thermal management systems, the flow behavior can be affected by different fluids and the operating conditions which might be out of the range covered by the correlation; this typically leads to inaccurate prediction of heat transfer and improper design of the thermal cooling system. Universal correlation can be considered

as the most effective way to generate a two-phase flow predictions, since these types of correlations have been derived from a large and comprehensive worldwide database, which cover a large range of geometrical and flow parameters that can achieve extraordinary prediction results [18, 19].

In order to overcome the limitations faced in both theoretical models and empirical / simi empirical correlations, the research interest has focused on utilizing the capability of computational fluid dynamics (CFD) simulations to order to have an improved predictive and visualization of two-phase interaction behavior. For instance, Figure 2 shows a single bubble during the flow boiling of water at 0.076 m/s was simulated using Level-Set scheme in 3D domain where the simulation used to predict the bubble shape through the flow domain.
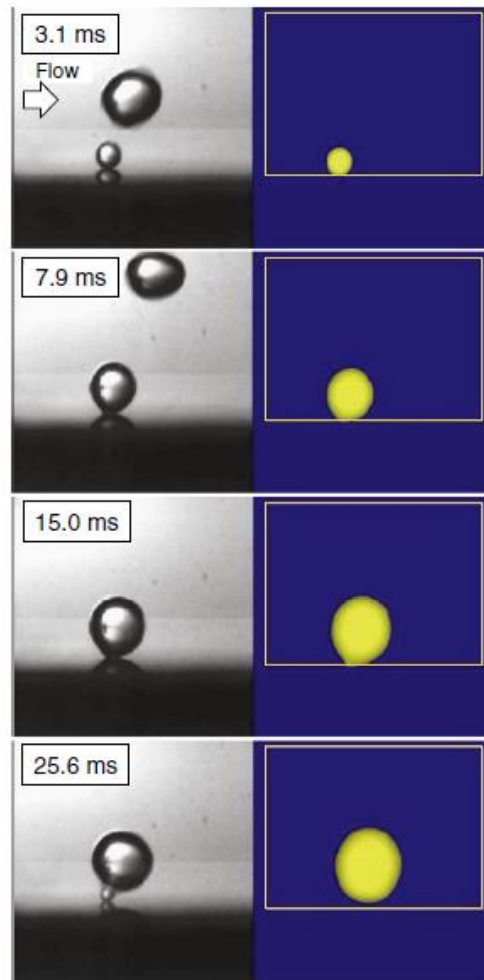
Figure 2: Simulation of bubble shape for single bubble during flow boiling in comparison with experimental results [20].

Computational fluid dynamics (CFD) has the capability to deal with transient flow and to provide a detailed analysis on the thermal and spatial distributions in the region of interest. Furthermore, this technique can predict the flow field velocity distribution, pressure differences and overall flow dynamic. However, the effectiveness of the CFD in multi-phase flows has not been fully studied and the accuracy of CFD existing models multi-phase heat and flow system has not been fully investigated. Currently, simulating

the two-phase flows are relatively computationally expensive and limited to ordinary flow configurations [21].

2.3 Two-Phase Computational Schemes

The existing numerical methods are used to provide visualization and analysis of two-phase flow of each phase and the interaction between the phases at the interface. Most computational fluid dynamics (CFD) solve the mass, momentum and energy equations based on the assumption of the continuum hypothesis, where in each portion of the fluid matter consist of a sufficient number of molecules [22]. This section will discuss the various methodologies used to simulate the two-phase flow with focus on the most popular methods that have been used in numerical simulation.

2.3.1 Lagrangian Methods

In the early stages of simulating a two-phase flow the Lagrangian approach was introduced and used by applying a separate boundary fitted grids to each phase, Takagi and Matsumoto used this method to simulate a 3D unsteady bubble rise in flow domain [23]. Ryskin and Leal [24] has simulated in 2D axisymmetric flow domain. Furthermore, Ryskin and Leal [24] solved the governing equations for each phase separately with equal boundary conditions in the interface region to simulate the bubble rise under buoyancy force. Using this method can provide a high level of accuracy in simulating the two-phase flow in comparison with other computational methods but it has a fixed meshes in the interface region. Therefore, moving-mesh Lagrangian method has the capability to

provide a moving grid between the phases during the interaction and deformation of phases as illustrated in Figure 3 [22].

Shopov et al. [32] simulated bubble deformation, that is affected by a buoyancy force, using the moving grid method. Additionally, Fukai et al. [33] adapted the same method to predict the effect of a droplet impacting the solid wall.
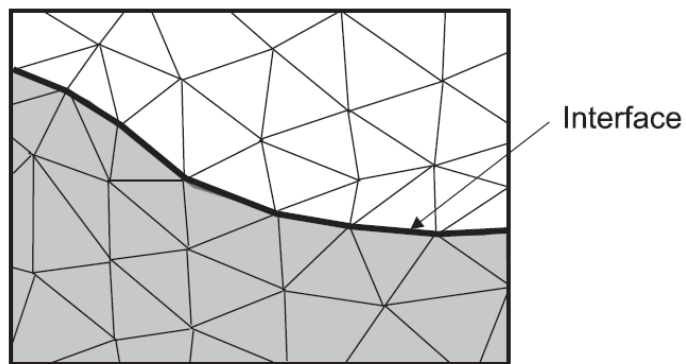
Figure 3: Lagrangian moving grid method [22].

In general, using a Lagrangian approach or moving-mesh methods need an extensive computational power. Therefore, these methods were limited to very simple two-phase flow configuration.

2.3.2 Interface-Capturing Methods

The most popular two-phase simulation method is the interface-capturing method, and this method adapts the Eulerian schemes in predicting the behavior of the phases.

Among interface-capturing methods, the volume of fluid (VOF), the level-set (LS) methods, and a coupled version of both methods are the most used approaches [25 – 27].

Volume of Fluid (VOF) Method

The Volume of fluid (VOF) method using the volume fraction approach which has a value between 0 and 1. In this method the 0 and 1 values represent a full phase without any interaction between the both phases. Moreover, the interfacial region identified by a value between 0 and 1 as shown in Figure 4 [21]. The VOF can be considered as fundamentally a conservative method, since the interface region tracked by 0 to 1 range value which is very beneficial in solving conservation equations.
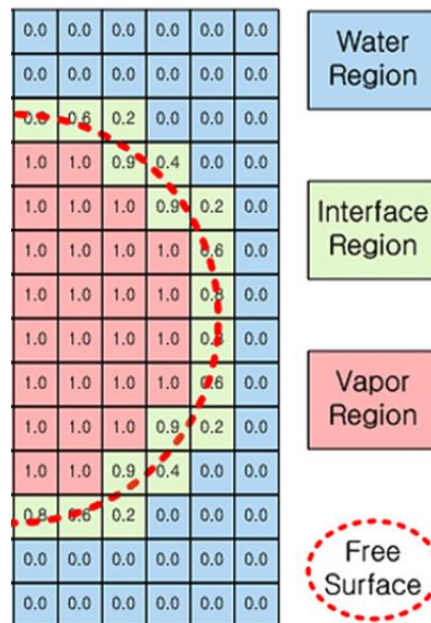
Figure 4: Volume fraction in each cell using VOF method [21].

In general, the VOF method has two main categories; the interface reconstruction and another type that do not adapt interface reconstruction. The most popular approach is the interface reconstruction method, and this approach has the capability to capture the interface region with negligible thickness where this region is solved by piecewise constant or linear schemes. The piecewise constant simple line interface calculation (SLIC) [25] assumes that the interface is orientated with perpendicular axis as shown in Figure 5.
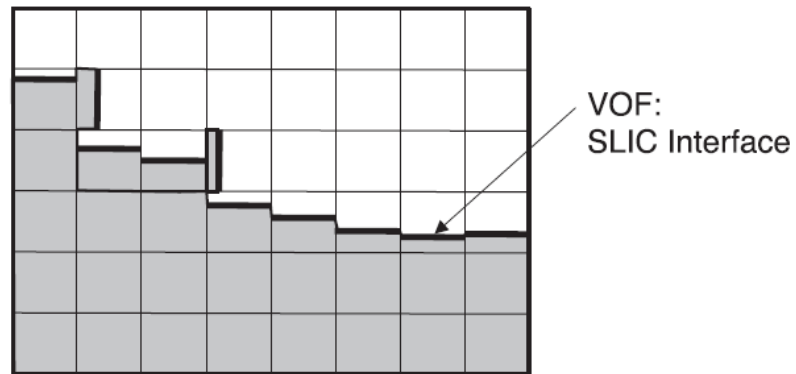
Figure 5: Volume of fluid (VOF) method SLIC scheme [22].

On the other hand, the linear schemes include piecewise linear interface calculation (PLIC) as shown in Figure 6, which demonstrate that the interface is a straight line or normal plane where the direction is normal to the interface. In PLIC scheme computing the direction of the interface based on the cell orientation obtained by interrogating volume fractions of all other cells that close to the calculated cell then it will be used to maintain the volume fraction of the cell [39].
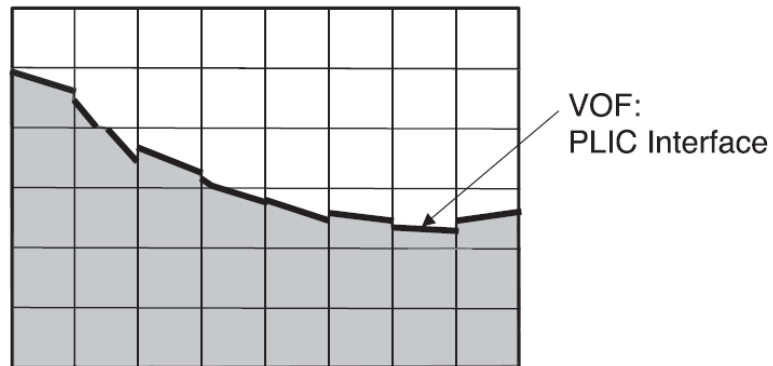
Figure 6: Volume of fluid (VOF) method PLIC scheme [22].

The second, and the less popular, method that does not include interface reconstruction uses 0.5 value to identify the interface with 0 and 1 for a complete full phase. Whereas the range from 0 to 1 occurs in the limited thickness interface surrounding with multiple cells which will lead to having a rough interface. This approach includes, a compressive interface capturing scheme for (CICSAM) developed by Ubbink and Issa, donor-acceptor scheme by Hirt and Nicholas and a flux corrected transport scheme by Rudman, [25 - 30].

In the volume of fluid (VOF) method for the two-phase flow domain all variables and properties are shared by the phases, and it follows that each local volume fraction is assigned with the appropriate variables and properties (e.g., density, viscosity). For instance, the density in each cell can be determined based on for the bounded tracked volume fraction cells and the other properties can be calculated in same manner. The velocity field in VOF model obtained from solving single momentum equation throughout

the flow domain, which depends on the properties, (e.g., density, viscosity) and the associated volume fractions of all the phases.

Level-Set (LS) Method

The Level-set (LS) method is an Eulerian scheme that uses a specific function to define a distance from the interface region where the function equal to zero at the interface intersection line, and it is positive or negative in both sides of the interface region. In (LS) method, the interface region is simulated by interpolating values of the function therefore the location is given implicitly by the predicted values. While the (LS) method can simulate complex interface patterns well, the function cannot remain smooth due to the inability to sustain the properties, which may lead to errors in calculating the curveture of the region and mass conservation. Sussman et al. [29] proposed a technique which is to reinitialize the (LS) equation after few time steps during the calculation, and this will transform the equation to a scaler field that has same zero level set at the interface region. The study conducted by Russo and Smereka [30] showed the proposed solution by Sussman et al. [29] may have inaccurate result in calculating the distance from the interface which will allow for a combined mass conservation errors. Therefore, the reviewed literatures recommended to use explicit methods to force mass conservation [31, 32].

Coupled Level-set/Volume of Fluid (CLSVOF) Method

The Coupled Level-set/Volume of Fluid (CLSVOF) method has been introduced in order to combine the advantages of both methods mentioned earlier. This CLSVOF

method reconstructs the interface region using VOF function where the direction of the interface normal vector is calculated by LS function [33]. Based on this reconfiguration, the Level-Set (LS) function will recalculate the distance from the interface line to reach accurate results for mass conservation [34]. The combination between the VOF and LS give the CLSVOF method the capability to compute different patterns of the interface accurately while having high level of accuracy calculating mass conservation. The Coupled Level-set/Volume of Fluid (CLSVOF) algorithm has been developed to follow the flow chart shown in Figure 7.
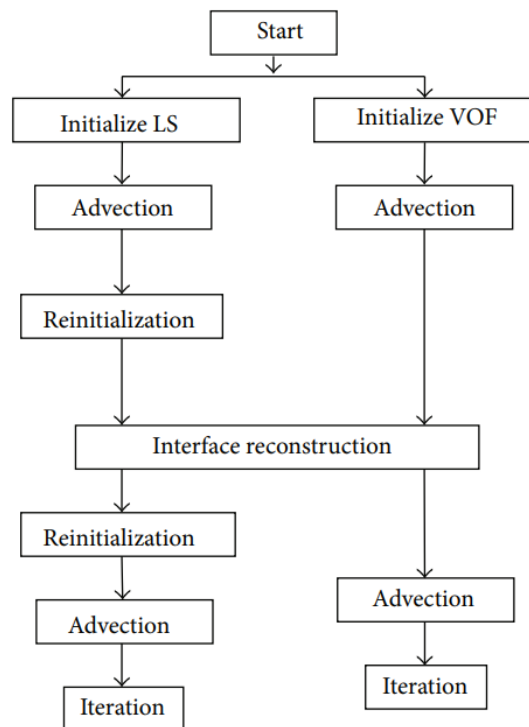
Figure 7: A flow-chart of Coupled Level-set/Volume of Fluid (CLSVOF) method [34].

2.3.3 Interface Front-Tracking

The Interface front-tracking (FT) method uses fixed and moving meshes by combining the abilities of Lagrangian and Eulerian schemes in dealing with these two types of meshes. Interface front-tracking (FT) methods can be demonstrated in various forms where Glimm et al. [35] solved each phase alone without interacting with the other, while Tryggvason et al. [36] used a combined set of equation for all phases. Furthermore, Unverdi and Tryggvason [37] simulated the flow by utilizing regular structured mesh to track the flow behavior in each phase. Juric and Tryggvason [38] adapted FT method to simulate film boiling, where considering the wall heat flux instead of fixed temperature. In their study they visualized the bubble and the associated film during the initial departure of boiling as shown in Figure 8.
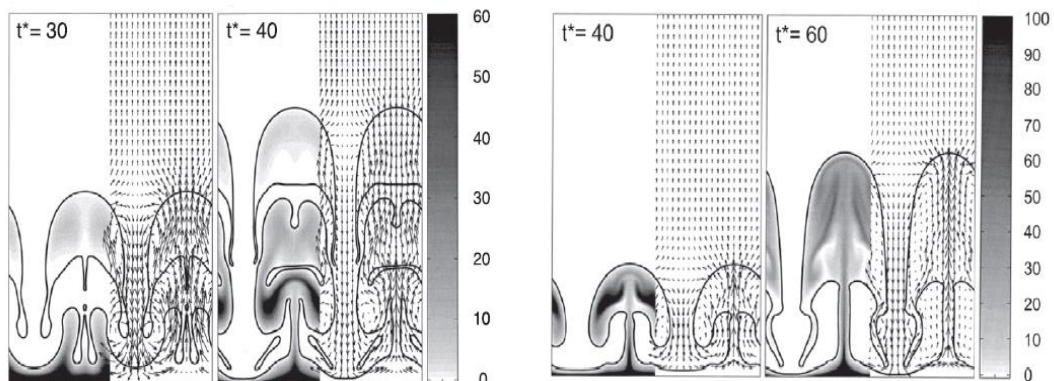
Figure 8: Simulations of film boiling domain using FT scheme.

Several studies have been conducted to develop other methods. For instance, Yabe et al. [39] adapted a fixed grids concept to develop a constrained interpolation profile

(CIP) method to avoid errors inside the computational cell that occurred from discretization process. The CTP method transforms the volume fraction equations to smooth equations by using a Lagrangian solution scheme for advection in comparison with earlier mentioned methods which uses a mathematical model to smooth the flow properties within multiple cells. Furthermore, phase field (PF) method is developed to diffuse the interface with limited thickness, whereas the interface tracking is calculated from advection-diffusion equations [40].

2.4 Bubble Condensation Phenomena

Condensation heat transfer can be considered a highly complicated phenomenon, which exists in many industrial applications, such as heating, ventilation, and air conditioning (HVAC), power plants, and electronics cooling. Therefore, the investigation of the complicated and dynamic phenomena of bubbles departure, bubbles break-up, bubbles coalescence, and the condensation of bubbles has crucial importance in understanding the subcooled boiling. Since it is difficult to develop a theoretical model that can accurately predict rising bubble condensation, various experimental works have been conducted to evaluate bubbles condensation process including the evaluation of interfacial heat transfer coefficient, surrounding liquid temperature and flow rate, bubble condensation rate, bubble's volume and the interfacial area between the vapor and liquid phases.

In experimental studies, the common method to investigate the bubble condensing process is visualization. In single bubble condensation experiments, the high-speed cameras show significant performance in revealing the condensation behaviors, and

consequently, it has been used for the subcooled condition. In the study performed by Pattanttyus-H [41], the overall temperature variation and collapsing time have obtained by neglecting the vapor temperature variation during the condensation. Kamei and Hirata [42] used frame-by-frame analysis technique to visualize the collapsing history, and they found the bubble starting the deformation from a sphere to a hemisphere, to an ellipsoid, to a sphere, and finally to collapse as shown in Figure 9. Additionally, the study found the time needed for bubble to collapse has increased by increasing the pressure for a range of pressures from atmospheric to 1 MPa [42].
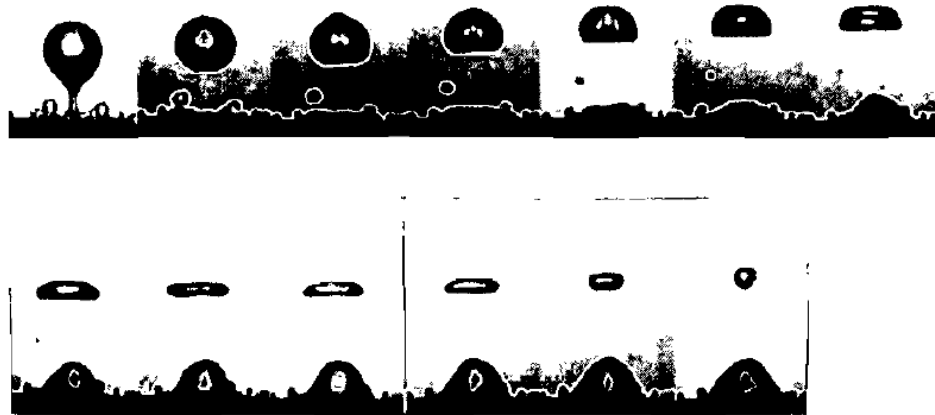
Figure 9: Bubble's collapse history [42].

Chen and Mayinger [43] investigated experimentally condensation of bubbles and their result showed that the heat transfer and volumetric changes of a bubble condensing in a subcooled liquid can be corelated using Jakob number, Prandtl number, Reynold number and Fourier number. Their experiment shows that the condensation is controlled

by the heat transfer at the phase interface if the Jakob number below 100, and for the values above this limit the inertial forces will have a significant effect. In addition, the bubble dynamics is closely related to the collapsing rate. Therefore, Moalem and Sideman [44] showed the radius-dependent translational bubble velocity has a correlation with the collapse rate of the single bubble, and it has inverse relationship with the stream cross flow. Under high pressure/temperature condition (7 MPa / 286 $^{\circ}$C), Lucas and Prasser [45] investigated the steam injected into subcooled water, and they found the change of the interfacial area has strong influence on the condensation process. Also, the study found that the increase in the injection nozzle diameter affected the condensation negatively. Isikan [46] studied the heat transfer at the top surface and in the wake of the bubble, and assumed the conduction in the tangential direction is much smaller than the conduction in the radial direction. Subsequently, energy and Navier–Stokes equations were used to obtain the bubble's velocity and the collapsing rate for spherical-cap shaped bubbles. Kalman [47] developed a theoretical model describing the condensation of the bubble during accelerating and decelerating zones that shows two different zones of collapse in miscible liquids, the model showed in the acceleration zone the rate of collapse is increasing rapidly, however in the decelerating zone the collapse rate abruptly decreases. On the other hand, research has also focused on obtaining the condensation heat transfer coefficient for vapor-liquid interface under different circumstances; bubble condensation in immiscible liquid environment (aqueous-glycerol solutions) [48], vertical conduits with subcooled bubbly flow [49], heated vertical flat plate associated with low-pressure subcooled flow [50], and narrow rectangular vertical channel [51].

The investigations mentioned above were based on experimental approaches or theoretical models associated with simplifying assumptions, where the bubble condensation is described under ideal situation. However, it is difficult to investigate the flow field effects or the changes that may occur on the characteristics of the condensation process. Therefore, the numerical simulations are adapted to study the behavior of the bubbles during the condensation. Jeon et al. [21] studied the dynamic behavior of a bubble condensation through flow boiling inside a conventional channel. The simulation conducted using VOF method to capture the liquid–vapor interface region. The VOF model was coupled with the UDF which includes empirical correlation derived by Kim and Park [52] and used to evaluate the heat and mass transfer in the interface region. The study concludes that as the condensation rate increases the rise distance is reduced due to the shorter lifetime of the condensing bubble. The obtained simulation predictions of bubble volume history show a good agreement with experimental measurements as shown in Figure 10.

| Time (Seconds) | 0 | 0.005 | 0.010 | 0.015 | 0.020 | 0.025 | 0.030 | 0.035 |
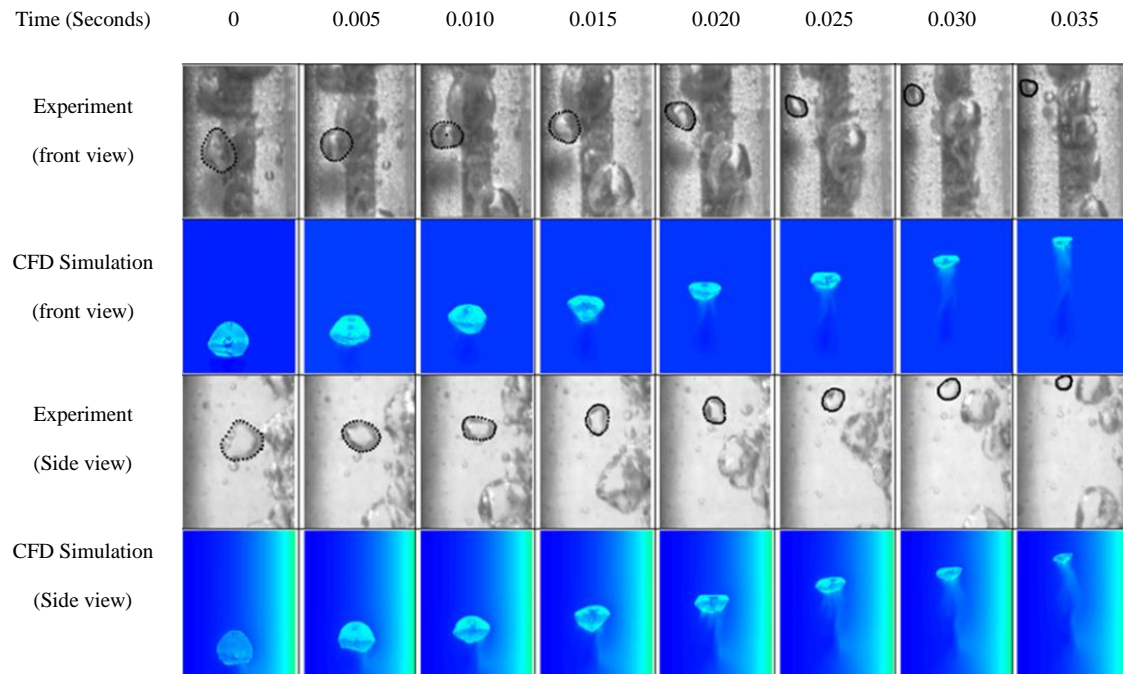
Figure 10: CFD simulation and experimental results Jeon et al. [21].

Pan et al. [53] investigated the single vapor bubble condensation behavior within two different scale vertical rectangular channels using the VOF. The simulation shows with the increasing temperature difference, condensing bubble lifetime reduces significantly. The study reported that the system pressure, subcooling of the flow, and the initial bubble size influences the bubble deformation significantly. The bubble could have a sharper deformation while increasing the subcooling of liquid and initial diameter. Furthermore, the sequence of bubble deformation will be weakening if the system pressure increased. The numerical study conducted by Bahreini et al. [54], investigated the effects of the velocity gradient, bubble size and temperature gradient on the behavior of condensing bubble. The simulation results showed that increasing the fluid velocity causes

some deformation in the bubble which is more pronounced than the velocity effect on bubble diameter as shown in Figure 11. The study concludes that the bubble will be condensed rapidly in the case without temperature gradient in compression with the case of temperature gradient.
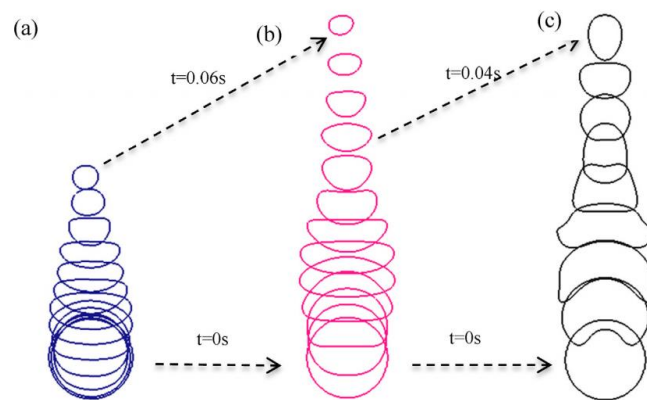
Figure 11: Bubble deformation at different velocities: (a) V = 0 m/s, (b) V = 0.1 m/s and (c) V = 0.3 m/s [54].

Samkhaniani and Ansari [55] simulated the phase change in the vapor bubble condensation process in quiescent water using the volume of fluid (CF-VOF) method. The study adopted the energy equation and Tanasawa mass transfer model to simulate the heat and mass transfer. The continuous surface force (CSF) method was used to consider surface tension between the phases. The simulation compared between initial shapes of the bubble (circle, horizontal ellipse, and vertical ellipse). The results show that bubble deformation sequences vary with different initial shapes but do not significantly affect bubble lifetime. Khosravifar et al. [56] conducted a 3D numerical modeling using VOF to investigate condensation of a bubble in subcooled liquid under a vertical and horizontal

uniform magnetic field. The results of the study showed that the pressure inside the bubble increased by magnetic field, and it also stretched the bubble along the field lines, which accelerates the bubble condensation in comparison with the condensation without magnetic field. Additionally, horizontal magnetic field decreases the bubble's rising velocity due to the increase of drag force on bubble, while the vertical magnetic field stretched the bubble vertically so the rising velocity increases. A VOF simulation has been carried out by Ganapathy et al. [57], to study flow condensation of the refrigerant R134a in a micro-channel. The study showed a reasonable agreement for Nusselt number between the obtained simulation results, and the experimental results as shown in Figure 12.
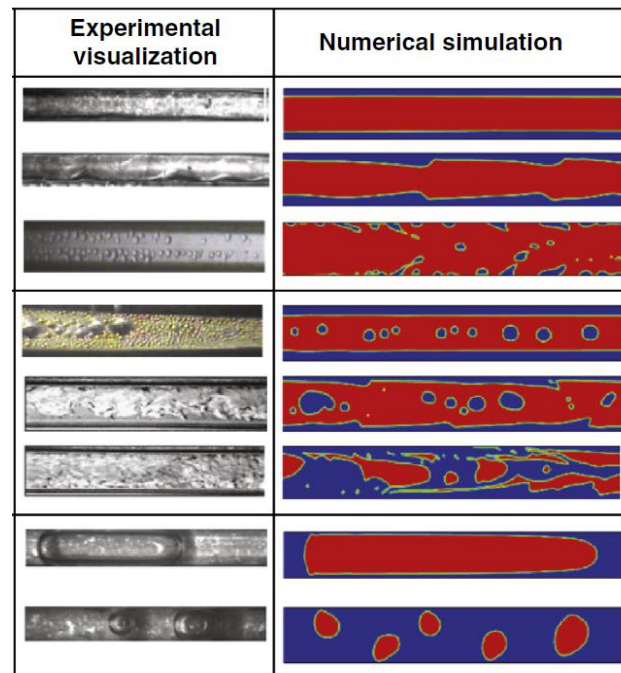
Figure 12: Simulations of predicted condensation flow along micro-channel using VOF scheme [57].

A numerical analysis is carried out using the Moving Particle Semi-implicit (MPS) method and movable boundary to find the topological position of the interfacial bubble [50]. The study showed that the bubble experienced various deformations at lower degrees of liquid subcooling, and the bubble lifetime is proportional to bubble size which agreed well with the experimental data of Kamei and Hirata [42, 59]. However, the behavior of the condensation has a strong relationship with the heat and mass transfer during the phase change process within the interface area. Thus, Pan et al. [60] investigated the condensation behavior of single bubble numerically by implementing the VOF (Volume of Fluid) supported by modified mass and energy transfer model in a UDF (User-Defined Function). Then, they analyzed under different conditions (System pressure 0.1-0.4 MPa, Subcooling Temperature 20-40 K, Mass flux 300-500 kg·m^{-2}·s^{-1}, and Bubble initial diameter 0.6-1.4 mm), the bubble size history, lifetime, deformation and the flow field characteristics, which showed a strong agreement with experimental data obtained by Chen et al. [61], and Kamei and Hirata [42]. Although simulating the bubble condensation has increased significantly the understanding of bubble dynamics mechanism in phase change phenomena, many simulation methods can be used, namely, the VOF introduced by [62], Level-set interface-capturing method (LS) used by Wang and Tong [63], to investigate the deformation and oscillations of single gas bubble. Furthermore, Coupled Level-Set/Volume of Fluid (CLSVOF) method was used by Ohta et al. [64] to study the effect of initial bubble conditions on the motion of the rising bubble. The Front-tracking method is used by Hua et al.[65] to study the rising of three dimensional bubbles in viscous liquids. Moreover, finite-volume based numerical method (Eulerian-Lagrangian) implemented to simulate isothermal two-phase flow, consisting of a rising deformable

bubble [66]. Volume of fluid methods, level set methods and phase field (diffuse interface) methods can be considered the most popular methods among front capturing techniques, which provides relatively simple treatment to capture the severe topological changes of the interface [67]. Therefore, the mentioned simulation techniques are reliable in analyzing the bubble condensation in the subcooled flow boiling under different initial conditions and flow stream characteristics.

The time derivative terms during the simulation is highly affected by the numerical method that handle the transient term such as forward Euler or Runge-Kutta [68]. Furthermore, these methods range from explicit to implicit time-stepping schemes and between these two extremes a semi-implicit or implicit-explicit schemes also available such as Pressure-Linked Equations (SIMPLE) and explicit Fractional Step (FS) [69]. These methods treat transient simulation differently and since the bubbles' condensation is transient phenomena, the most accurate and efficient schemes should be chosen.

There is a great potential for the different two-phase numerical simulation techniques; however, there is still notable challenges related to the enforcement of mass, momentum and kinetic energy conservation and properties discontinuity. In addition, accurate prediction of bubble dynamics and bubble condensation using CFD methods is still a challenge. These challenges stand against capturing the interface and coupling it with the conservation momentum equation in a cost-effective, accurate and physically consistent numerical method [70].

Although many previous investigations have been conducted to study bubbles condensation and bubbles dynamic behaviors under different conditions, there are still

many applications that have not been addressed properly in the literature. In the present work, a semi-empirical formulation and a numerical CFD investigation are carried out to study bubbles condensation and dynamic behaviors during and after breaking up a single bubble into multiple smaller bubbles in the flow. The study analyzed bubble separation and the resultant smaller bubbles behavior, and the condensation enhancement achieved by bubbles separation. Additionally, this work introduced a mesh-based structure to achieve breaking up the rising bubble into smaller bubbles without applying any changes in the fluid operating condition, which leads to enhance the condensation rate in many cooling systems without changing the working paraments in the system. Introducing the mesh-based structure in this work provides a great observation of the interaction between the bubble and the walls in a narrow channel and spacing between the channels in the flow direction and it shows the behavior of bubbles moving from wide to narrow channel along the flow direction. The effects of having various gap sizes in the mesh structure are introduced to investigate the breaking up behavior and how it will affect the bubble's deformation, size, trajectory, velocity, condensation rate, and other thermal or dynamic behaviors.

Chapter 3: Mathematical Model

3.1 Condensation Concept

The condensation phenomenon is the process when the state of the fluid phase changes from the gas to liquid. In this study, the condensing fluid of interest is water, which its phase is affected by the temperature and pressure. Figure 13 illustrate the different phases of water under different operating parameters of temperature and pressure. The saturation line in Figure 13, separates the vapor domains that denoted as V (vapor) and the liquid domain denoted as L (liquid), where water condensation occurs when the temperature goes below the saturation temperature at a given pressure. During the condensation process, the latent heat is released from the vapor as the phase change gradually from the vapor phase to the liquid phase, which also equal to the latent heat absorbed in the evaporation process. In particular, the condensation process can be categorized into three different types: homogeneous, surface, and direct contact. The condensation that occurs between the vapor and liquid phase through the interface region is called direct contact condensation, which is the main phenomena of interest of this study.
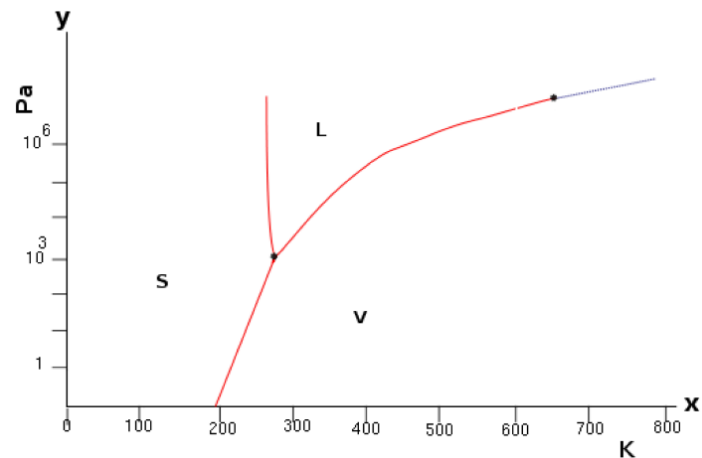
Figure 13: Water Phase diagram.

3.2 Semi-empirical Mathematical Model

In this study, a theoretical model is developed for a rising condensing bubble that accounts for the force balance on the bubble during the condensation process. A MATLAB code is also developed in order to calculate the instantaneous bubble velocity, bubble radius, condensation heat transfer, and the mass loss of the vapor bubble in each time step. Where the assumption is stated as the following:

- Bubble in three-dimensional space domain

- The gravity effect is in the downward direction

- Liquid domain dimensions are assumed to be much larger than the size of the bubble

- The Flow consist of water-liquid and water-vapor

- Saturation temperature $T_{sat} = 373.2$ K

- Local pressure $P = 101.3$ kPa

The force balance applied on a bubble shown in Figure 14 is given as.

$$\sum F = \text{upward forces} + \text{downward forces} \qquad (1)$$
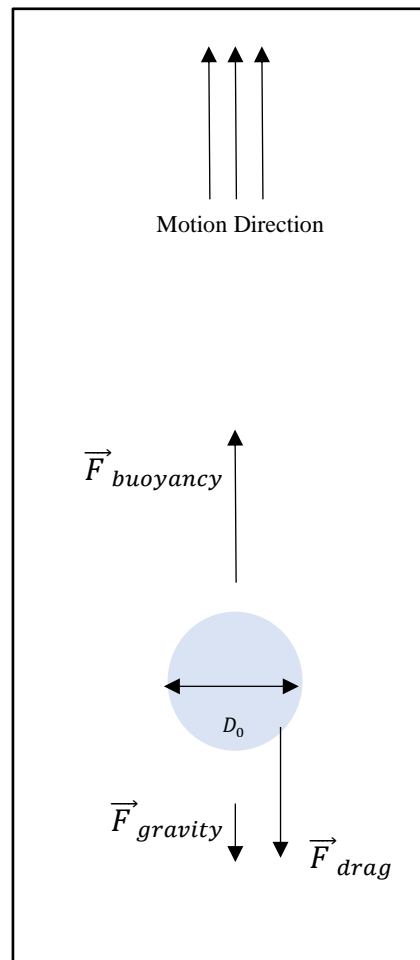
Figure 14: Schematic diagram of computational flow domain.

The net force acting on the bubble can be considered as the summation of upward and downward forces. The forces that acting downward includes the drag force F_d and weights. The upward force includes the buoyancy forces F_b due to the low density of the bubble within liquid pool. The drag force can be calculated as

$$F_d = \frac{1}{2}\pi r^2 C_d\, \rho_L\, U^2 \tag{2}$$

where r is the instantaneous bubble radius, C_d is the drag coefficient, ρ_L is the liquid density and U the instantaneous bubble velocity.

Since the velocity and bubble radius changes continuously during condensation heat transfer, it is appropriate to use a variable drag coefficient that account for such variation. A correlation of the drag coefficient is used which is obtained based on experimental data reported by Higeta et al. [74]; this correlation can be used to calculate the drag coefficient for various range of Reynold numbers as shown in Equations (3) and (4).

$$C_d = \frac{24}{R_e} + \frac{1}{5+R_e} + 1.5 \qquad\qquad \text{for } R_e < 100 \tag{3}$$

$$C_d = \frac{240}{R_e} + 1.44 \times 10^{-5}\, Re^{1.5} \qquad\qquad \text{for } R_e > 100 \tag{4}$$

The hydrostatic force has an upward effect on the bubble movement which consist of the buoyancy force. Therefore, it can be obtained from integrating the hydrostatic component of the pressure over the vapor bubble and can be written as:

$$F_b = \frac{4}{3}\pi r^3 (\rho_L - \rho_v)g \tag{5}$$

where ρ_v is vapor density.

The condensation heat transfer coefficient, Nusselt number, is evaluated based on a semi-empirical correlation developed from the experimental data reported by Kim et al. [9], on single bubble condensation is adapted given as:

$$Nu_v = f(Re_v, Ja, Pr_l) = 0.2527 Re^{0.7} Ja^{-0.2043} Pr^{-0.4564} \tag{6}$$

where Re_v is the bubble Reynolds number based on time dependent bubble diameter, Pr_l is the Prandtl number of the liquid phase, and Ja is the Jakob number. The Bubble Reynolds number Re_v is defined as:

$$Re_v = \frac{\rho_l U D_V}{\mu_l} \tag{7}$$

where μ_l liquid phase viscosity and D_V bubble time-dependent diameter. The liquid Prandtl number Pr_l is defined as:

$$Pr_l = \frac{C_{pl}\mu_l}{k_l} \tag{8}$$

whereas C_{pl} is the liquid specific heat and k_l thermal conductivity.

The Jakob number (Ja) is calculated as:

$$Ja = \frac{\rho_l C_{pl}\Delta T}{\rho_v h_{fg}} \tag{9}$$

where ΔT is temperature difference between the vapor and liquid phase, and h_{fg} is the latent heat of evaporation. As a result, after substituting from Equations from (7) to (9) into Equation (6), the time-dependent interfacial heat transfer coefficient (h) will be obtained from the following equation:

$$h = \frac{k_l Nu_v}{D_b} \tag{10}$$

The total heat transfer rate between two phases is evaluated by

$$Q = h . \Delta T . A_b \tag{11}$$

whereas A_b is the bubble interface area with liquid phase. From Equation (11) the total mass transfer rate from vapor phase to liquid phase could be defined from:

$$m_i - m_f = \frac{Q}{h_{fg}} = \frac{h . \Delta T . A_b}{h_{fg}} \tag{12}$$

Based on the initial bubble's mass the final mass will be calculated from Equation (12). Therefore, the new diameter can be calculated from the following form;

$$D_{i+1} = \sqrt[3]{\frac{m_f}{(4/3) \, \rho_v \pi}} \tag{13}$$

Summarizing, the MATLAB code (Appendix A) developed to calculate the acting force on the bubble in each time step. The new velocity will be calculated from the force balance based on the drag force and buoyancy force. The Nu used to define the heat transfer coefficient. Furthermore, the new mass will be used to determine the next time step bubble diameter.

3.3 Numerical CFD Model

In multiphase flow, the fluids are interacted on a microscopic scale with different velocity and temperature fields, which can be obtained for each fluid. Depending on the multiphase flow characteristic and how it is modeled, the phases can be homogeneous flow where the phases can have single mixture flow field variables, or inhomogeneous flow which have separate flow field variables for the different phases such as velocity and temperature. The homogeneous flow can be used when the surface area to volume ratio increases with decreasing size of the particle, which rapidly reaches equilibrium with the continuous phase change. Therefore, the inhomogeneous model is suitable for larger particles.

Several approaches exist to simulate the condensation process in ANSYS Fluent [71] are available, which can be divided into two categories:

1. Wet steam model

2. Euler-Euler multiphase models with condensation

In the following subsections, each of these approaches will be described.

3.3.1 Wet Steam Model

In ANSYS Fluent the wet steam model adapts Euler-Euler approach for simulating wet steam, which can be utilized when rapid expansion occurred in superheated dry steam. The governing equations in this model for the gas-liquid mixture, with two additional transport equations in compressible Navier-Stokes equations: for the number of droplets per unit volume and mass fraction of the liquid. In this model, the default properties are

fixed and cannot be changed, also and the material properties tab is disabled while using this model. Furthermore, the free stream needs to be pure water vapor only, and additional species are not allowed in this model [71].

3.3.2 Euler-Euler Multiphase Models with Condensation

In the Euler-Euler approach, the volume fractions for each phase are introduced and assumed to be continuous functions of space and time. In ANSYS Fluent introduced three different Euler-Euler multiphase models: the volume of fluid (VOF) model, the mixture model, and the Eulerian model, which will be described in the following subsections.

<u>Mixture Model</u>

The Mixture model can be utilized to solve for single or multiple numbers of phases, which calculates the continuity, momentum, and energy equation for phases mixture. This model can handle both a homogeneous and inhomogeneous flows, whereas, a single velocity field is shared by all phases in homogeneous flow, and the relative velocities are solved by algebraic expressions between the different phases in inhomogeneous flow. This model can be considered a simplified and computationally cheap approach to simulate multiphase flow, and simple algebraic equations need to be handled during the simulation compared with other Euler-Euler multiphase models.

<u>Eulerian Model</u>

The Eulerian model deal with each phase separately, by solving the continuity and momentum equations for the different phases. This model considers the flow setup as

inhomogeneous with discrete temperature and velocity fields for each phase. The Eulerian model can simulate the interactions between solids, liquids and gases. Nonetheless, this model has expensive computational power due to the complexity in capturing the physics of the flow.

Volume of Fluid (VOF) Model

The Volume of Fluid (VOF) Model is a surface-tracking approach where the region of the interface between the flow phases is of interest, this model tracking the volume fraction in each cell through the computational domain for all phases.

In this work the VOF model has adapted to simulate bobble dynamics and condensation through a liquid domain. The heat and mass transfer between the bubble interface and the surrounded liquid are captured by formulating governing equations of flow, momentum and energy. Also, to define the conservation of mass and energy equations by introducing the source terms of condensation, mass and energy.

3.3.3 Governing Equations of The Volume of Fluid Model

The conservation of mass is used to represent the added or subtracting mass in the following equation:

$$\frac{\partial \rho}{\partial t} + \nabla \cdot (\rho \vec{v}) = S_m \tag{14}$$

where S_m is the mass source term. The conservation of energy is:

$$\frac{\partial}{\partial t}(\rho E) + \nabla.(\vec{v}(\rho E + p)) = \nabla.(k\nabla T + (\bar{\tau}.\vec{v})) + S_h \tag{15}$$

where $\bar{\tau}$ is the stress tensor, and S_h volumetric heat source term. The stress tensor is defined as,

$$\bar{\tau} = \mu(\nabla v + \nabla v^T) \tag{16}$$

The Navier-Stokes equation for conservation of momentum as the following:

$$\frac{\partial}{\partial t}(\rho\vec{v}) + \nabla.(\rho\vec{v}\vec{v}) = -\nabla p + \nabla.\bar{\tau} + \rho g + \vec{F} \tag{17}$$

In every cell accumulation and convective momentum terms for the momentum equation are pressure p, shear, gravitational body forces and additional forces, $\vec{F}$ (e.g., surface tension force) which can be included based on the problem.

The governing equations in the VOF model solved based on volume fraction in each cell along the flow domain. During the computational stage each phase 'k' is identified by a volume fraction α_k ranged between 0.0 to 1.0 in each cell. The cells with full primary phase identified as $\alpha_k = 0.0$, and for the secondary phase $\alpha_k = 1.0$. In the interface region the cells contain the both phases with a value between the upper and lower range $0.0 < \alpha_k < 1.0$. In each control volume the summation of volume fractions for all phases is equal to one, as shown below:

$$\sum_{k=1}^{n} \alpha_k = 1 \tag{18}$$

The solution of the continuity Equation (14) in VOF model yields tracking capability of the interface between the two phases. For each phase k the volume fraction equation is given as:

$$\frac{\partial \alpha_k}{\partial t} + \vec{v} \, \nabla \alpha_k = \frac{S_m}{\rho_k} \tag{19}$$

For the two-phase flow domain in VOF all variables and properties are shared by the phases, and based on that for each local volume fraction will be assigned with the appropriate variables and properties (e.g., density, viscosity). For instance, the density and viscosity in each cell for the tracked volume fraction can be determined as the using Equation (20), and other properties can be calculated in a same manner.

$$\rho = \alpha_{k2}\rho_{k2} + (1 - \alpha_{k2})\rho_{k1}$$

$$\tag{20}$$

$$\mu = \alpha_{k2}\mu_{k2} + (1 - \alpha_{k2})\mu_{k1}$$

The momentum equation given in Equation (17) can be revised for the VOF model to take the form given in Equation (21) The velocity field depends on the properties, ρ and μ and the associated volume fractions of all the phases throughout the flow domain can be obtained after solving Equation (21).

$$\frac{\partial}{\partial t}(\rho\vec{v}) + \nabla(\rho\vec{v}\,\vec{v}) = -\nabla p + \nabla\mu\left(\nabla\vec{v} + \overrightarrow{\nabla v^T}\right) + \rho\vec{g} + \vec{F} \tag{21}$$

The mass-averaged of the velocity can be determined as:

$$v = \frac{(\alpha \rho v)_{k1} + (\alpha \rho v)_{k2}}{\rho} \tag{22}$$

From energy conversation equation (15):

$$\frac{\partial}{\partial t}(\rho E) + \nabla . (\vec{v}(\rho E + p)) = \nabla . (k_{eff} \nabla T) + S_h \tag{23}$$

where the VOF model treats the temperature T and energy E as mass-averaged variables and can be described as:

$$E = \frac{\sum_{k=1}^{n} a_k \rho_k E_k}{\sum_{k=1}^{n} a_k \rho_k} \tag{24}$$

3.3.4 Time-Dependent Heat Transfer Coefficient of Phases Interface in Condensation

The condensation heat transfer coefficient is evaluated based on the following form:

$$Nu_v = f (Re_v, Pr_l, Ja, Fo_{v,\text{initial}}) \tag{25}$$

where Re_v is the bubble Reynolds number based on time dependent bubble diameter, Pr_l is the Prandtl number of the liquid phase, Ja is Jakob number and $Fo_{v,\text{initial}}$ is the Fourier number for the initial diameter of the bubble.

The Bubble Reynolds number Re_v is defined as:

$$Re_v = \frac{\rho_l U_{rel} D_V}{\mu_l} \tag{26}$$

where ρ_l is liquid density, U_{rel} bubble's relative velocity, μ_l liquid phase viscosity and D_V bubble time-dependent diameter. Also, the bubble relative velocity is defined by:

$$U_{rel} = \sqrt{U_{v.x}^2 + \left(U_{v.y} - U_l\right)^2 + U_{v.z}^2} \tag{27}$$

where $U_{v.n}$ is the instantaneous absolute bubble velocities at each coordinate (x, y, z) and U_l is the local liquid phase velocity. the $U_{v.n}$ defined as the summation of instantaneous absolute velocities in each vapor cell as following:

$$U_{v.n} = \frac{\sum u_n \rho_v V}{\sum \rho_v V} \tag{28}$$

where $u_n \rho_v V$ is the instantaneous absolute velocities in each vapor cell, vapor density and vapor cell's volume respectively. The liquid Prandtl number Pr_l is defined as:

$$Pr_l = \frac{C_{pl} \mu_l}{k_l} \tag{29}$$

whereas C_{pl} is the specific heat and μ_l thermal conductivity of the liquid. The Jakob number (Ja) is calculated as:

$$Ja = \frac{\rho_l C_{pl} \Delta T}{\rho_v h_{fg}} \tag{30}$$

where ΔT is difference between the vapor temperature and liquid phase temperature, and h_{fg} is the latent heat of evaporation. Fourier number $Fo_{v.initial}$ is defined as:

$$Fo_{\text{v.initial}} = \frac{\chi\, t}{D_b^2} \tag{31}$$

whereas χ, t, D_b is the thermal diffusivity, time and bubble initial diameter.

As a result, after substituting from Equations (26) to (31) in Equation (25), the time-dependent interfacial heat transfer coefficient (h) will be obtained from the following equation:

$$h = \frac{k_l Nu_v}{D_b} \tag{32}$$

3.3.5 Mass and Energy Transfer

The total heat transfer rate between two phases is evaluated by

$$\dot{Q} = h.\Delta T. A_b \tag{33}$$

whereas A_b is the bubble interface area with liquid phase.

from Equation (33) the total mass transfer rate from vapor phase to liquid phase could be defined from:

$$\dot{M} = \frac{\dot{Q}}{h_{fg}} = \frac{h.\Delta T. A_b}{h_{fg}} \tag{34}$$

in the interface region during the bubble condensation the total mass transfer rate $\dot{M}$ is the sum of each cell's mass transfer rate. Thus, the mass transfer rate per unit vapor volume is obtained as:

$$m_c = \frac{\dot{M}}{\sum_n a_v \ x \ V_n} = \frac{h \cdot \Delta T \cdot A_b}{h_{fg} \sum_n a_v \ x \ V_n} \tag{35}$$

where V_i is the vapor cell's volume in the interface region, and then the cell's mass transfer rate each in the interface region, which is the mass source, is given by:

$$S_m = a_v \ x \ m_c = \frac{a_v \ (h \cdot \Delta T \cdot A_b)}{h_{fg} \sum_n a_v \ x \ V_n} \tag{36}$$

Finally, the energy source S_h is obtained as:

$$S_h = S_m \times h_{fg} \tag{37}$$

3.3.6 Turbulence Model

Based on the computational power limitation in the computer the choice will be made whether or not the resources can handle to resolve all the turbulent that will be occurred in the flow. Whereas, the time and scale of the flow is much larger than the time and length scales, then its will be beneficial to decompose into two quantities ensemble averaged and fluctuating components:

$$\emptyset = [\emptyset] + \emptyset' \tag{38}$$

where $[\emptyset]$ is the ensemble averaged part of $\emptyset$ and the $\emptyset'$ represent the fluctuating component of $\emptyset$. Where the ensemble average represented as:

$$[\emptyset] = \frac{1}{N} \sum_{i+1}^{N} \emptyset_i \tag{39}$$

the N is the total number of physical tests, and $\emptyset$ represents the value at one test sample of specific time and space. Substituting Equation (38) into Equations (14) and (17) yields,

$$\frac{\partial[\rho]}{\partial t} + \nabla.\left(\rho[\vec{v}] + [\overrightarrow{v'}]\right) = S_m \tag{40}$$

$$\frac{\partial}{\partial t}\left(\rho[\vec{v}]\right) + \nabla.\left(\rho[\vec{v}] + [\overrightarrow{v'}]\right) = -\nabla[p] + \nabla.[\bar{\tau}] + \rho g + \vec{F} \tag{41}$$

The difference between Equations (17) and (41) is the additional value of the Reynolds stress tensor $[\overrightarrow{v'}]$ which has to be modeled for the system of equations. Boussinesq approximation can be considered one of the most common types in modeling Reynolds stress tensor,

$$[\overrightarrow{v'}] = -\langle u_i' u_j' \rangle = v_t\left(\frac{\partial\langle u_i\rangle}{\partial x_j} + \frac{\partial\langle u_j\rangle}{\partial x_i}\right) + \frac{2}{3} + \delta_{ij}k \tag{42}$$

where δ_{ij}, $k\ and\ v_t$ are Kronecker delta, turbulent kinetic energy and eddy viscosity respectively, where the k can be defined from:

$$k = \frac{1}{2}\langle u_i' u_j' \rangle \tag{43}$$

where the Equation (41) can be opened in following form:

$$\frac{\partial \langle u_i \rangle}{\partial t} + \frac{\partial}{\partial x_i} \left(\langle u_i \rangle \langle u_j \rangle \right)$$

$$= -\frac{\partial}{\partial x_i} \left(\langle P \rangle + \frac{2}{3} k \right) + \frac{\partial}{\partial x_j} \left[v_t \left(\frac{\partial \langle u_i \rangle}{\partial x_j} + \frac{\partial \langle u_j \rangle}{\partial x_i} \right) \right] + \rho g \qquad (44)$$

$$+ \vec{F}$$

then the transport form of k is obtained from the dot product of Equation (44) with the velocity vector,

$$\frac{\partial \langle k \rangle}{\partial t} + \frac{\partial \langle u_i \rangle \langle k \rangle}{\partial x_j} = P_k - \langle \varepsilon \rangle + \frac{\partial}{\partial x_j} \left(\frac{\langle v_t \rangle}{\sigma_k} \frac{\partial \langle k \rangle}{\partial x_j} \right) \qquad (45)$$

where the turbulence dissipation rate ε is given as:

$$\frac{\partial \langle \varepsilon \rangle}{\partial t} + \frac{\partial \langle u_i \rangle \langle \varepsilon \rangle}{\partial x_j} = \frac{\langle \varepsilon \rangle}{\langle k \rangle} C_{\varepsilon 1} P_k - C_{\varepsilon 2} \langle \varepsilon \rangle + \frac{\partial}{\partial x_j} \left(\frac{\langle v_t \rangle}{\sigma_k} \frac{\partial \langle \varepsilon \rangle}{\partial x_j} \right) \qquad (46)$$

whereas the additional variables eddy viscosity v_t and Turbulence production P_k have the following forms:

$$\langle v_t \rangle = C_\mu \frac{\langle \varepsilon \rangle^2}{\langle k \rangle} \qquad (47)$$

$$P_k = -\langle u_i' u_j' \rangle \frac{\partial \langle u_i \rangle}{\partial x_j} = C_\mu \langle \varepsilon \rangle \, S^2 \qquad (48)$$

the C_μ and S^2 are the eddy viscosity coefficient and turbulent strain rate, respectively.

Chapter 4: Semi-Empirical Mathematical Modeling Results

The condensation and collapsing of bubbles in a heat transfer environment is a very complex phenomenon. The rate of collapse can be assumed to be controlled by the bubbles external and internal thermal behavior and the temperature difference. However, this simplicity in the assumption does not shows the realistic condition of the collapsing and the condensation process. Therefore, the process can be affected by bubble dynamics, shape, and flow field thermal parameters.

This chapter investigates the influence of bubble dynamics and bubble size on the interfacial heat transfer coefficient. It is to be noted that the analysis that accounts for variations in all operational parameters is extremely complex. A semi-empirical model is developed to analyze heat transfer and condensation of a rising spherical bubble. The developed model includes bubble shrinkage during condensation, and it can be used to analyze the total energy loss from the bubble, the rising velocity and bubble condensation rate of a single bubble compared to multiple bubbles with the same total thermal energy. The developed model consists of motion, heat, and mass transfer equations. For the validation, the model results were compared with a bubble condensation experiment data from the literature [52], and results obtained from the model showed a good agreement with the experimental results which will be illustrated in the next section. In the developed mathematical model from chapter 3, the dynamic term of the model is developed using the force balance on a gravity-driven bubble, including hydrodynamic drag force and gravity/buoyancy force, which acting with and against the bubble's motion direction. For the thermal part of the model, a condensation correlation has been adapted to represent

the Nusselt number as a function of Reynolds number (Re), Jakob number (Ja), and Prandtl number (Pr). Figure 15 is a flow chart of the calculation steps of the equations, and it is written in a MATLAB code. The MATLAB code is developed in order to calculate the instantaneous velocity, the radius, and the mass loss of the vapor bubble in each time step as shown in Appendix A. Moreover, the fundamental behavior for a single bubble and multiple bubbles are also investigated in various initial conditions with the same total thermal energy. The effects of the initial bubble radius and the temperature difference between the liquid and vapor phases are analyzed for both scenarios in order to examine the condensation rate. It was found that the thermal behavior of the condensing bubble can be improved by forcing the bubble to break up into sub bubbles, which will increase the total interfacial area and the rising velocity. Further, due to the generated sub-bubbles, the resultant velocity increased the flow's turbulence and the heat transfer rate accordingly. This study can lead to enhanced heat transfer in bubble condensation.

Start

$$\rho_l \,,\rho_v \,,h_{fg} \,,\mu_l \,,C_p \,,T_{sat} \,,T_l \,,k \,,g$$

$$Ja = \frac{\rho_l * C_p * (T_{sat} - T_l)}{\rho_v * h_{fg}} \,,P_r = \frac{C_p * \mu_l}{k}$$

$$t_{max} \,,Iterations\ Number$$

$$\Delta t = t_{max}/Iterations\ Number$$

$$t_0, r_0, u_0, m_0$$

$$t_{i+1} = t_i + \Delta t$$

$$t_i, r_i, u_i, m_i$$

$$Re_i = \frac{\rho_l * u_i * D_i}{\mu_l}$$

$$0 \leq Re_i \leq 100$$

false

true

$$C_d = \frac{240}{R_e} + 1.44\ x\ 10^{-5}\ Re^{1.5}$$

$$C_d = \frac{24}{R_e} + \frac{1}{5 + R_e} + 1.5$$

$$F_b = \frac{4}{3}\pi r^3 (\rho_L - \rho_v)g \quad , \quad F_d = \frac{1}{2}\pi r^2 C_d\, \rho_L\, U^2$$

$$\sum F = \frac{4}{3}\pi r^3 (\rho_v + 0.5\rho_L)\left(\frac{u_{i+1} - u_i}{\Delta t}\right) - F_b + F_d$$

$$Nu_v = f(Re_v, Ja, Pr_l) = 0.2527 Re^{0.7} Ja^{-0.2043} Pr^{-0.4564}$$

$$h_i = \frac{k_l Nu_v}{D_b}$$

$$Q = \frac{m_i + m_{i+1}}{\Delta t} h_{fg} = h_i (4\pi r^2)(T_{sat} - T_l)$$

$$r_{i+1} = \sqrt[3]{\frac{m_{i+1}}{\rho_v \frac{4}{3}\pi}}$$

$$r_{i+1} \leq 0$$

false

true

$$t_i = t_{max}$$

false

true

End
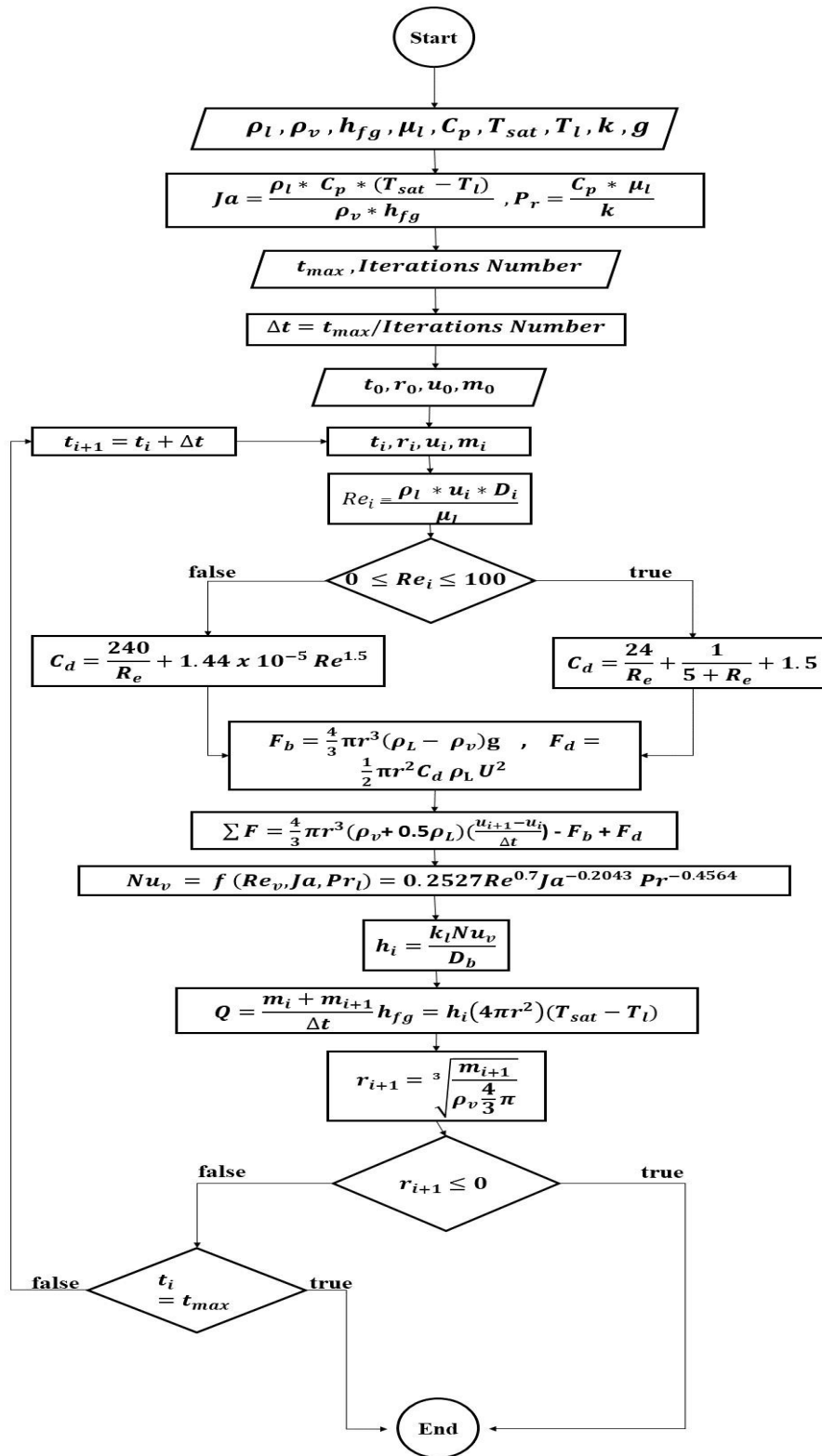
Figure 15: MATLAB's scrip diagram.

4.1 Bubble Configuration and Parameter

In this section, a spherical shape for a bubble in three-dimensional space domain is considered as an assumption for the analysis. The gravity effect is in the downward direction as shown in Figure 14, which is against the direction of the flow domain and the bubble's motion. The liquid domain dimensions are assumed to be much larger than the size of the bubble.

Figure 16 shows the initial position of the bubble and D_0 is the initial diameter. The calculations are conducted for water-liquid and water-vapor with the following conditions; three different temperature difference, between the bubble and the surrounding liquid with fixed bubble initial diameter. Additionally, the largest temperature difference is fixed to conduct the analysis for three different initial bubble diameters. The influence of dividing the total volume of single bubble into smaller bubbles are also analyzed under the same conditions of saturation temperature $T_{sat} = 373.2\ K$ and temperature difference between the bubble and liquid at $\Delta T = 15\ K$.
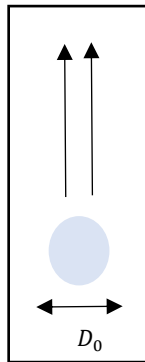
Figure 16: Schematic diagram of computational flow domain.

4.2 Model Validation and Comparison with The Experimental Results

Figure 17 shows the variation of rising bubble volume over time during the condensation comparing between the mathematical model results and the experimental data [52]. The initial and operating conditions for the liquid pool and the bubble used in both the mathematical modeling and the experimental-study are listed in Table 1. As time progresses the bubble moves up and starts to condensate through the flow domain. The differences between the bubble volume in the model-based results and the experimental data It is difficult to observe the turbulent mixing phenomena of the rising bubble and the changes on the bubble shape from the symmetrical sphere shape to ellipsoidal shape in the mathematical model which causes some variation in the heat transfer area. Considering the simplifying assumption of spherical shaped bubble in the mathematical model there is a good agreement of the volume variation pattern between the theoretical and experimental results. The variation of bubble volume over time is a representation of condensation rate over time. In the following section, investigation will be carried out to evaluate the condensation rate and the thermal behavior under different initial and flow field conditions.

Table 1: Initial condition for the fluid and the bubble.

Parameter	Value	Units
Saturation temperature	373.2	K
Initial liquid temperature	358.2	K
Bubble inlet velocity	Zero	m/s
Bubble initial volume	60	mm^3

Figure 17: Model predicted and experimentally measured bubble volume over time [52].
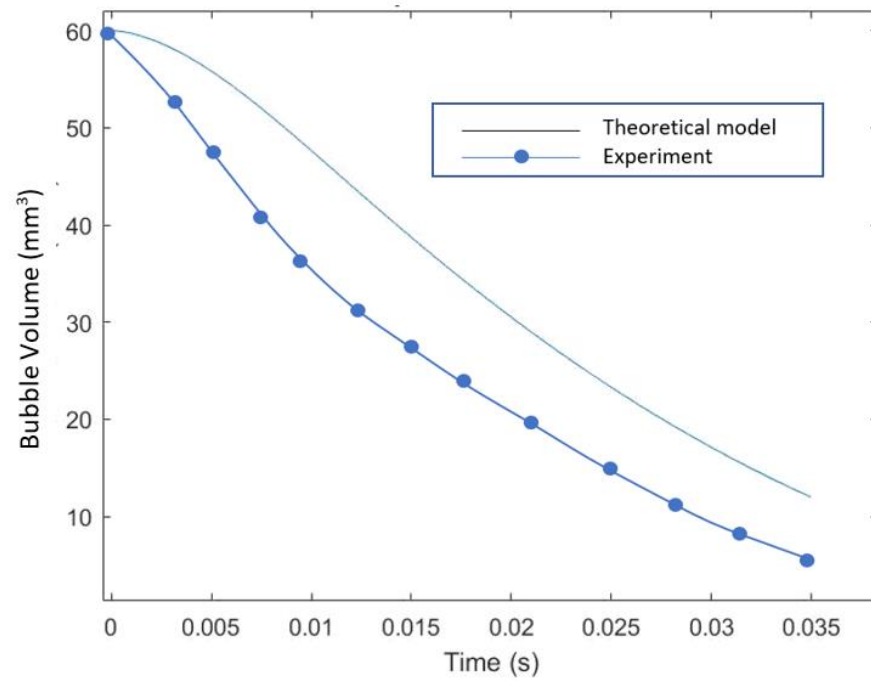
4.3 Parametric Study Simulation and Results

To investigate the bubble behavior under various flow and operating conditions, MATLAB code was developed describing the mathematical model written to examine three different initial liquid temperatures, and the corresponding parameters used in the three cases are listed in Table 2.

Table 2: Parameters used in the three different initial liquid temperatures.

Case Number	1	2	3
Local pressure (kPa)	101.3	101.3	101.3
Bubble temperature (K)	373	373	373
Liquid temperature (K)	368	363	358
Temperature difference ΔT (K)	5	10	15
Liquid density (kg/m^3)	961.9	965.3	968.6
Vapor density (kg/m^3)	0.5975	0.5975	0.5975
Liquid viscosity (kg/m.s)	0.0002972	0.0003144	0.0003333
Liquid thermal conductivity (W/m.K)	0.6634	0.6613	0.6590
Liquid specific heat (kJ/kg.K)	4.210	4.204	4.199
Latent heat of vaporization (kJ/kg)	2270	2283	2295

The variation of bubble volume over time for different liquid temperature is shown in Figure 18. The initial bubble diameter in the three cases is constant at $D_0 = 4.8\ mm$, which corresponds to 60 mm^3 bubble volume. The solid line represents the bubble volume history with a temperature difference of 5 K while dash lines for 10 K and dot lines for 15 K. It is shown that for the same initial volume, the bubble volume decreases faster when the temperature difference increases. For bubbles with high difference in temperatures the heat transfer rate is higher than the others. This is mainly because increasing temperature

difference increases the heat transfer rate under the same interfacial surface area as shown in *Figure 18*. As shown in Figure 19, the heat transfer increases rapidly from the initial time until it reaches a maximum value, and this is due to the increase in bubble rising velocity. Then after, condensation increases which results in reduction bubble volume and bubble surface area which reduces the heat transfer rate.
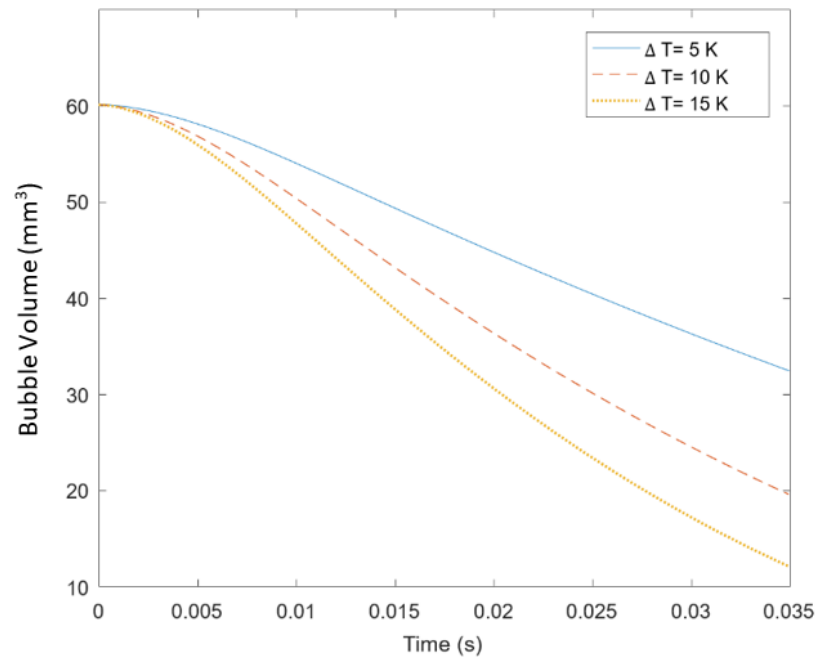
Figure 18: Time-dependent bubble volume history for $\Delta T = 5\ K, 10\ K\ and\ 15\ K$.
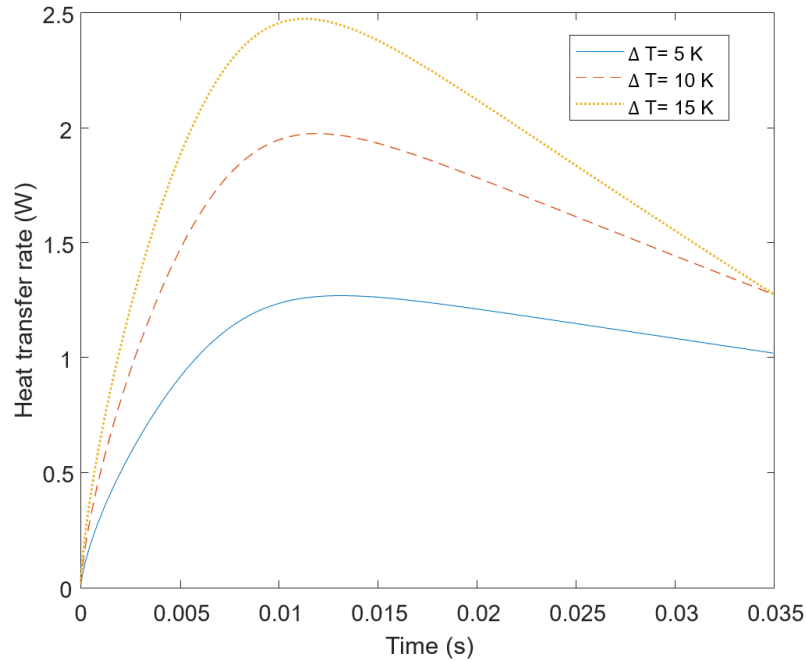
Figure 19: Time-dependent bubble's heat transfer rate for $\Delta T = 5\ K, 10\ K\ and\ 15\ K$.

Figure 20 illustrates the bubbles under the same operating conditions, and at $\Delta T = 15\ K$, but with different initial bubble's volume which corresponds to different initial diameters of 5 mm, 6 mm and 7 mm. The bubble with the largest volume requires longer time to fully condense due to the larger bubble volume and the vapor amount compared with the smaller sized bubbles. In the largest bubble $D_3 = 7\ mm$ a phenomenon should be noted that, the slope of the bubble volume over time has the highest negative slope which indicates a higher heat transfer rate in comparison with smaller bubble sizes. One explanation is the large initial diameter represents a larger interfacial area which allows for more heat transfer rate as shown in Figure 21.
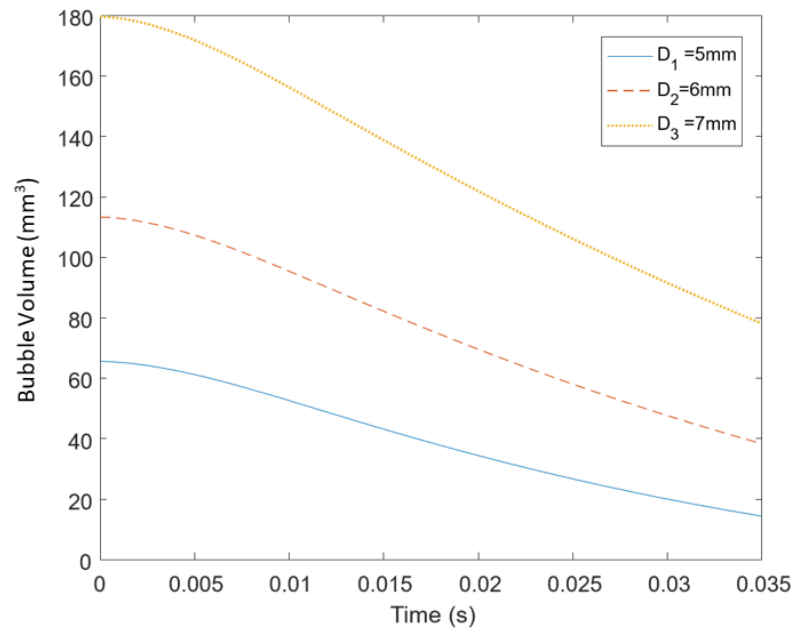
Figure 20: Time-dependent bubble volume history for $D_0 = 5, 6 \ and \ 7 \ mm$ and $\Delta T = 15 \ K$.
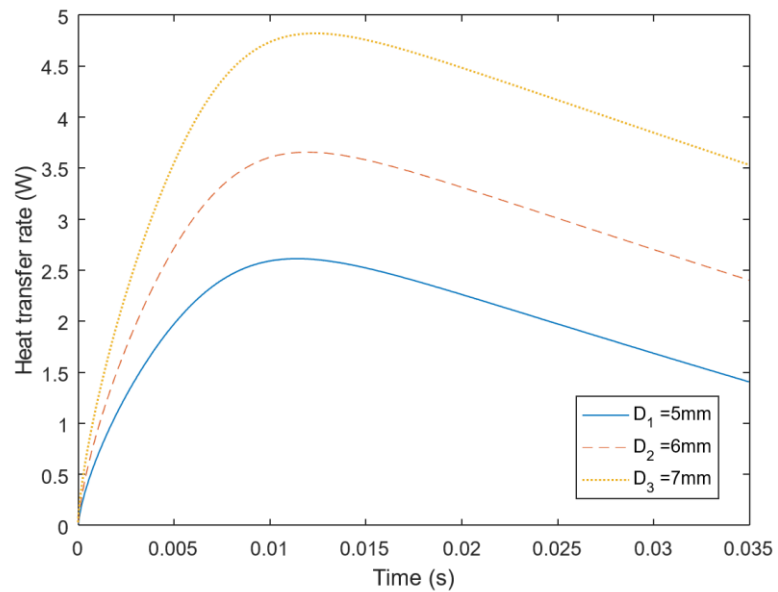
Figure 21: Time-dependent bubble's heat transfer rate for $D_0 = 5, 6 \ and \ 7 \ mm$ and $\Delta T = 15 \ K$.

During the condensation process the heat transfer rate of the bubble increase rapidly until it reaches the maximum rate then it starts to decrease. This phenomenon can be explained by the decreasing rate of the bubble's diameter versus the changing in heat transfer coefficient. Figure 22 shows the heat transfer coefficient increases dramatically in the beginning of the condensation process then the rate of change decay gradually. It is to be noted that the heat transfer coefficient is affected by the Reynold number, and the Reynold number changes continuously due to the variation in bubble volume, inertial forces, and buoyancy forces. The variation in Reynolds number over time is shown in Figure 23. Therefore, the decrease of Reynold number decreases the heat transfer coefficient while the bubble diameter continues with same decreasing rate.
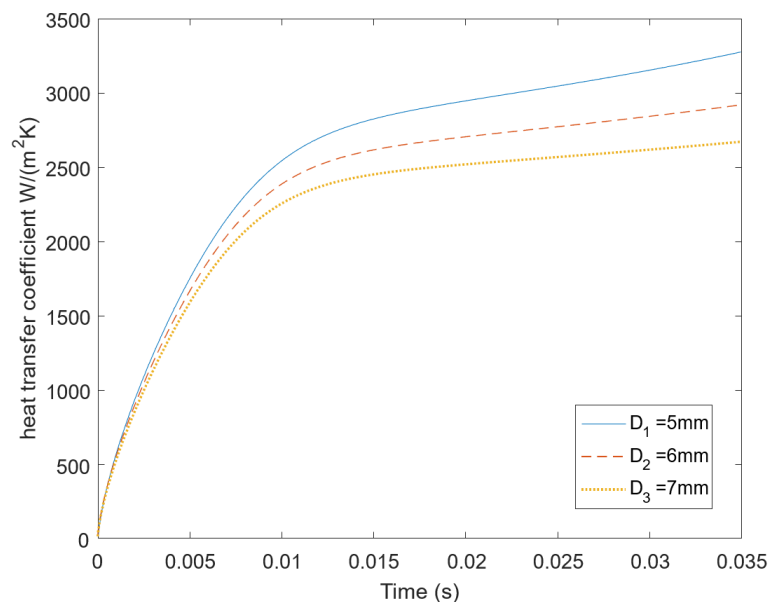
Figure 22: Time-dependent bubble's heat transfer coefficient for different diameters $D_0 = 5, 6 \ and \ 7 \ mm$.
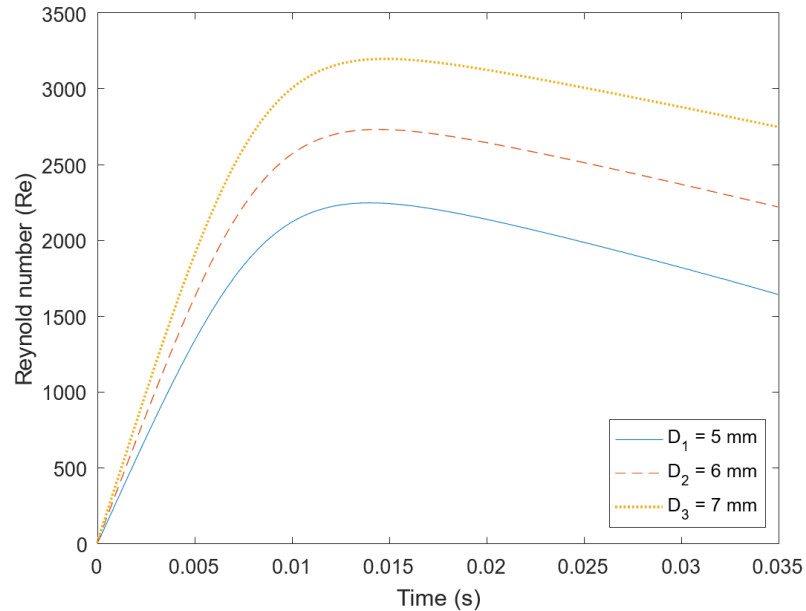
Figure 23: Bubble's Reynold number for $D_0 = 5, 6$ and 7 mm.

4.3 Effects of Bubble Break Up on Condensation Heat Transfer Rate

Based on the calculated results for a single bubble with an initial diameter of $D_0 = 4.86$ mm, and temperature difference of $\Delta T = 15$ K with fluid parameter listed for Case 3 in Table 2, an investigation is done to examine the bubble thermal behavior if the bubble divided into two, four and six smaller bubbles. To investigate the bubble lifetime the MATLAB code performed for the three cases (A, B and C) with fixed time duration $t_{final} = 0.05$ s. Figure 24 illustrates the original bubble lifetime and variation of bubble over time due to condensation. It is shown that the original bubble completely condensed and transferred from vapor phase to liquid phase approximately at 0.065 second.
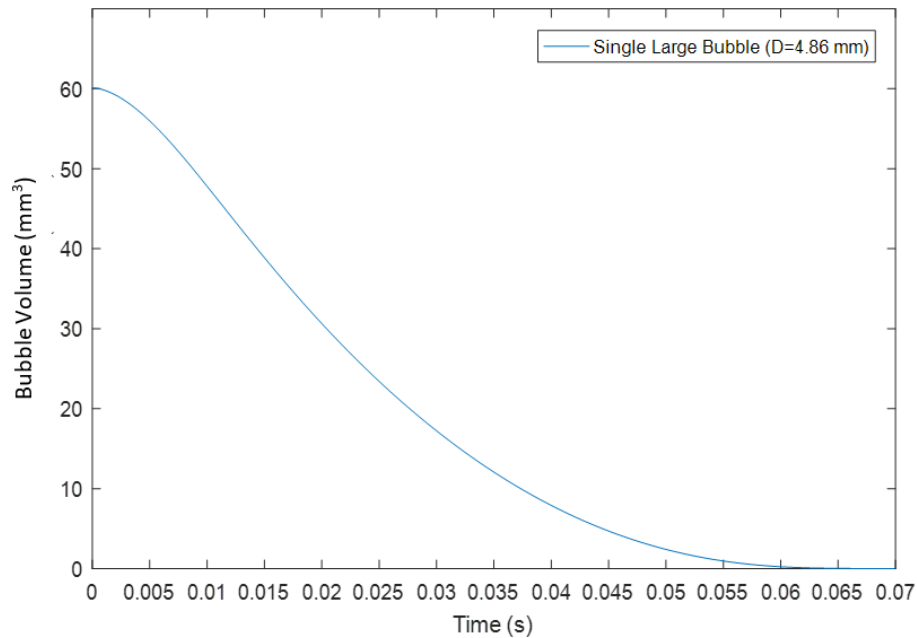
Figure 24: Time-dependent bubble volume history for original bubble before breaking up into smaller bubbles.

The original bubble has an initial volume of $V_0 = 60$ mm ^{3} is divided into smaller bubbles that have a total volume equal to the original bubble $(60$ mm $^3)$. Figure 20 illustrates three cases (A,B and C) of breaking the bubble into smaller bubbles, in the first case the original bubble is divided into two equal bubbles with initial volume of $V_0 = 30$ mm ^{3} for each bubble, and equivalent to initial diameter of $D_0 = 3.86\ mm$, the second case the original bubble is divided into four bubbles with initial volume of $V_0 = 15$ mm ^{3} for each bubble, and equivalent to initial diameter of $D_0 = 3.06\ mm$, the last case have six smaller bubbles with an initial volume of $V_0 = 10$ mm ^{3} and initial diameter $D_0 = 2.67\ mm$.

$D_0 = 4.86\ mm$

$D_0 = 3.86\ mm$

$D_0 = 4.86\ mm$

$D_0 = 3.06\ mm$

$D_0 = 4.86\ mm$

$D_0 = 2.67\ mm$

Case A   Case B   Case C
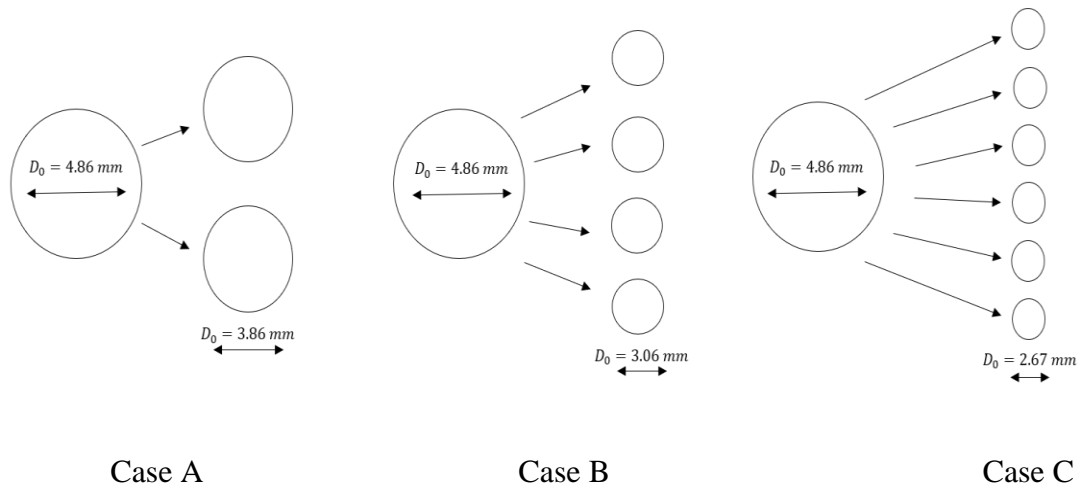
Figure 25: Three cases of breaking up the original bubble into smaller bubbles.

Figure 26 shows the bubble volume variation over time for Single bubble and multiple smaller bubbles. In Figure 26 (A) the smaller bubble has completely condensed and reached the liquid phase during $t_{total} = 0.045$ s, while the original bubble still in a vapor-phase. The volume of the smaller bubble decreases rapidly in the first half of time duration $t = 0.025$ s, which reaches $V = 8$ mm^3 that equivalent to 26% of smaller bubble initial volume, compared with original bubble reached $V = 24$ mm^3 that equivalent to 40% of original bubble initial volume. By considering the first half lifetime of the smaller bubble before $t = 0.0225$ s the volume of the bubble decreased from initial volume $V = 30$ mm^3 to $V = 10$ mm^3, which is 66.67% reduction from the initial volume, while the remaining 33.3% of the vapor phase has taken the second half of the bubble lifetime to completely condense and its phase change to liquid phase. Breaking up the original bubble into half of its original volume can reduce the total condensation time from $t_{total} = 0.065$ s to $t_{total} = 0.045$ s, which is reduction of 33.8% from the original

bubble lifetime. Furthermore, Figure 26 (B) illustrates the variation in the bubble volume which is into four smaller bubble with initial volume of $V = 15$ mm^3 for each small bubble. The four bubbles have a lifetime of $t_{total} = 0.0375$ s to completely condense. Additionally, in the first half of the four bubbles lifetime the volume decreased to the third of initial bubble volume, which is a similar behavior as shown in Case (A). Figure 26 (C) shows that if the original bubble is divided into six smaller bubbles the total lifetime for the bubble to completely condense will be decreased from $t_{total} = 0.065$ s to $t_{total} = 0.03$ s. The bubbles lifetime and the amount of reduction in the total condensation time due to original bubble break up listed in Table 3. The analysis shows for a single bubble with initial bubble volume of $V_0 = 60$ mm^3 needs to break up minimum into 1/6 of its original volume to decrease the total condinsation time to approximately half of the original lifetime.
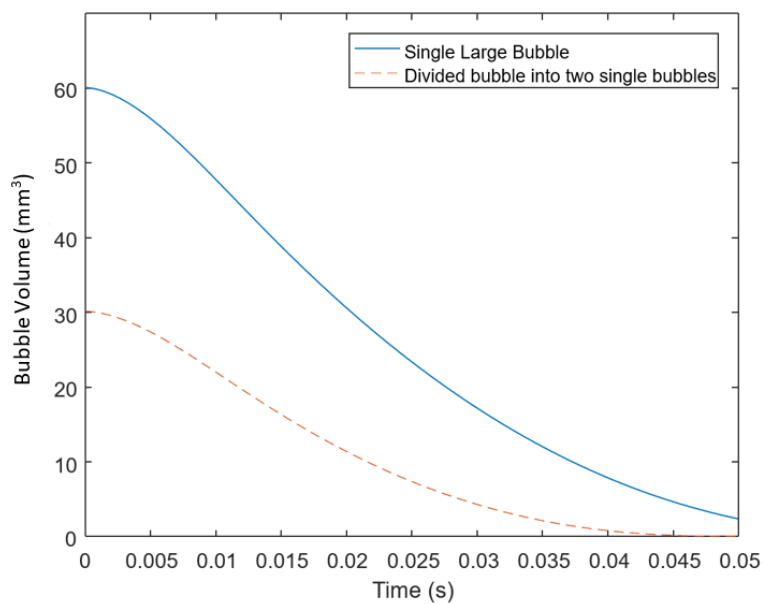
Case (A)
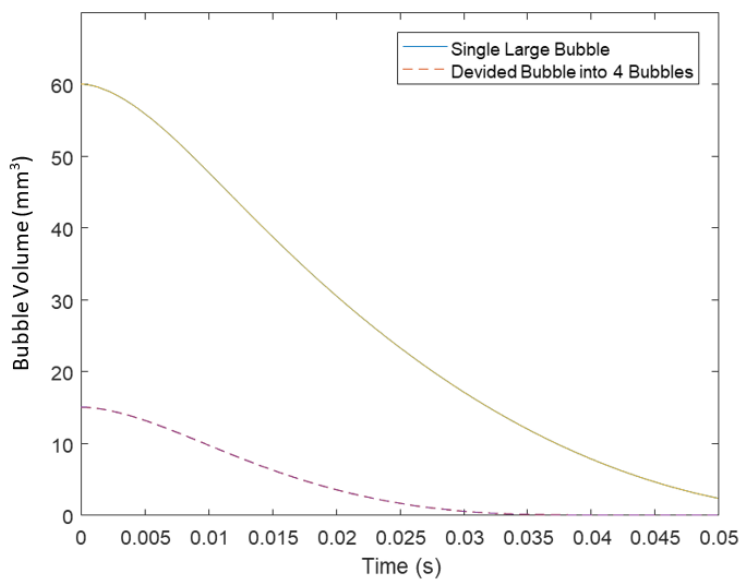
Case (B)

Figure 26: Time-dependent bubble volume history for Single bubble and sub bubbles in three cases (A, B and C).
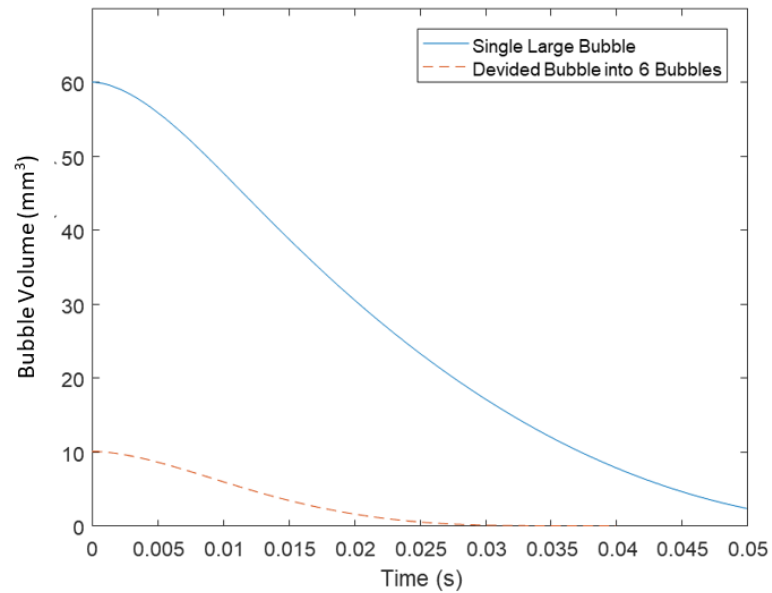
Case (C)

Figure 26: Time-dependent bubble volume history for Single bubble and sub bubbles in three cases (A, B and C) (continued).

Table 3: Bubble lifetime in single large bubble and the bubbles in Cases (A, B and C).

Number of Bubbles	Single original bubble	2	4	6
Lifetime (second)	0.065	0.045	0.0375	0.03
Reduction from original bubble lifetime (%)	-	33.8	42.3	53.8

To investigate the effect of breaking up the bubble into half of its initial bubble volume, the bubbles volume history for the three chases (A, B and C) was plotted in one

figure as shown in Figure 35. Since the bubbles in Case (B) has initial volume of $V_0 =$ 15 mm ^{3} which is half of the volume of the bubbles in Case (A), the smaller the volume, the smaller is the condensing time for Case (B). In Case (B) the bubbles have a lifetime of $t_{total} = 0.0375$ s and the lifetime in Case (A) $t_{total} = 0.045$ s, this means that the condensation time has reduced by 16.6%, however, the condensation time has reduced by 33.8% in Case (A) although in both scenarios the initial volume has divided into half. This indicates whenever the bubbles break up into half the resultant bubbles will not behave linearly.
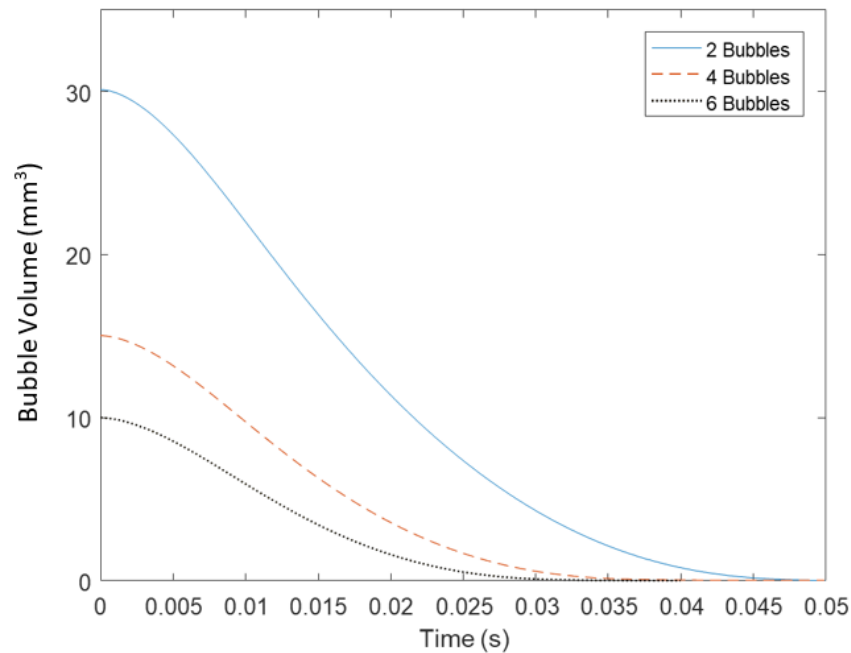
Figure 27: Time-dependent bubble volume history for the bubbles in three cases (A, B and C).

The heat transfer rate of a condensing bubble is shown in Figure 28, and it indicates that if a large bubble is divided into smaller bubbles with the same original volume, the

heat transfer rate of smaller bubbles will be higher than that of a single bubble. As a result, the consequences of collapsing the original bubble into sub bubbles improves the total heat transfer rate by approximately 35% in Case (A) at the peak time as shown in Figure 28 (A). Figure 28 (B) shows the heat transfer rate for four bubbles has increased to 4 Watt compared with 3.2 Watt in Case (A) that produced an additional 20% enhancement in the peak of total heat transfer rate. Figure 28 (C) illustrates After breaking up the bubble into six bubbles the heat transfer rate reached 4.5 Watt, which gives 11.1% additional enhancement on the heat transfer rate in Case (B).

This is due to the increase of the total interfacial area between the vapor phase and the liquid phase, the original bubble has diameter of $D_0 = 4.86\ mm$ which is equivalent to a surface area of 74.11 mm^2, however the two bubbles in Case (A) have a total surface area of 93.38 mm^2 in. The total surface area and the correlated peak heat transfer rate for the three Cases (A, B and C) is shown in Figure 29. Thermal behavior of the bubbles in Figure 28 and Figure 29 reveal that under the same operating conditions the bubble's heat transfer can be enhanced by dividing the bubble into smaller bubbles before the start of the condensation process.
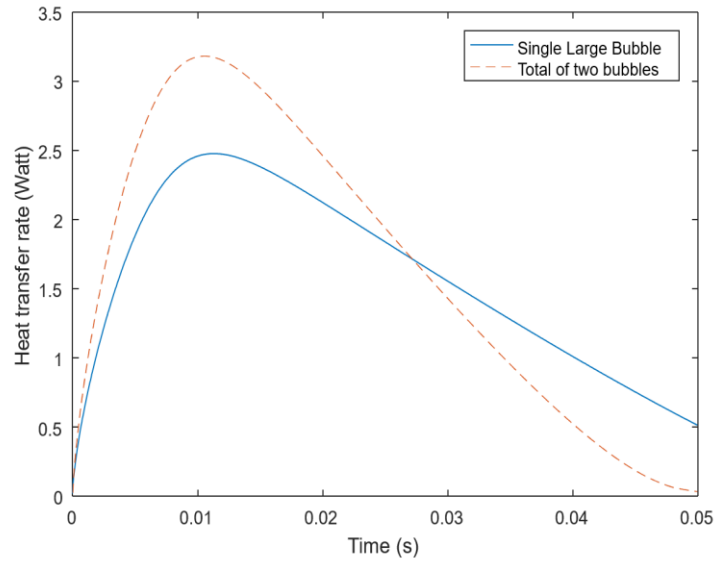
Case (A)
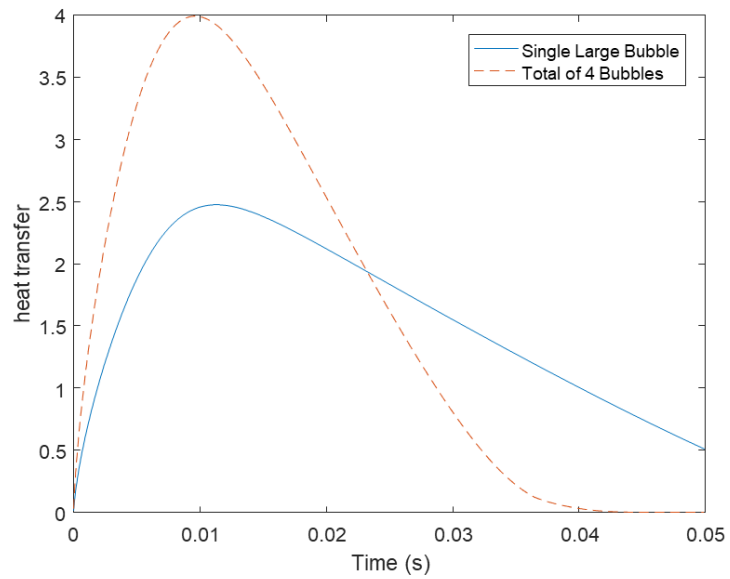
Case (B)

Figure 28: Heat transfer rate for single bubble and total sub bubbles over time.
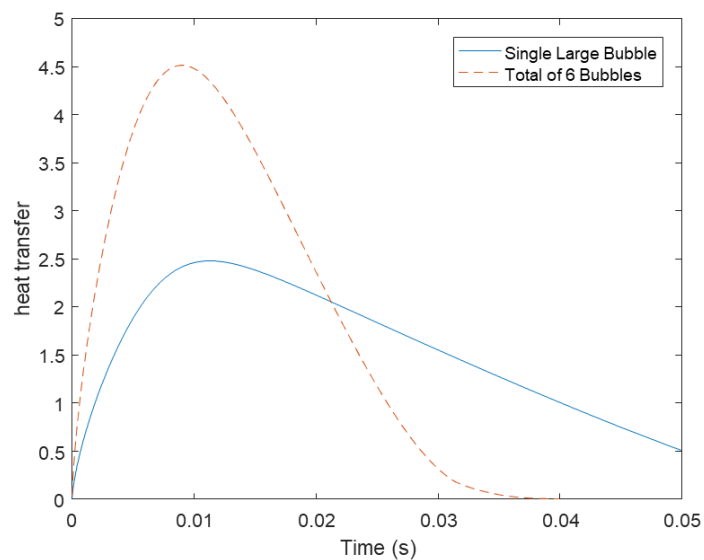
Case (C)

Figure 28: Heat transfer rate for single bubble and total sub bubbles over time (continued).
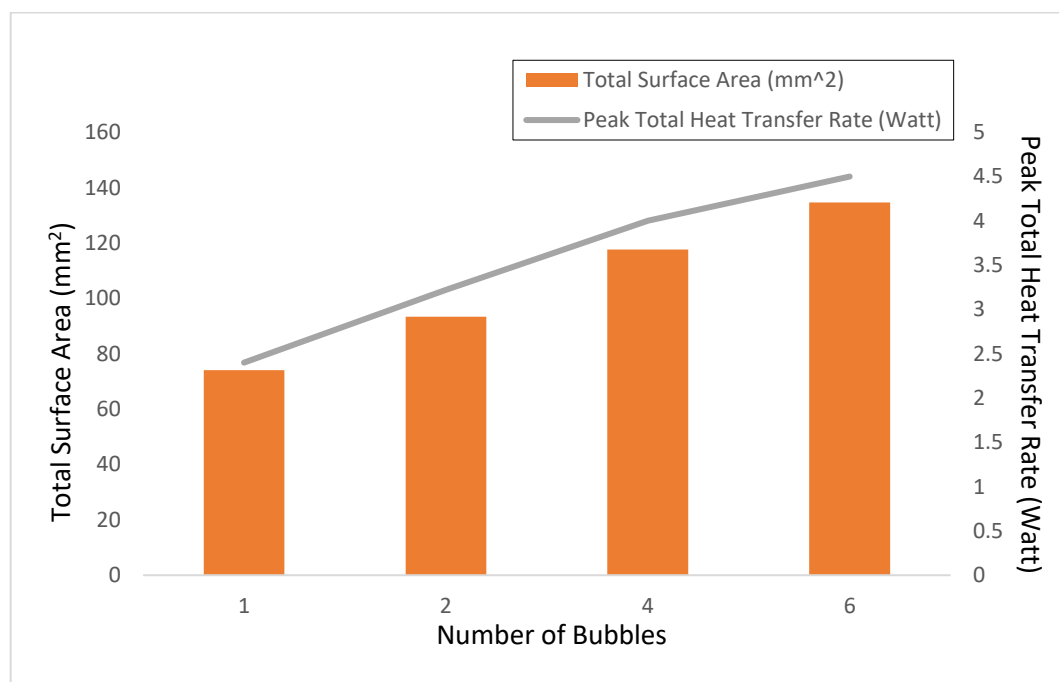
Figure 29: Bubbles total surface area versus peak total heat transfer rate.

Chapter 5: Numerical CFD Simulation Results

In the previous chapter, the semi-empirical model showed that if the original bubble is divided into smaller bubbles, it will positively affect the condensation rate. Therefore, the need for a solution that features a collapsing mechanism for the bubble during the condensation is highlighted. In this chapter, a mesh-based structure is introduced as a geometrical modification of the flow structure. The mesh-based structure is a physical barrier contained many small gaps placed normal to the flow direction, which can be modified to fit in various types of flow structure shapes, as shown in Figure 30. The mesh will allow the flow to move freely through the desired direction, but if the flow field contains any bubbles, it will be disturbed. The bubbles can follow several trajectories while crossing the mesh gaps since they will not follow a uniform path. The bubbles can cross through the middle of the gap or collide with the middle barrier between the gaps as shown in Figure 31. In both scenarios, the bubble will follow a different behavior which will be discussed in this chapter. in the following sections a single gap mesh structure is chosen to demonstrate the bubble dynamic behavior while crossing the mesh in the middle of the gap and multiple gaps mesh structure is chosen to demonstrate the behavior of the bubble while it collides with the middle barrier between the gaps.
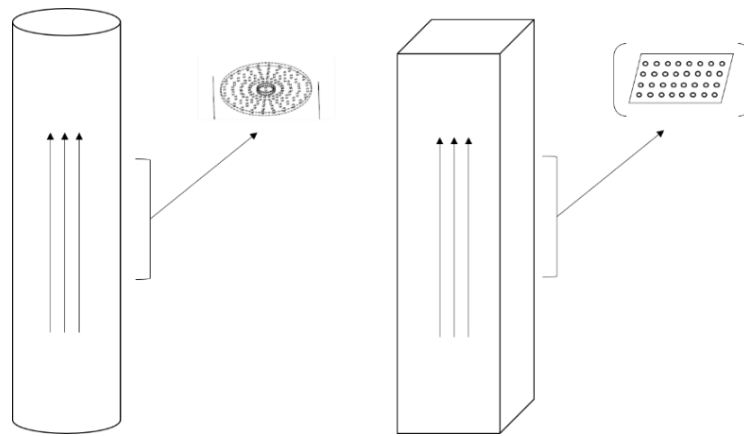
Figure 30: Schematic diagram of various structure shapes.
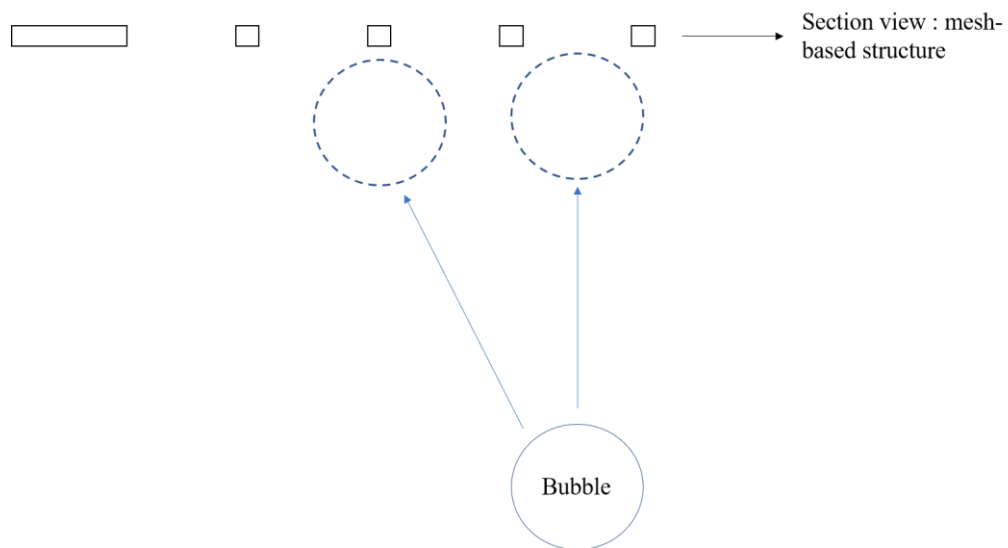
Figure 31: Schematic diagram of various bubble trajectories.

To investigate these behaviors, a numerical study has conducted using CFD code in ANSYS Fluent, which has been used for a variety of applications as mentioned in literature. This CFD finite volume package along with Design Modeler and ANSYS

Meshing are used to design the geometry and meshing respectively for the simulation. The

methodology followed to perform the numerical simulation can be summarized in Figure

32. The ANSYS Fluent model used is a 2-D planer space model. The volume of fluid VOF

coupled with user-defined function (UDF) is utilized to demonstrate the bubble behavior

under various conditions.

| Create geometry in design modeler | Meshing in ANSYS meshing tool | Import the mesh into Fluent solver | Assign solver general parameter | Assign boundary conditions | Assign initial conditions and patch the volume fraction | Set solver settings & run the solver | Post CFD results |
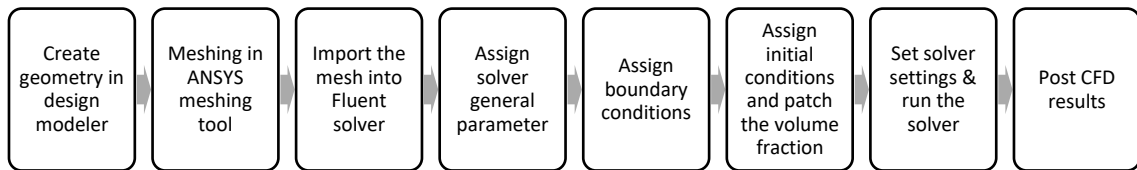
Figure 32: Flowchart summarizing the numerical methodology.

This chapter investigated a single bubble crossing through the middle of the

mesh's gap and multi gaps. The numerical study is conducted for three single gap sizes

(10 mm, 8 mm, and 6 mm) and for multi gaps (double gaps and 3 gaps) to analyze the

behavior of the bubble in terms of deformation, velocity distribution, and moving

trajectory. The calculations are conducted for water-liquid and water-vapor multiphase

flow with the following constant properties: $\rho_l = 1000 \; kgm^{-3}$, $\rho_g =$

$1.266 \; kgm^{-3}$, $\mu_l = 1.137 \times 10^{-3} \; kgms^{-1}$, $\mu_g = 1.78 \times 10^{-5} \; kgms^{-1}$ and $\sigma =$

$0.0719 \; N/m$ with $Gravity = 9.81 \; ms^{-2}$ in the negative Y-axis (-y).

5.1 Geometry and Meshing

A two-dimensional (2D) planer computational domain is created to include vapor chamber, flow path and mesh's gap as shown in Figure 33. The geometry consists of two zones the flow and the vapor chamber. The flow is the fluid domain that contains water liquid and has a dimension of 100 mm by 20 mm. additionally, this zone includes the mesh's gap, which is 40 mm above the vapor chamber with a thickness of 1 mm. Furthermore, the vapor chamber is placed at the bottom of the flow domain with a dimension of 10 mm by 2 mm and contains water vapor. Generally, to analyze the effect of grid resolution on simulation of an adiabatic bubble, it has been reported 16 CPD (Cells per bubble diameter) is appropriate to simulate bubble behavior with VOF model [68, 69]. However, 16 CPD cannot be maintained since the bubble diameter may vary during bubble deformation inside the mesh's gap. Therefore, a greater CPD is used for the simulation. To ensure that mesh size less than 1/16 of the bubble diameter, the cell size has been chosen to be Quadrilateral and less than 1/16 of the gap width in each simulation. That will ensure capturing rich dynamic features in the simulation, as shown in Figure 34.
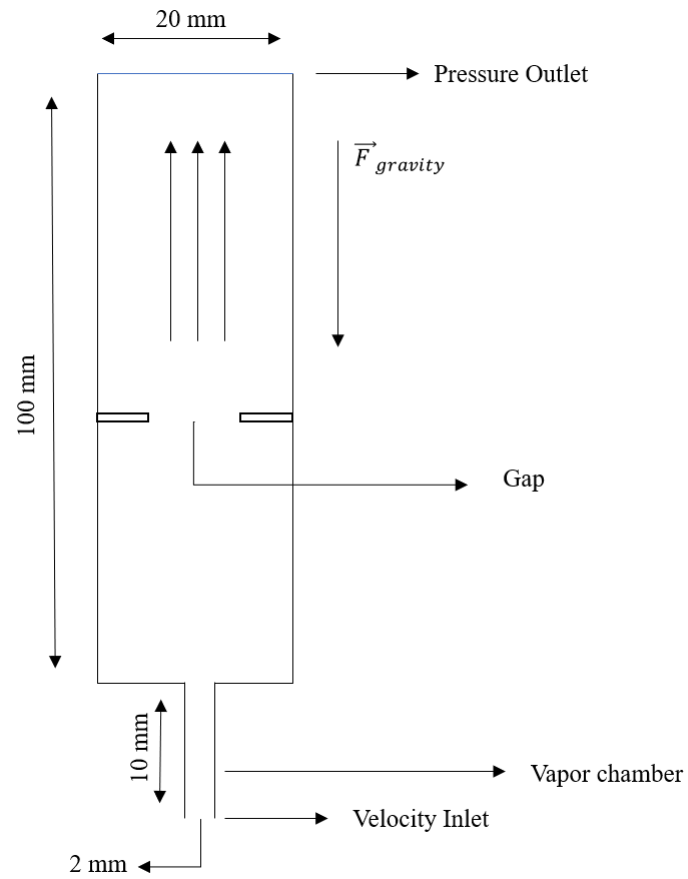
Single Gap (A)

Figure 33: Schematic diagram of computational flow domain in single, double and four gaps.

20 mm

Pressure Outlet

$\vec{F}_{gravity}$

100 mm

Double Gaps

10 mm

Vapor chamber

Velocity Inlet

2 mm
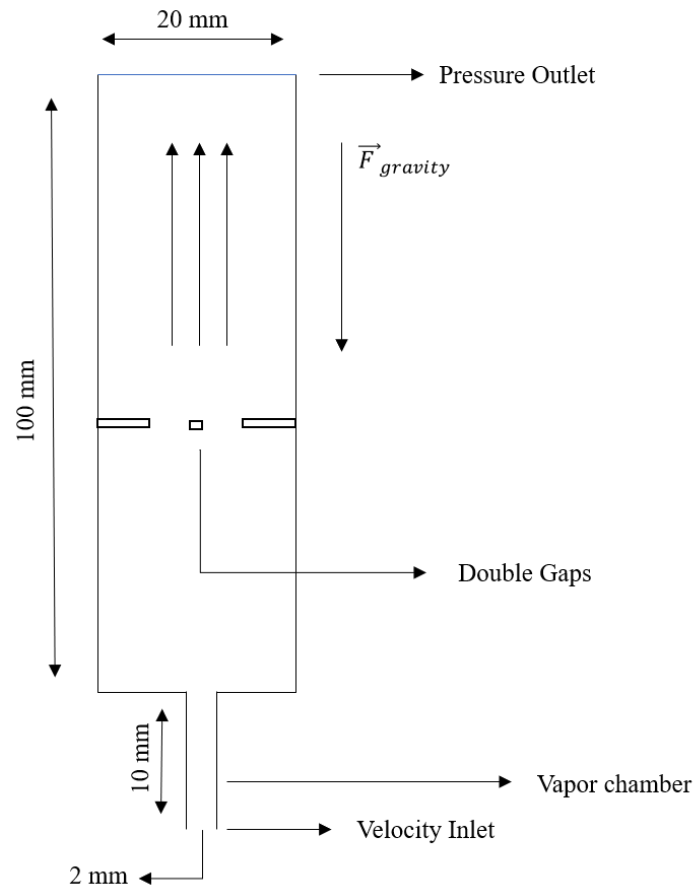
Double Gap (B)

Figure 33: Schematic diagram of computational flow domain in single, double and four gaps (continued).
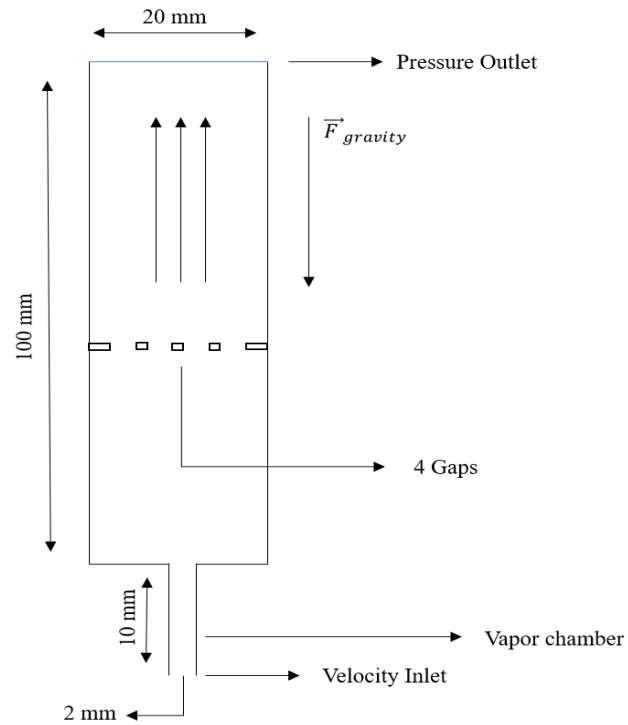
Four Gaps (C)

Figure 33: Schematic diagram of computational flow domain in single, double and four gaps (continued).
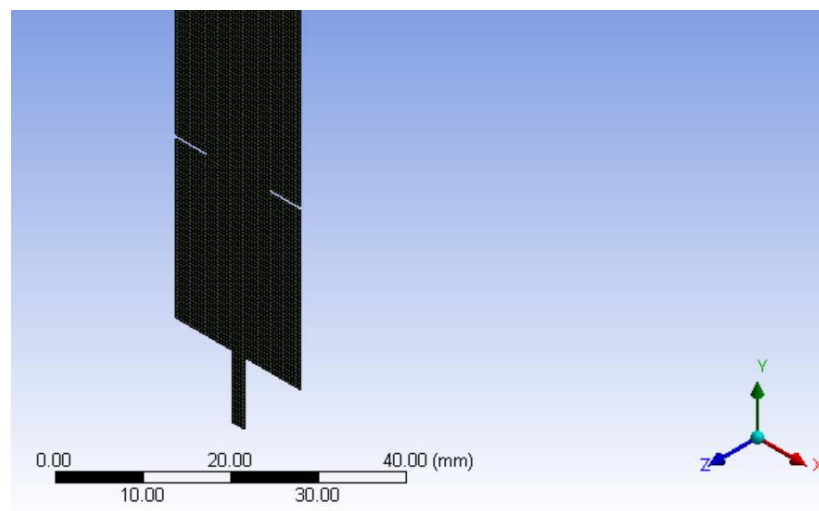
Figure 34: Meshing for computational flow domain.

5.2 Boundary Conditions and Solver Settings

A numerical solution method for the transient, incompressible Navier-Stokes equations has been adapted to simulate the bubble behavior. In order to have a close solution domain, the boundary conditions must be specified. In the cases studied in this work have three types of boundary conditions are used. In most cases, the boundary conditions employed at the boundary's cells with a grid of zero thickness which allows the conditions to be applied explicitly. Figure 33 shows the inlet conditions are defined to be a velocity inlet in the positive Y-axis (+y), a UDF (user-define-function) is utilized to limit the inlet velocity of 3 m/s for 0.008 seconds only in order to generate the required bubble (Appendix B). Outlet boundary conditions are specified to be pressure outlet with constant static (gauge) pressure at the outlet and equal to 0 Pa since we have an inlet flow rate, and the parameters are unknown at the outlet. The wall boundary conditions are used to bound fluid and solid regions where wall motion is stationary and the shear condition is no slip conditions for the side walls are applied with zero tangential velocity component. To ensure the bubble will be created by the vapor phase, the vapor chamber's initial condition is specified to be full of vapor phase where the vapor phase is set to have a value of 1 volume fraction and the liquid phase is 0. The initial condition of the liquid domain is specified to have the listed parameters in Table 4.

Table 4: Initial condition parameters in the liquid phase domain.

Parameter	Value	Unit
Gauge pressure	0	Pa
X velocity	0	m/s
Y velocity	0	m/s
Turbulent Kinetic Energy	1	m^2/s^2
Turbulent Disspation Energy	1	m^2/s^2

The VOF for multiphase and the $k - \varepsilon$ equation were incorporated in the above-described conditions to adapt the different volume fractions for liquid and vapor phases and to solve the velocity distribution, pressure equations, and turbulence model equations in the domain. Although the liquid regime initially is laminar, the $k - \varepsilon$ model with enhanced wall treatment option yielded better results in simulating the bubble movement and deformation since high inlet velocity 3 m/s will create turbulent eddies through the flow domain. Time integration, or time-stepping, is solved using PISO (Pressure-Implicit with Splitting of Operators), recommended for all transient flow calculations and VOF model [71]. The time step used in the simulations was determined by the Courant number, which governs the propagation speed of information on the domain mesh. The Courant number is defined as:

$$C_0 = \frac{u\Delta t}{\Delta x}$$

where u is velocity magnitude, Δt is the time step size, and Δx is the mesh length. For this simulation, a time step size of 6×10^{-5} was used to keep the courant number below 1.

5.3 Simulation and Results

5.3.1 Single Gap Geometry

For three gap sizes ($10\ mm, 8\ mm, and\ 6\ mm$) the time evolution of the bubble generation is shown in Figure 35. The water-vapor entered the flow domain with the inlet velocity of 3 m/s, forming a spherical shape bubble due to high surface tension force compared to the buoyancy force. The bubble extended by the water-vapor rapidly until the velocity cut-off time reached and resultant of $67.12\ mm^2$ equivalent to 9 mm diameter of the vapor bubble. The bubble exerted by the buoyancy force, which will detach the bubble from the inlet source and raised rapidly through the flow domain. The velocity vector field during detaching is presented in Figure 36. The velocity vectors in the axial direction decrease away from the flow field. In the redial direction, the velocity increases rapidly and moved from the tip of the bubble on both sides, creating a vortex that moves the fluid underneath the bubble then deforming the bubble to bullet-like shape. After the bubbles detached from the water vapor source the bubble continues rising up toward the mesh's gap influenced by the momentum gained by vapor inlet velocity and the buoyancy force.

| 0 s | 0.0009 s | 0.03 s | 0.06 s | 0.09 s | 0.12 s |
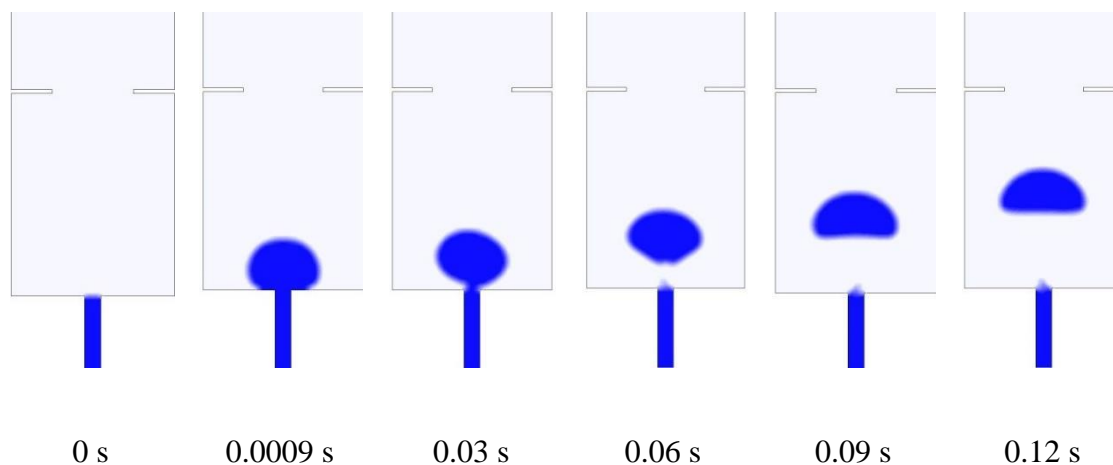
Figure 35: Water- vapor volume fraction contour for bubble generation.
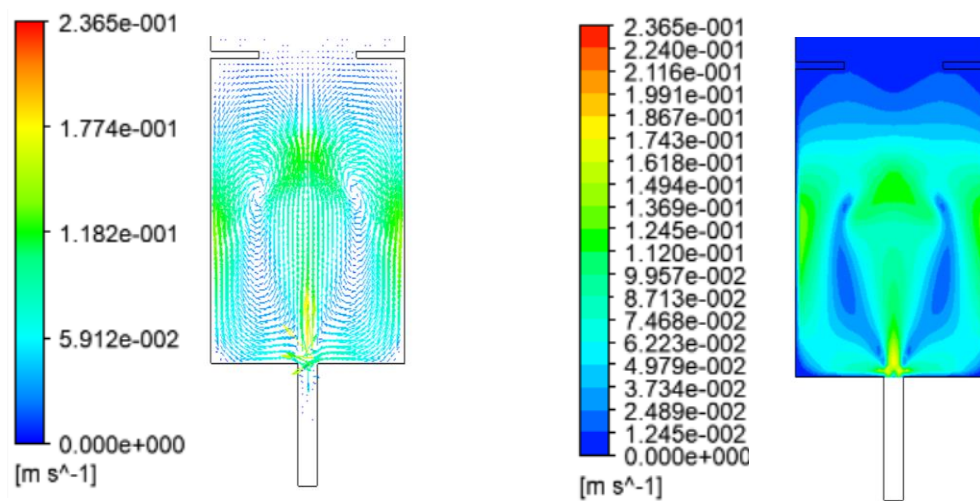
(A) Velocity vector

(B) Velocity contour

Figure 36: Velocity vector and contour for the bubble at t= 0.12 s.

Figure 37 illustrates the volume fraction contour for the bubble dynamic behavior

in 10 mm gap from $t = 0.15\ s$ until the bubble exiting the mesh's gap. Over time the

bubble reaches the bottom section of the gap where the deformation is occurred on the bubble shape. Before entering the gap the bubble shape deformed from elliptical to hemispherical shape due to the collision that occurred between the bubble and the bottom section of the gap. Afterward, the attraction force shrunk to the bubble and return it to spherical shape which will allow the bubble to pass the gap. While the bubble crossing the mesh's gap the surface tension will deform the bubble and adapt the gap width. The hydrodynamic force exerting the bubble motion inside the gap which deformed the bubble toward axial direction. The unbalance between the hydrodynamic force and attraction force caused the bubble to exit without collapsing the bubble. Subsequently, after leaving the mesh's gap the bubble will be influenced again by the buoyancy force which retained the bubble to its elliptical shape. The velocity contour in Figure 38 shows the bubble collided the bottom section of the gap with the approximate velocity of $0.2\ m/s$ and let bubble to bounce from the bottom surface of the gap. The rapid decrease in bubble's velocity decreases the fluid velocity underneath the bubble therefore, the bubble will be affected by the hydrodynamic force only while crossing the mesh. Surface tension and adhesion reduced the rising velocity of the bubble through the gap while the bubble adapt the gap width. Furthermore, Figure 38 (K and L) shows the bubble started to accelerate due to the influence of hydrodynamic force while exiting the gap.
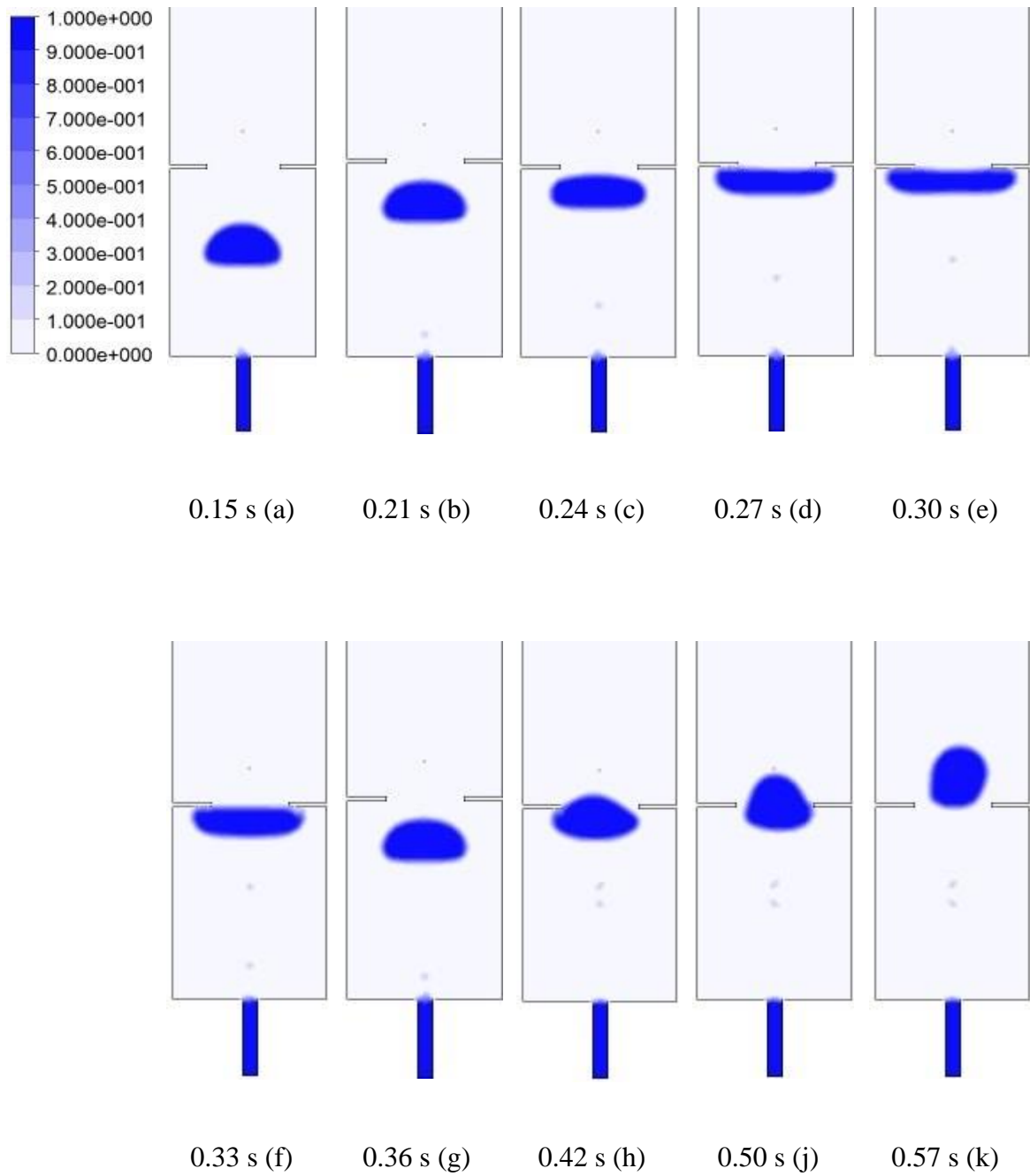
Figure 37: Water- vapor volume fraction contour for bubble behavior across the mesh 10 mm gap.
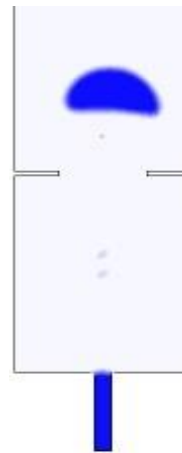
0.63 s (l)

Figure 37: Water- vapor volume fraction contour for bubble behavior across the mesh 10 mm gap (continued).
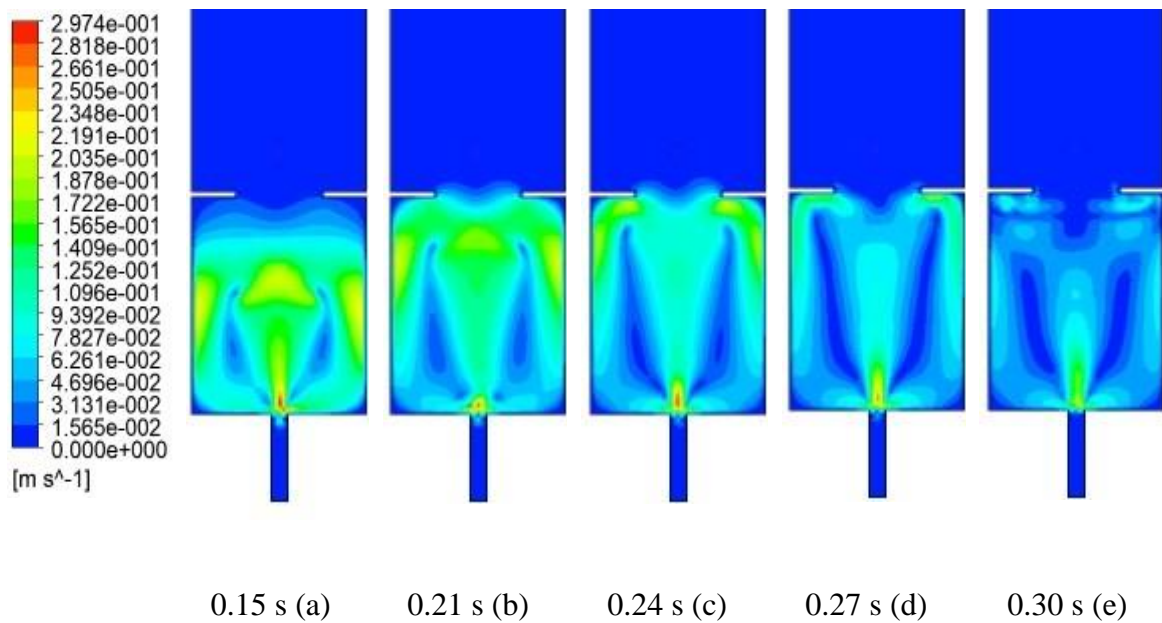
0.15 s (a)   0.21 s (b)   0.24 s (c)   0.27 s (d)   0.30 s (e)

Figure 38: Velocity contour (10 mm gap).

0.33 s (f)   0.36 s (g)   0.42 s (h)   0.50 s (j)   0.57 s (k)

0.63 s (l)
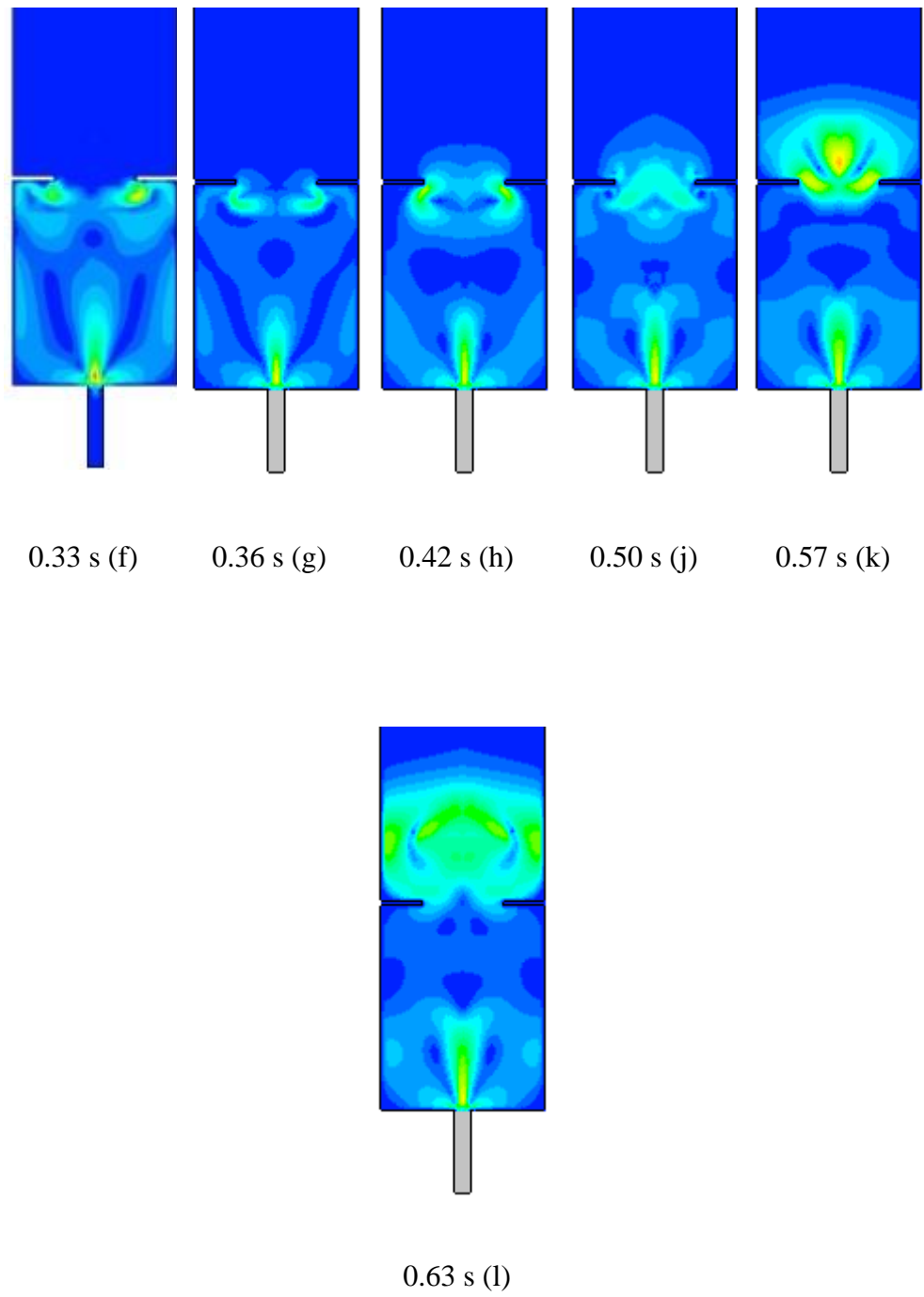
Figure 38: Velocity contour (10 mm gap) (continued).

Figure 39 shows the bubble behavior crossing 8 mm gap. In this smaller gap size, the bubble exposed to higher reaction forces by the bottom surface after the collision. This gap size has smaller exiting area which affecting negatively the influence of the buoyancy force as shown in Figure 39 (G). Subsequently, higher deformation is occurred on the bubble shape to adapt the width of the gap. Within the gap sides, the surface tension force is applied toward the inside in the bubble through the interface between the two phases in order to maintain the shape which will ensure the attraction between the vapor phase. the smaller open area of the gap reduced the ability of the buoyancy force to pull the bubble upward. Therefore, the bubble crossing velocity decreased while the bubble crossing the mesh's gap. Figure 40 (M), shows the bubble at $t = 0.66\ s,$ the bubble will start to accelerate rapidly again in comparison with 10 mm gap the bubble started to accelerate at $t = 0.57$ s as shown in Figure 38 (K). Additionally, due to smaller gap size the bubble exposed to higher deformation which took the bubble till $t = 0.66\ s$ to exit the gap while in 10 mm gap the bubble exited at $t = 0.57\ s$. Figure 41 shows in both gap sizes (10 mm and 8 mm) the bubble position follows similar trend until $t = 0.5s$, where the bubble in 10 mm started to exit while the 8 mm gap bubble still within the gap walls. The delayed occurred on 8 mm gap increased the total time of the bubble within the flow domain, whereas 8 mm gap bubble reached 38 mm vertically while 10 mm gap bubble exceed 45 mm at the same time step. Furthermore, after exiting the gap the bubble position in both gap sizes will follow similar pattern but with positive shift for the of 10 mm gap. Figure 42 (Region A) shows in 10 mm and 8 mm gap sizes the bubble will exposed to sharp decrease in the velocity until $t = 0.33\ s$ where the bubble start to adapt the gap width. In 10 mm gap the bubble velocity increasing rate is higher than 8 mm gap, which can indicate

the 10 mm gap allow for a higher buoyancy force as shown in Figure 42 (Region B). after exiting the gap in both sizes, the bubble will be exposed to sudden increase in the velocity due to sudden release from the gap width and increase in the buoyancy force. At the same time instance $t = 0.72\ s$ in both sizes the bubble will reach the same velocity.
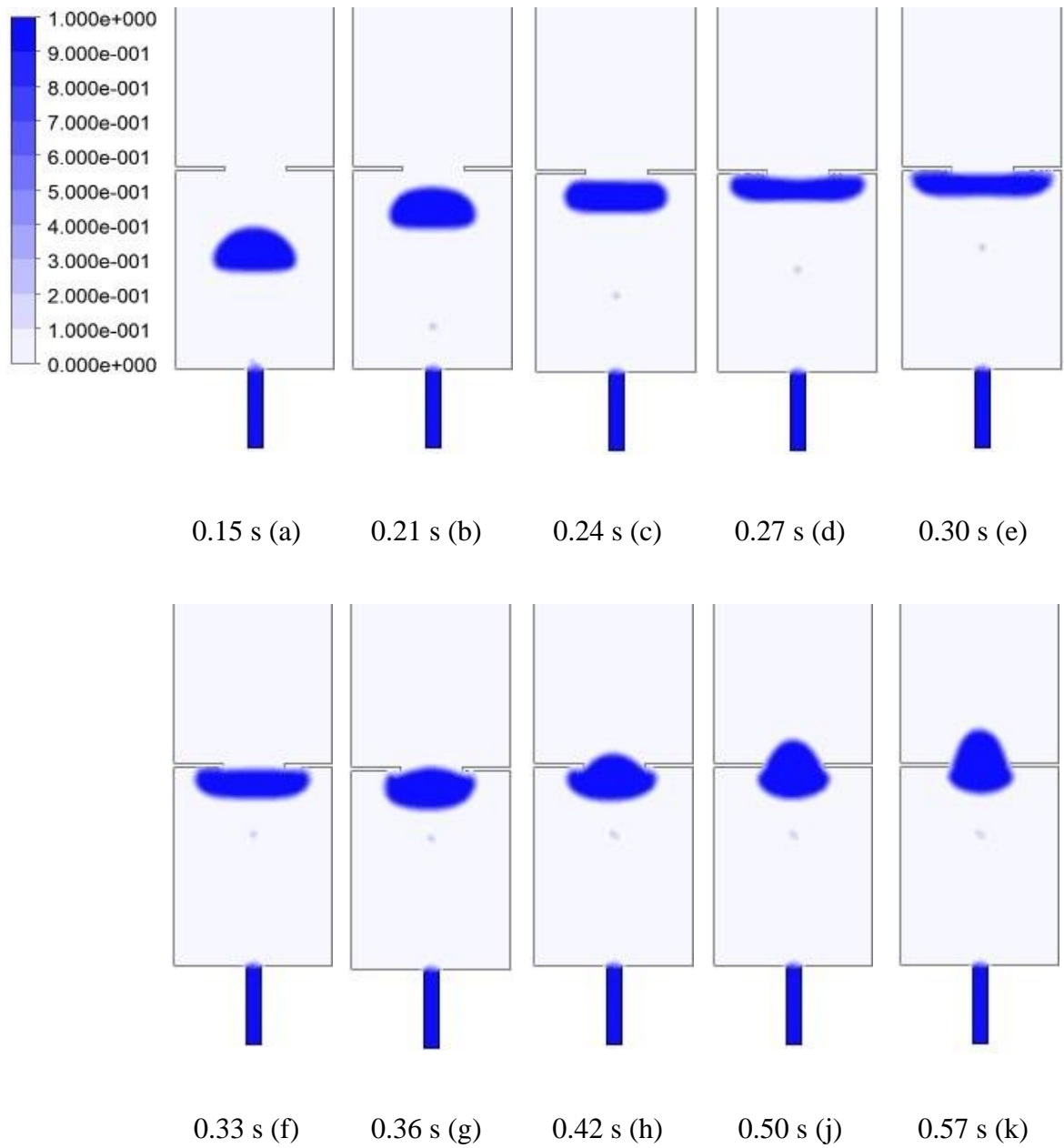
Figure 39: Water- vapor volume fraction contour for bubble behavior across the mesh 8 mm gap.

0.63 s (l)   0.66 s (l)   0.69 s (l)   0.72 s (l)
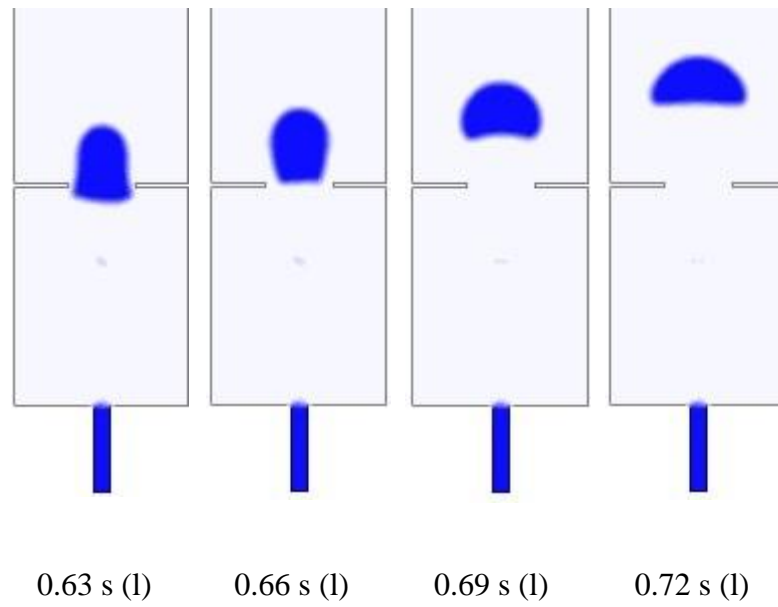
Figure 39: Water- vapor volume fraction contour for bubble behavior across the mesh 8 mm gap (continued).
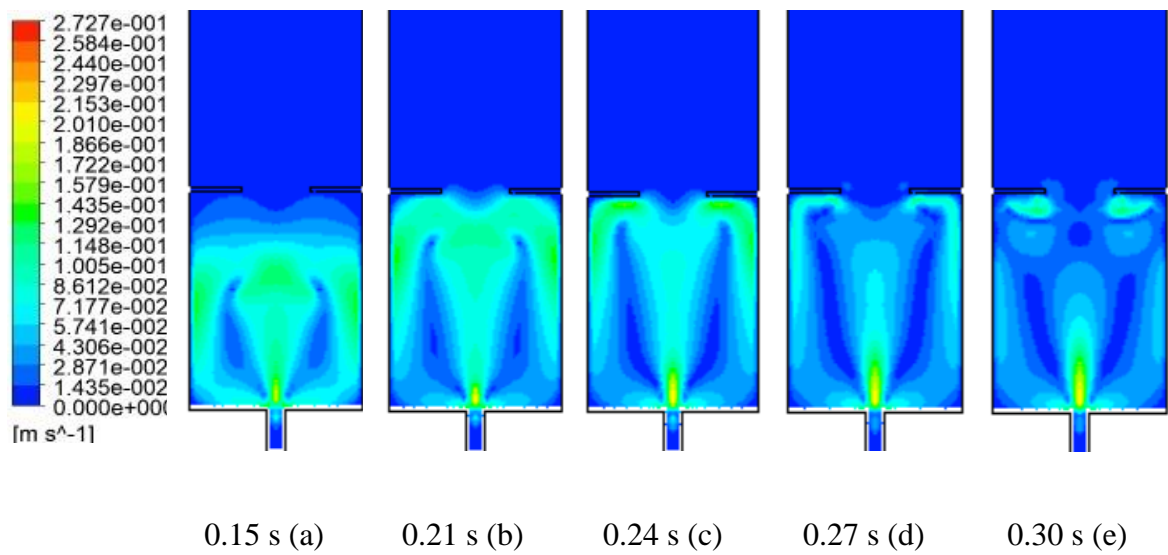
0.15 s (a)   0.21 s (b)   0.24 s (c)   0.27 s (d)   0.30 s (e)

Figure 40: Velocity contour (10 mm gap).

0.33 s (f)   0.36 s (g)   0.42 s (h)   0.50 s (j)   0.57 s (k)

0.63 s (l)   0.66 s (m)   0.69 s (n)   0.72 s (o)
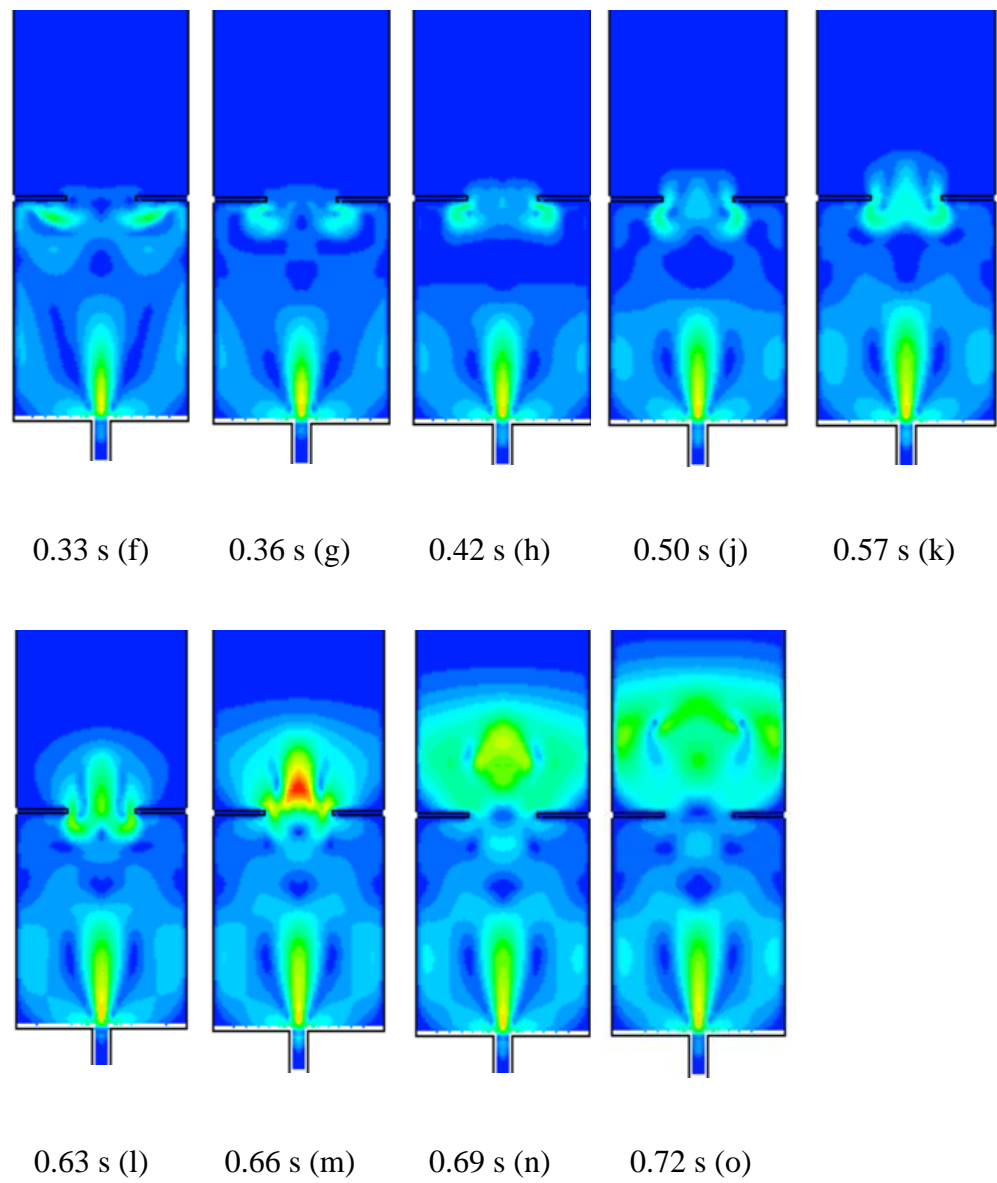
Figure 40: Velocity contour (10 mm gap) (continued).
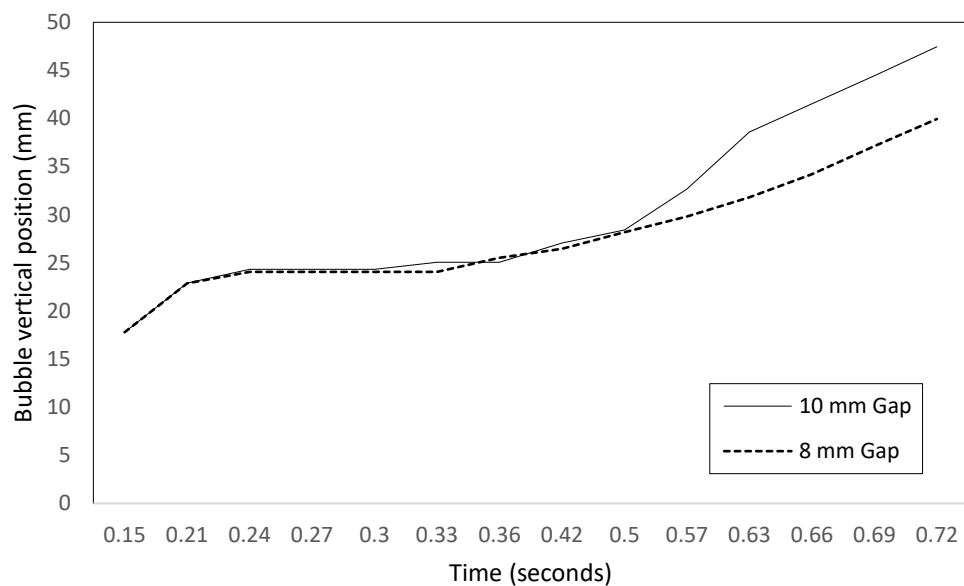
Figure 41: Bubble vertical position (10 mm and 8 mm gap sizes).
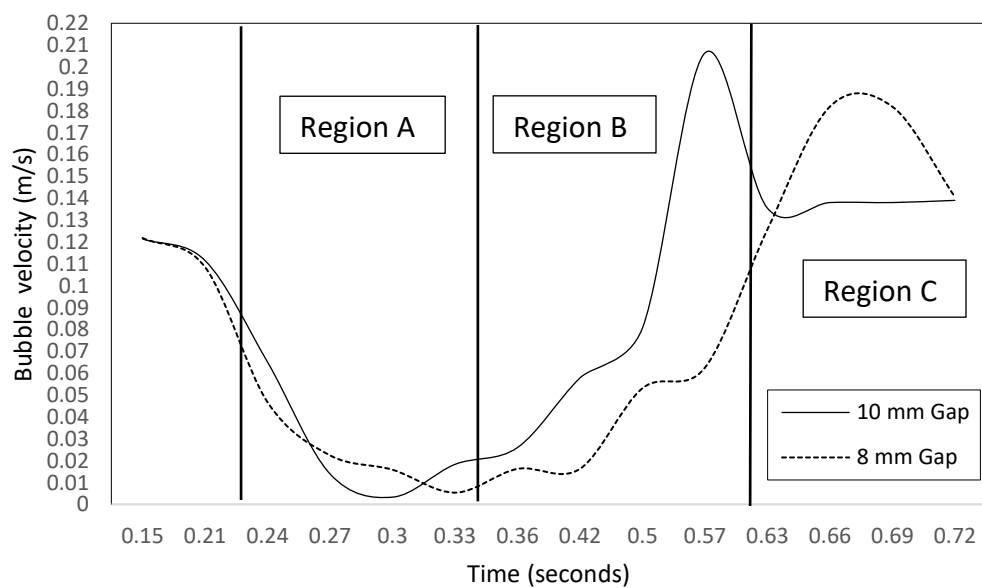
Figure 42: Bubble rising velocity (10 mm and 8 mm gap sizes).

The bubble in $6\ mm$ gap size behaved differently compared with the other sizes, as shown in Figure 43. When the bubble reached the bottom of the gap, the bubble deformation changed from ellipse shape to a flatten shape with concave-up deformation on the tip of the bubble and stuck in this form and position, as illustrated in Figure 43. This behavior can be a result of the balance between the buoyancy force and the surface tension force, such that this equivalent effect produces this behavior on the bubble. The 6 mm gap does not allow for sufficient open area for the bubble to be exerted by buoyancy force, therefore the bubble has not pulled inside the gap.

In the three gap sizes (10 mm, 8 mm and 6 mm) the bubble dynamic showed a strong relation between the gap size and the bubble behavior in term of bubble deformation, bubble velocity and bubble position through the flow domain. The 10 mm gap have the less effect on the bubble behavior in comparison with other sizes, where the bubble behavior disturbed within the gap then it retains to its ellipse shape. In 8 mm gap the bubble exposed to smaller gap width which impacted the bubble crossing velocity and resulted increase in the total time of the bubble inside the flow domain, whereas this delay can grant additional time for the bubble to condensate within the flow domain which will enhance the overall condensation performance. The 6 mm gap did not allow the bubble to pass the gap due to the size of the gap and weak upward forces, from heat transfer perspective that may lead to overheat in the lower section of the mesh where the bubbles will be concentrated. This comparison analyses between three gap sizes shows a relation between the bubble size and the gap size whereas the ratio between the bubble size and the gap size will determine the bubble behavior if the bubble crossing the gap from the middle.

0.15 s (a)   0.21 s (b)   0.24 s (c)   0.27 s (d)   0.30 s (e)

0.33 s (f)   0.36 s (g)
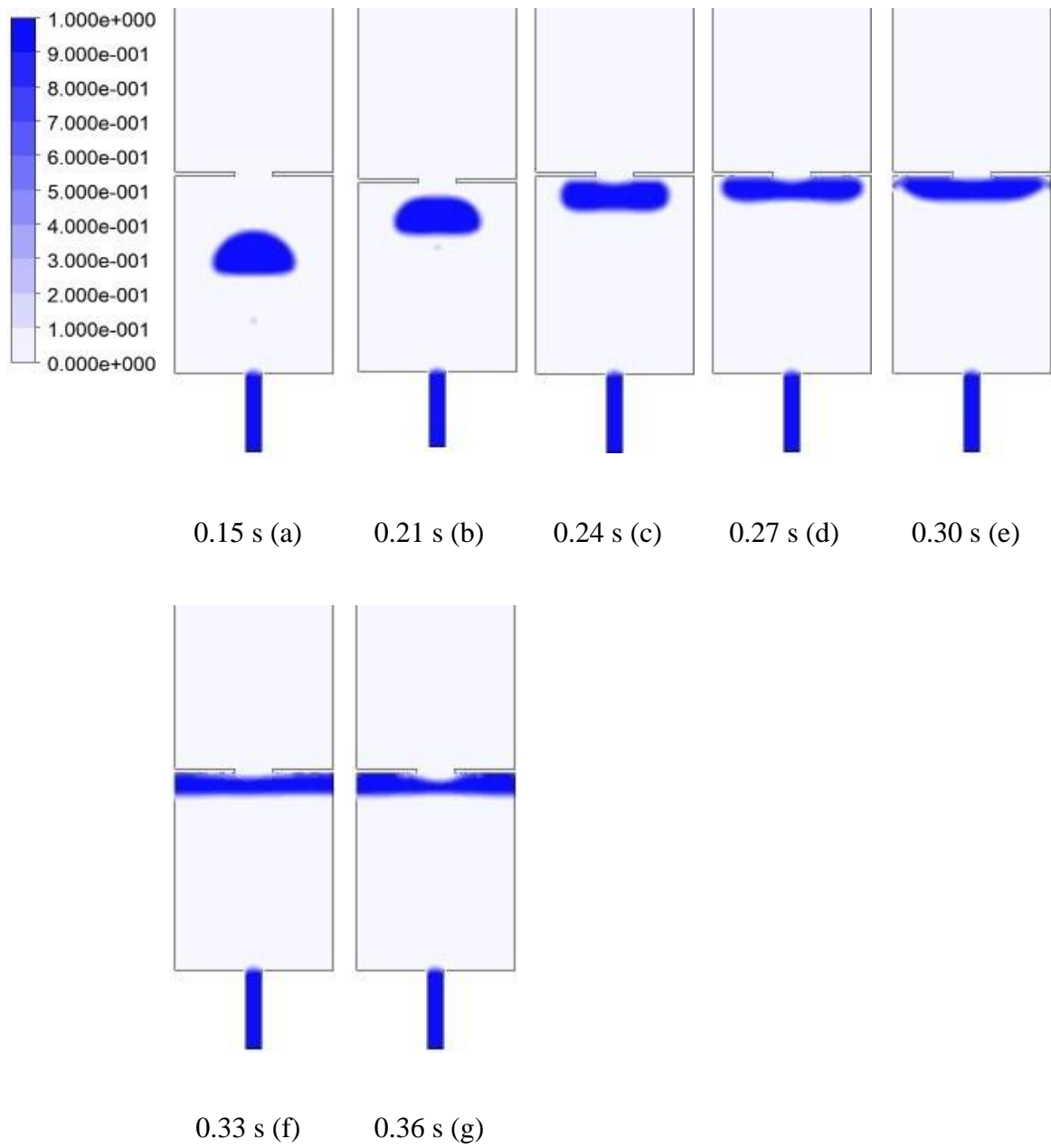
Figure 43: Bubble behavior across the mesh 6 mm gap.

5.3.2 Multi Gaps Geometry

To investigate the bubble behavior if the bubble crossing the mesh between multiple gaps, the geometrical modification applied on the flow domain to have double gaps and 4 gaps as shown in Figure 33 (B and C). This section numerically demonstrates the interaction between the bubble and the gaps through the mesh.

Figure 44 shows the bubble's behavior through its movement between the two gaps of the mesh. The volume fraction contour shows the bubble reached the bottom of the mesh's gaps in elliptical shape similar to the bubble shape in single gap demonstration. Afterward, the bubble gradually touched the wall between that separate the gaps. At $t = 0.34 \, s$ the middle wall forced the bubble top to deform in order to adapt the shape of the wall. Figure 44 (D and E) shows the deformation on the bubble has bullet-like shape this deformation due to the moving fluid from the bubble sides toward the bottom of the bubble caused loses mass while the bubble is rising. $At \, t = 0.36 \, s$ the bubble passing the two gaps and exerted to high level of deformation caused by the middle wall. At this time instance the surface tension in the middle of the bubble will be weaken, since the bubble exposed to high level of buoyancy forces from both sides and high stress coming from the mid wall and these forces acting on opposite directions as shown in Figure 45. Based on unbalance forces the original bubble divided into two smaller bubbles. Additionally, the bottom end of the bubble experienced low surface tension which results on having micro bubbles on both sides as shown in Figure 44 (G – I). On the other hand, having four gaps instead of two gaps will follow similar behavior with minor differences while the bubble is breaking up as shown in Figure 46 The resulted smaller bubbles will not be affected by

the others mid walls between the gaps, the smaller bubbles have very high surface tension which allow the bubbles to pass around the walls while adapting the deformation. Additionally, in 4 mesh gaps the bubble deformation will have a thinner surface area in both sides in comparison with double gaps while will lead to have higher number of micro bubbles in both sides as shown in Figure 46 (G - I).

0.25 s (a)   0.28 s (b)   0.32 s (c)   0.34 s (d)

0.36 s (e)   0.38 s (f)   0.40 s (g)   0.42 s (h)

0.44 s (i)
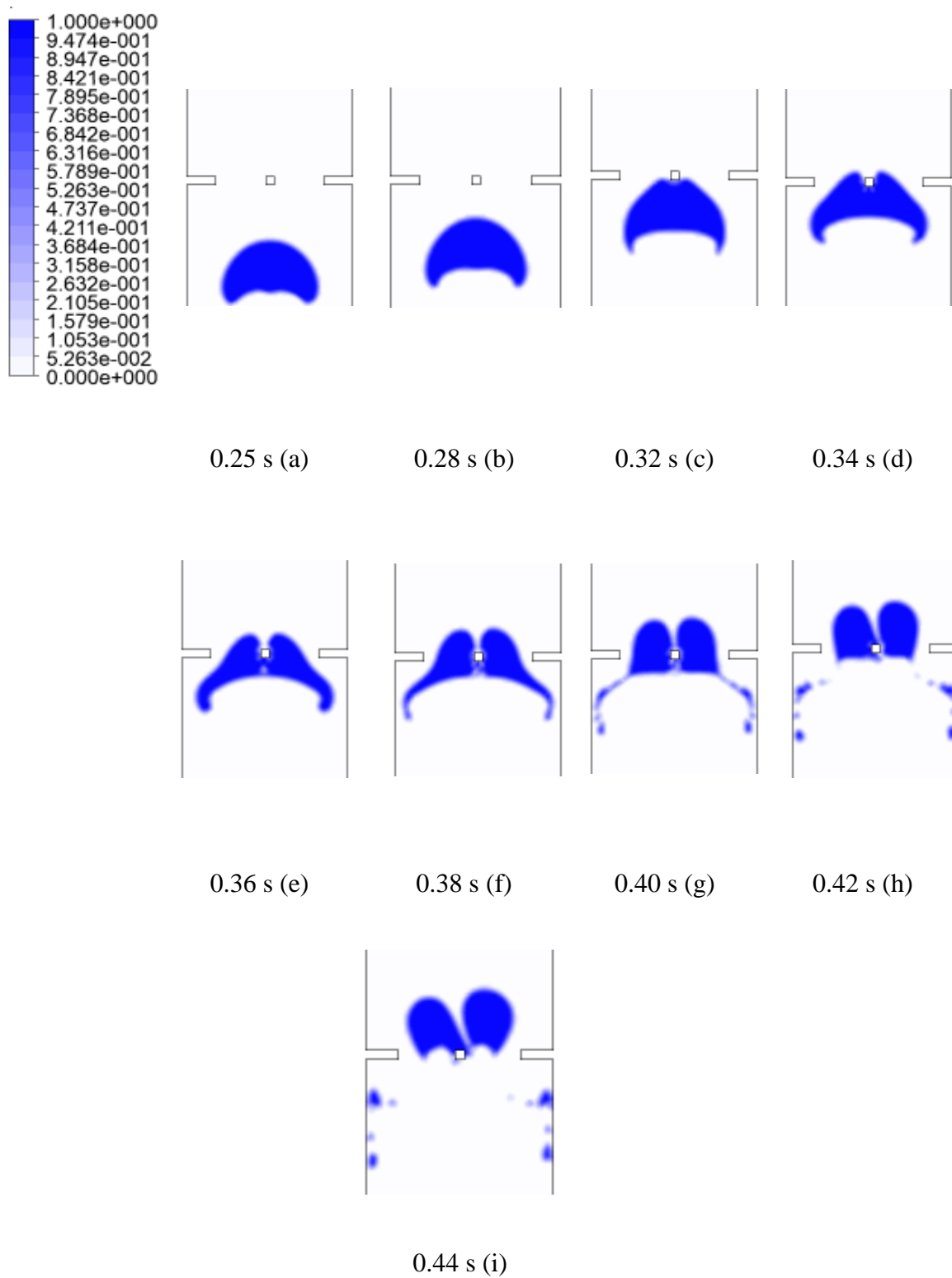
Figure 44: Bubble behavior across double gaps.
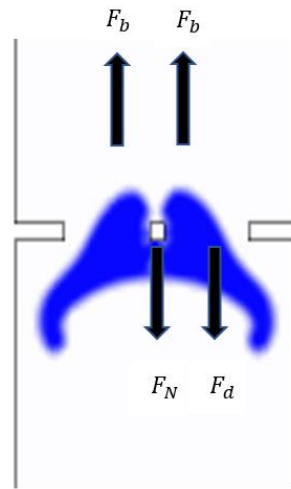
Figure 45: Acting forces on the bubble.
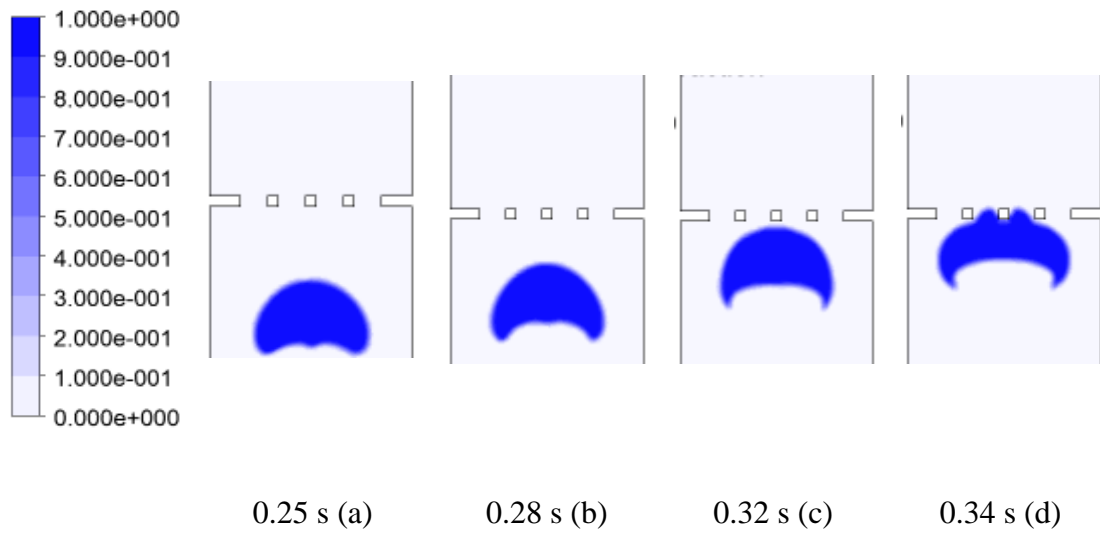
0.25 s (a)　　　0.28 s (b)　　　0.32 s (c)　　　0.34 s (d)

Figure 46: Bubble behavior across four gaps mesh.

| 0.36 s (e) | 0.38 s (f) | 0.40 s (g) | 0.42 s (h) |

0.44 s (i)
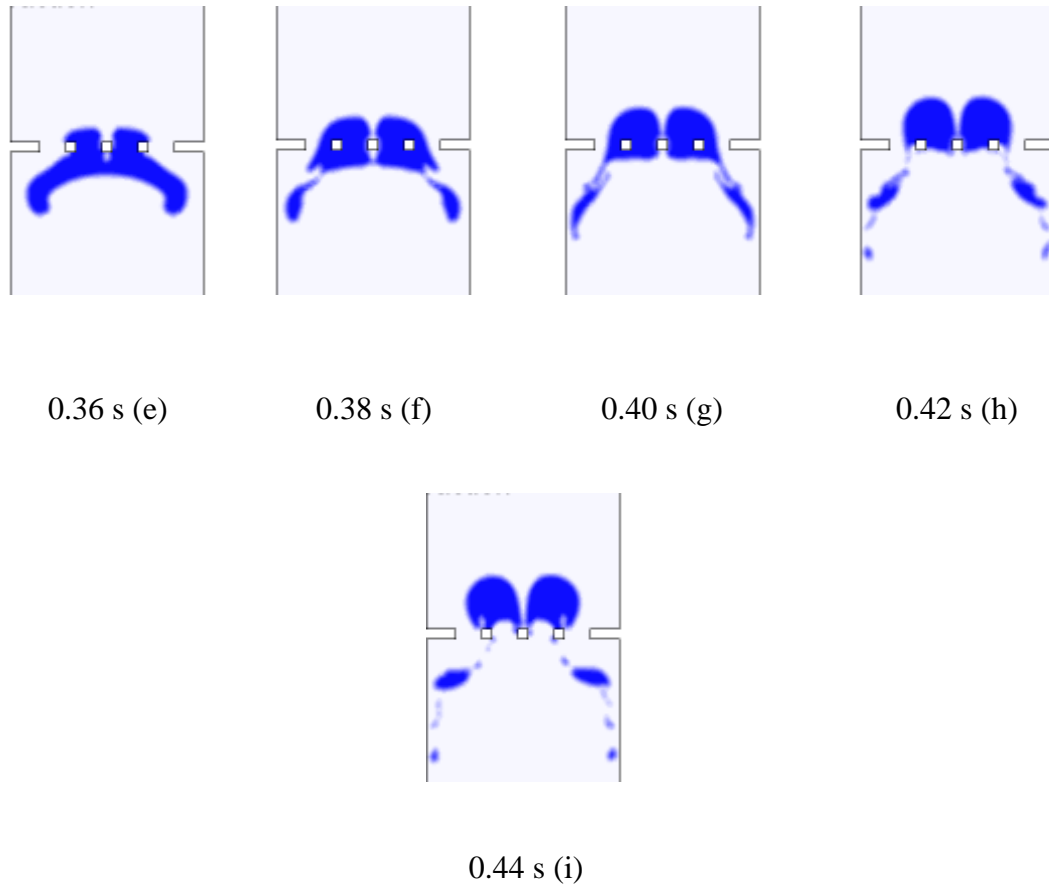
Figure 46: Bubble behavior across four gaps mesh (continued).

Figure 47 illustrate the effect of double gaps and multi gaps on the total surface area of the bubble. In both configurations the bubble surface area follows the same pattern. During the passing stage the bubble stretched to adapt the gaps shape where in the same instance the bubble exerted to the buoyancy force which leads to elongate the bubble in the vertical direction and caused the total surface area to be increased. Additionally, starting from collapsing stage at $t = 0.4\ s$ the total surface area increased from $105\ mm^2$ to $111.1\ mm^2$, this is due to additional micro bubbles occurred during collapsing stage. For the double gaps' configuration, the total surface area increased from $104\ mm^2$ to

$107\ mm^2$. In comparison between the two configurations the four gaps will have a slightly higher total surface area which equivalent to additional 4% on the total surface area resultant from double gap configuration. In both configurations the total surface area increased by approximately 27%.

The multi gaps configuration demonstrated the ability for the mesh structure to break up the bubble into smaller bubbles. From heat transfer perspective having a mechanism to break up the bubble will lead to higher surface area which will impact positively the heat transfer rate between the two phases as demonstrated in the previous chapter. Four gaps configuration may result on higher total surface area but it will affect the flow rate, since it will include additional walls. The gap sizes and number of gaps placed on the bubble trajectory have great effects on the bubble deformation and the ability to collapse into smaller bubbles.
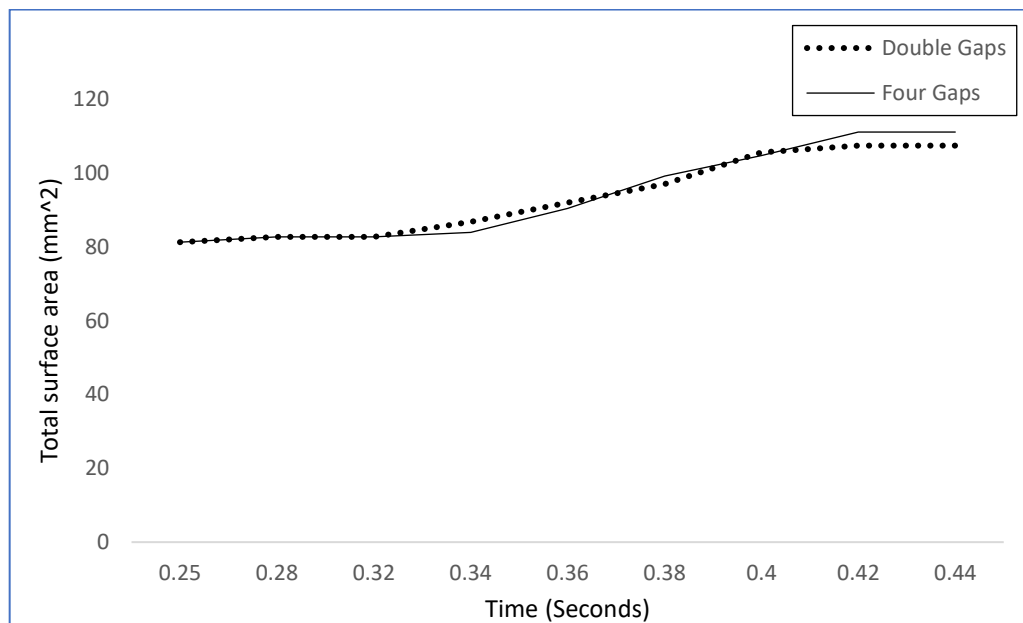
Figure 47: Bubbles total surface area in double gaps and four gaps.

Chapter 6: Conclusion and Recommendations

6.1 Conclusion

This chapter concludes the thesis work and detailed the major findings and achievements. A numerical study for a vapor bubble condensation process and the enhancement technique via affecting the bubbles; dynamic using a mesh-based structure is analyzed in this work. The analysis included bubble dynamics and thermal behavior by considering the heat and mass transfer through the bubble's interface area between the vapor and liquid regions and the resulting condensation effects. The relation between the bubble condensation's thermal and dynamic parameters is analyzed under different operating conditions and flow configurations using a MATLAB code and Computational fluid dynamic analysis. The model's dynamic term is developed using the force balance on a gravity-driven bubble, including hydrodynamic drag force and gravity/buoyancy force, which are acting with and against the bubble's motion direction. For the thermal part of the model, a condensation correlation has been adapted to represent the Nusselt number as a function of Reynolds number (Re), Jakob number (Ja), and Prandtl number (Pr). The combination between the semi-empirical correlation and the theoretical equations is developed to demonstrate the bubble condensation rate through the flow field where the condensation is occurred and is affected by the fluid parameters.

A MATLAB code was developed to perform the calculation based on the mathematical model. The initial results have been compared with the experimental results and showed a good agreement. The first analysis was performed on a single bubble with three different initial liquid temperatures difference conditions ($\Delta T=5$ K, $\Delta T=10$ K, and

ΔT=15 K), under a constant bubble diameter $D_0 = 4.8\ mm$, the results showed the higher difference in temperature coincides with a higher condensation rate and less bubble lifetime. Additionally, the effect of different initial diameters (5 mm, 6 mm and 7 mm) on the bubble condensation rate was analyzed. The results showed the smallest bubble will have a shorter lifetime, but the biggest bubble's reduction rate is higher. The MATLAB code is used to evaluate the effect of bubble break up on the condensation heat transfer rate. By fixing the initial diameter of $D_0 = 4.86\ mm$, and temperature difference of ΔT=15 K an investigation is done to examine the bubble's thermal behavior if the bubble is divided into two, four, and six smaller bubbles. It has been found by breaking the bubble into two smaller bubbles the total lifetime of the bubble will be reduced by 33.8%, while breaking the bubble into 4 smaller bubbles reduced the lifetime by 42.3%, and if the bubble was divided into 6 bubbles, the lifetime will be reduced by 53.8%. Additionally, the results indicate that the total surface area increased, positively impacting the heat transfer rate.

A numerical study conducted using CFD code in ANSYS Fluent to simulate the bubble's dynamic behavior under different geometrical modifications. A mesh-based structure is introduced as a geometrical modification of the flow structure to achieve the breakup of the bubble. Two bubble trajectory scenarios were examined, where the bubble may pass the mesh-based structure from the mid of the mesh's gap or the bubble may collide with the walls between the gaps. For a single gap, the simulation was conducted for three gap sizes (10 mm, 8 mm, and 6 mm). The bubble dynamic results showed a strong relation between the gap size and the bubble behavior in terms of bubble deformation, bubble velocity, and bubble position through the flow domain. The 10 mm

gap has less effect on the bubble's behavior in comparison with other sizes. A 6 mm gap did not allow the bubble to pass the gap due to the gap's size. The simulation concluded that the relation between the bubble size and the gap size should be considered as a design parameter, whereas the ratio between the bubble size and the gap size will determine the bubble behavior in terms of deformation and velocity. For the second scenario, where the bubble will collide with the mid walls between the gaps, the simulation was performed for a modified flow geometry, including 2 gaps and 4 gaps. The results found in multi gaps configuration; the original bubble collapsed into two smaller bubbles, and the total surface area increased from $82\ mm^2$ to $107\ mm^2\ and\ 111.1\ mm^2$. Furthermore, the implemented multi gaps mesh structure increased the total surface area by approximately 27%. This achievement indicates the mesh-based structure's ability to enhance the condensation rate by considering the ratio between number of gaps, gap size, mid walls size, and the initial bubble size.

6.2 Recommendations for Future Studies

In this work, a numerical investigation was performed to evaluate the bubble condensation enhancement by modifying the flow path structures. A MATLAB code was developed based on the semi-empirical model to perform the calculation, and a CFD numerical simulation was conducted the simulate the bubble's dynamic behaviors after implementing the geometrical enhancement. This study can be extended to consider the following points:

- Evaluate the semi-empirical model under different mediums.
- Extend the numerical simulation from 2-D to 3-D space.

- Evaluate mesh-based structure with multi-initial bubbles.

- Extend the CFD simulation by integrating the heat transfer and evaluate the condensation performance.

- Investigate the effect of mesh's gap internal structure and examine different internal gap shapes.

References

[1] I. Mudawar, "Assessment of high-heat-flux thermal management schemes," in *ITHERM The Seventh Intersociety Conference on Thermal and Thermomechanical Phenomena in Electronic Systems (Cat. No. 00CH37069)*, 2000, vol. 1, pp. 1–20, 2000.

[2] I. Mudawar, "Two-phase microchannel heat sinks: theory, applications, and limitations," *Journal of electronic packaging*, vol. 133, no. 4, 2011. https://doi.org/10.1115/1.4005300

[3] I. Mudawar, "Recent advances in high-flux, two-phase thermal management," *Journal of Thermal Science and Engineering Applications*, vol. 5, no. 2, 2013. https://doi.org/10.1115/1.4023599

[4] C. W. Chan, E. Siqueiros, J. Ling-Chin, M. Royapoor, and A. P. Roskilly, "Heat utilisation technologies: A critical review of heat pipes," *Renewable and Sustainable Energy Reviews*, vol. 50, pp. 615–627, 2015.

[5] P. J. Marto and V. J. Lepere, "Pool boiling heat transfer from enhanced surfaces to dielectric fluids," *Journal of Heat Transfer*. May 1982, vol. 104, no. 2, pp. 92-299, 1982.

[6] I. Mudawar and T. M. Anderson, "Parametric investigation into the effects of pressure, subcooling, surface augmentation and choice of coolant on pool boiling in the design of cooling systems for high-power-density electronic chips," *Journal of* Electron, vol. 112 no. 4, pp. 375-382, 1990.

[7] S. Mukherjee and I. Mudawar, "Pumpless loop for narrow channel and micro-channel boiling," *J. Electron. Packag.*, vol. 125, no. 3, pp. 431–441, 2003.

[8] J. A. Shmerler and I. Mudawwar, "Local heat transfer coefficient in wavy free-falling turbulent liquid films undergoing uniform sensible heating," *International journal of heat and mass transfer*, vol. 31, no. 1, pp. 67–77, 1988.

[9] J. A. Shmerler and I. Mudawwar, "Local evaporative heat transfer coefficient in turbulent free-falling liquid films," *International journal of heat and mass transfer*, vol. 31, no. 4, pp. 731–742, 1988.

[10] T. C. Willingham and I. Mudawar, "Forced-convection boiling and critical heat flux from a linear array of discrete heat sources," *International journal of heat and mass transfer*, vol. 35, no. 11, pp. 2879–2890, 1992.

[11] J. Lee and I. Mudawar, "Low-temperature two-phase microchannel cooling for high-heat-flux thermal management of defense electronics," *IEEE transactions on components and packaging technologies*, vol. 32, no. 2, pp. 453–465, 2009.

[12] J. Lee and I. Mudawar, "Critical heat flux for subcooled flow boiling in micro-channel heat sinks," *International Journal of Heat and Mass Transfer*, vol. 52, no. 13–14, pp. 3341–3352, 2009.

[13] D. C. Wadsworth and I. Mudawar, "Enhancement of single-phase heat transfer and critical heat flux from an ultra-high-flux simulated microelectronic heat source to a rectangular impinging jet of dielectric liquid," *Journal of Heat Transfer*, vol. 114, no. 3 pp. 764-768 1992.

[14] M. E. Johns and I. Mudawar, "An ultra-high power two-phase jet-impingement avionic clamshell module,"*Journal of Electron*, vol. 118, no. 4, pp. 264-270, 1996.

[15] D. D. Hall and I. Mudawar, "Experimental and numerical study of quenching complex-shaped metallic alloys with multiple, overlapping sprays," *International journal of heat and mass transfer*, vol. 38, no. 7, pp. 1201–1216, 1995.

[16] I. A. Mudawwar and M. A. El-Masri, "Momentum and heat transfer across freely-falling turbulent liquid films," *International journal of multiphase flow*, vol. 12, no. 5, pp. 771–790, 1986.

[17] S.-M. Kim and I. Mudawar, "Theoretical model for annular flow condensation in rectangular micro-channels," *International journal of heat and mass transfer*, vol. 55, no. 4, pp. 958–970, 2012.

[18] M. M. Shah, "An improved and extended general correlation for heat transfer during condensation in plain tubes," *Hvac&R Research*, vol. 15, no. 5, pp. 889–913, 2009.

[19] S.-M. Kim and I. Mudawar, "Universal approach to predicting heat transfer coefficient for condensing mini/micro-channel flow," *International Journal of Heat and Mass Transfer*, vol. 56, no. 1–2, pp. 238–250, 2013.

[20] D. Li and V. K. Dhir, "Numerical study of single bubble dynamics during flow boiling," *Journal of* Heat Transfer, vol. 129, no. 7, pp. 864-876, 2007.

[21] S.-S. Jeon, S.-J. Kim, and G.-C. Park, "Numerical study of condensing bubble in subcooled boiling flow using volume of fluid model," *Chemical engineering science*, vol. 66, no. 23, pp. 5899–5909, 2011.

[22] C. R. Kharangate and I. Mudawar, "Review of computational studies on boiling and condensation," *International Journal of Heat and Mass Transfer*, vol. 108, pp. 1164–1196, 2017.

[23] J. Havlica *et al.*, "A case study on bubble formation: numerics vs. measurements," *Journal of Chemical Engineering*, vol. 77, pp. 458–464, 1999.

[24] G. Ryskin and L. G. Leal, "Numerical solution of free-boundary problems in fluid mechanics. Part 2. Buoyancy-driven motion of a gas bubble through a quiescent liquid," *Journal of Fluid Mechanics*, vol. 148, pp. 19–35, 1984.

[25] W. F. Noh and P. Woodward, "SLIC (simple line interface calculation)," in *Proceedings of the fifth international conference on numerical methods in fluid dynamics, Twente University, Enschede*, pp. 330–340, 1976.

[26] C. W. Hirt and B. D. Nichols, "Volume of fluid (VOF) method for the dynamics of free boundaries," *Journal of computational physics*, vol. 39, no. 1, pp. 201–225, 1981.

[27] O. Ubbink and R. I. Issa, "A method for capturing sharp fluid interfaces on arbitrary meshes," *Journal of computational physics*, vol. 153, no. 1, pp. 26–50, 1999.

[28] M. Rudman, "Volume-tracking methods for interfacial flow calculations," *International journal for numerical methods in fluids*, vol. 24, no. 7, pp. 671–691, 1997.

[29] D. Hartmann, M. Meinke, and W. Schröder, "Differential equation based constrained reinitialization for level set methods," *Journal of Computational Physics*, vol. 227, no. 14, pp. 6821–6845, 2008.

[30] G. Russo and P. Smereka, "A remark on computing distance functions," *Journal of computational physics*, vol. 163, no. 1, pp. 51–67, 2000.

[31] Y.-C. Chang, T. Y. Hou, B. Merriman, and S. Osher, "A level set formulation of Eulerian interface capturing methods for incompressible fluid flows," *Journal of computational Physics*, vol. 124, no. 2, pp. 449–464, 1996.

[32] Y. Zhang, Q. Zou, and D. Greaves, "Numerical simulation of free-surface flow using the level-set method with global mass correction," *International Journal for Numerical Methods in Fluids*, vol. 63, no. 6, pp. 651–680, 2010.

[33] M. Sussman and E. G. Puckett, "A coupled level set and volume-of-fluid method for computing 3D and axisymmetric incompressible two-phase flows," *Journal of computational physics*, vol. 162, no. 2, pp. 301–337, 2000.

[34] Y. Liu, J. Li, Y. Tian, X. Yu, J. Liu, and B.-M. Zhou, "CLSVOF method to study the formation process of taylor cone in crater-like electrospinning of nanofibers," *Journal of Nanomaterials*, vol. 2014, 2014. https://doi.org/10.1155/2014/635609

[35] J. Glimm, J. Grove, X. L. Li, R. Young, Y. Zeng, and Q. Zhang, "Front tracking: A parallelized approach for internal boundaries and interfaces," in *International Workshop on Applied Parallel Computing*, pp. 257–266, 1995.

[36] G. Tryggvason *et al.*, "A front-tracking method for the computations of multiphase flow," *Journal of computational physics*, vol. 169, no. 2, pp. 708–759, 2001.

[37] S. O. Unverdi and G. Tryggvason, "A front-tracking method for viscous, incompressible, multi-fluid flows," *Journal of computational physics*, vol. 100, no. 1, pp. 25–37, 1992.

[38] D. Juric and G. Tryggvason, "A front-tracking method for dendritic solidification," *Journal of computational physics*, vol. 123, no. 1, pp. 127–148, 1996.

[39] T. Yabe, F. Xiao, and T. Utsumi, "The constrained interpolation profile method for multiphase analysis," *Journal of Computational physics*, vol. 169, no. 2, pp. 556–593, 2001.

[40] D. Jacqmin, "Calculation of two-phase Navier–Stokes flows using phase-field modeling," *Journal of Computational Physics*, vol. 155, no. 1, pp. 96–127, 1999.

[41] E. Pattantyús-H, "Temperature variation and collapse time at the condensation of vapour bubble," *International Journal of Heat and Mass Transfer*, vol. 15, no. 12, pp. 2419–2426, 1972.

[42] S. Kamei and M. Hirata, "Condensing phenomena of a single vapor bubble into subcooled water," *Journal of Thermal Energy Generation*, vol. 3, no. 2, pp. 173–182, 1990.

[43] Y. M. Chen and F. Mayinger, "Measurement of heat transfer at the phase interface of condensing bubbles," *International journal of multiphase flow*, vol. 18, no. 6, pp. 877–890, 1992.

[44] D. Moalem and S. Sideman, "The effect of motion on bubble collapse," *International Journal of Heat and Mass Transfer*, vol. 16, no. 12, pp. 2321–2329, 1973.

[45] D. Lucas and H.-M. Prasser, "Steam bubble condensation in sub-cooled water in case of co-current vertical pipe flow," *Nuclear Engineering and Design*, vol. 237, no. 5, pp. 497–508, 2007.

[46] M. O. Isikan, "Condensation of spherical-cap shaped bubbles," *International Journal of Heat and Mass Transfer*, vol. 33, no. 6, pp. 1099–1103, 1990.

[47] H. Kalman, "Condensation of bubbles in miscible liquids," *International journal of heat and mass transfer*, vol. 46, no. 18, pp. 3451–3463, 2003.

[48] J. Isenberg and S. Sideman, "Direct contact heat transfer with change of phase: bubble condensation in immiscible liquids," *International Journal of Heat and Mass Transfer*, vol. 13, no. 6, pp. 997–1011, 1970.

[49] O. Zeitoun, M. Shoukri, and V. Chatoorgoon, "Interfacial heat transfer between steam bubbles and subcooled water in vertical upward flow," *Journal of heat transfer*, vol. 117, no. 2, pp. 402–407, 1995.

[50] G. R. Warrier, N. Basu, and V. K. Dhir, "Interfacial heat transfer during subcooled flow boiling," *International Journal of Heat and Mass Transfer*, vol. 45, no. 19, pp. 3947–3959, 2002.

[51] D. Yuan, L. Pan, D. Chen, and X. Wang, "Condensation heat transfer coefficient at vapour-liquid interface of subcooled flow boiling in vertical narrow rectangular channel," *Nuclear Power Engineering*, vol. 30, no. 5, pp. 30–34, 2009.

[52] S.-J. Kim and G.-C. Park, "Interfacial heat transfer of condensing bubble in subcooled boiling flow at low pressure," *International Journal of Heat and Mass Transfer*, vol. 54, no. 13–14, pp. 2962–2974, 2011.

[53] L. Pan, Z. Tan, D. Chen, and L. Xue, "Numerical investigation of vapor bubble condensation characteristics of subcooled flow boiling in vertical rectangular channel," *Nuclear engineering and design*, vol. 248, pp. 126–136, 2012.

[54] M. Bahreini, A. Ramiar, and A. A. Ranjbar, "Numerical simulation of bubble behavior in subcooled flow boiling under velocity and temperature gradient," *Nuclear Engineering and Design*, vol. 293, pp. 238–248, 2015.

[55] N. Samkhaniani and M. R. Ansari, "Numerical simulation of bubble condensation using CF-VOF," *Progress in Nuclear Energy*, vol. 89, pp. 120–131, 2016.

[56] P. Khosravifar, S. A. Zonouzi, H. Aminfar, and M. Mohammadpourfard, "Numerical investigation of the condensation of a rising bubble inside a subcooled liquid under magnetic field," *International Journal of Thermal Sciences*, vol. 160, pp. 106674, 2021. https://doi.org/10.1016/j.ijthermalsci.2020.106674

[57] H. Ganapathy, A. Shooshtari, K. Choo, S. Dessiatoun, M. Alshehhi, and M. Ohadi, "Volume of fluid-based numerical modeling of condensation heat transfer and fluid flow characteristics in microchannels," *International Journal of Heat and Mass Transfer*, vol. 65, pp. 62–72, 2013.

[58] W. Tian, Y. Ishiwatari, S. Ikejiri, M. Yamakawa, and Y. Oka, "Numerical computation of thermally controlled steam bubble condensation using Moving Particle Semi-implicit (MPS) method," *Annals of Nuclear Energy*, vol. 37, no. 1, pp. 5–15, 2010.

[59] S. Kamei and M. Hirata, "Study on condensation of a single vapor bubble into subcooled water-Part 2; Experimental analysis," *Heat Transfer-Japanese Research;(USA)*, vol. 19, no. 1, pp. 1-10, 1990.

[60] L. Pan, Z. Tan, D. Chen, and L. Xue, "Numerical investigation of vapor bubble condensation characteristics of subcooled flow boiling in vertical rectangular channel," *Nuclear Engineering and Design*, vol. 248, pp. 126–136, 2012.

[61] D. Chen, L. Pan, D. Yuan, and X. Wang, "Dual model of bubble growth in vertical rectangular narrow channel," *International Communications in Heat and Mass Transfer*, vol. 37, no. 8, pp. 1004–1007, 2010.

[62] A. Tomiyama, I. Zun, A. Sou, and T. Sakaguchi, "Numerical analysis of bubble motion with the VOF method," *Nuclear Engineering and Design*, vol. 141, no. 1–2, pp. 69–82, 1993.

[63] Z. Wang and A. Y. Tong, "Deformation and oscillations of a single gas bubble rising in a narrow vertical tube," *International Journal of Thermal Sciences*, vol. 47, no. 3, pp. 221–228, 2008.

[64] M. Ohta, T. Imura, Y. Yoshida, and M. Sussman, "A computational study of the effect of initial bubble conditions on the motion of a gas bubble rising in viscous liquids," *International journal of multiphase flow*, vol. 31, no. 2, pp. 223–237, 2005.

[65] J. Hua, J. F. Stene, and P. Lin, "Numerical simulation of 3D bubbles rising in viscous liquids using a front tracking method," *Journal of Computational Physics*, vol. 227, no. 6, pp. 3358–3382, 2008.

[66] A. Agarwal, C. F. Tai, and J. N. Chung, "Unsteady development of a deformable bubble rising in a quiescent liquid," *Computer Methods in Applied Mechanics and Engineering*, vol. 199, no. 17–20, pp. 1080–1090, 2010.

[67] S. Mirjalili, C. B. Ivey, and A. Mani, "Comparison between the diffuse interface and volume of fluid methods for simulating two-phase flows," *International Journal of Multiphase Flow*, vol. 116, pp. 221–238, 2019.

[68] S. Turek, "A comparative study of time-stepping techniques for the incompressible Navier-Stokes equations: from fully implicit non-linear schemes to semi-implicit projection methods," *International Journal for Numerical Methods in Fluids*, vol. 22, no. 10, pp. 987–1011, 1996.

[69] S. V. Patankar and D. B. Spalding, "A calculation procedure for heat, mass and momentum transfer in three-dimensional parabolic flows," in *Numerical Prediction of Flow, Heat Transfer, Turbulence and Combustion*, Elsevier, pp. 54–73, 1983.

[70] S. Mirjalili, S. S. Jain, and M. Dodd, "Interface-capturing methods for two-phase flows: An overview and recent developments," *Center for Turbulence Research Annual Research Briefs*, pp. 117–135, 2017.

[71] "Ansys Fluent 12.0 Theory Guide." https://www.afs.enea.it/project/neptunius/docs/fluent/html/th/main_pre.htm (accessed Mar. 07, 2021).

[72] D. Bothe, M. Schmidtke, and H. J. Warnecke, "VOF-simulation of the rise behavior of single air bubbles in linear shear flows," *Chemical Engineering and Technology*, vol. 29, pp. 1048–1053, 2006.

[73] S. S. Rabha and V. V. Buwa, "Volume-of-fluid (VOF) simulations of rise of single/multiple bubbles in sheared liquids," *Chemical Engineering Science*, vol. 65, no. 1, pp. 527–537, 2010.

[74] K. Higeta, Y.H. Mori, K. Komotori, "Condensation of a single vapor bubble rising in another immiscible liquid," AICHE Symp. vol. 75, no. 189, pp. 256–265, 1979.

List of Publications

[1] F. Alnaimat, O. Alhammadi, and B, Mathew, "Numerical Investigation of Single Bubble Dynamics Passing A Mesh-Based Structure," *ASME 2020 Summer Heat Transfer Conference SHTC2020,* Florida USA, July 13 – July 15, 2020. https://doi-org.uaeu.idm.oclc.org/10.1115/HT2020-9063

[2] F. Alnaimat, O. Alhammadi, and B, Mathew, "Condensation Heat Transfer Model: A Comparison Study of Condensation Rate between A Single Bubble and Multiple Rising Bubbles," *ASME 2021 Heat Transfer Summer Conference HT2021,* Florida USA, June 16 – June 18, 2021.

Appendix A

This section provides the details of implementation of the MATLAB code in Chapter 4.

```
%This code demonstrates the ability to calculate the bubble's condensation (velocity &
radius)
%while raising in the flow field for a period of time for data T = 5

clear
clc

% Constants

rho_l=961.9;            %iquid density [kg/m3]
rho_g=0.5975;           %vapor density [kg/m3]
Hfg=2270*1000;          %Latent heat of vaporization [J/kg]
muo=0.0002972;          %liquid viscosity [kg/m.s]
Cp=4.21*1000;           %Liquid specific heat [J/kg.K]
Tsat= 373.2;            %Local liquid sat temperature [K]
Tl=368.2;               %Local liquid temperature [K]
k=0.6634;               %liquid thermal conductivity [W/m.K]
g=9.81;                 %Gravety constant [m/s^2]
% Cd=2.6;               %drug coefficient for 10^3 < Re < 10^4

Ja=(rho_l*Cp*(Tsat-Tl))/(rho_g*Hfg);      % Jakob number
Pr=(Cp*muo)/k;                            % Constant Prandtl number


%Time duration , time steps and step size

tmax = 0.035;           % Final time (seconds)
nt = 1000;              % Number of time steps (iterations)
dt = tmax/nt            % Step Size (seconds)

%Initial conditions

t0=0;
r0=(4.86/1000)/2;           % Initial bubble radius at T=0 (m)
u0=0.0001;                  % Initial bubble velocity at T=0 (m/s)
mi=rho_g*(4/3)*pi*r0^3;     % Initial bubble mass  at T=0 (kg)
dis0=0;                     % Initial bubble location (m)
```

%Initiating the parameters radius (r),velocity(u),mass(m),time(t) &
%displacement (dis)

```matlab
r(1)=r0;
u(1)=u0;
m(1)=mi;
t(1)=t0;
dis(1)=dis0;

for i=1:nt

    t(i+1,1)=t(i)+dt

    syms uf mf rf

    Re(i,1)=(rho_l*u(i)*(r(i)*2))/muo;              % Bubble Reynold number

    if (Re(i) >= 0) && (Re(i) <= 100)               % Drug coefficient
        Cd(i,1)=(24/Re(i))+(1/(5+Re(i)))+1.5;
    else
        Cd(i,1)=(240/Re(i))+((1.44*10^(-5))*(Re(i)^1.5));
    end




    Fb(i,1)=(4/3)*pi*(r(i))^3*g*(rho_l-rho_g);        % Buoyancy force (N)
    Fd(i,1)=(pi*(r(i))^2*Cd(i)*((rho_l*(u(i)^2))/2));  % Drag force (N)

    F=((4/3)*pi*r(i)^3*(rho_g+(0.5*rho_l))*((uf-u(i))/dt))-Fb(i)+Fd(i); % Force balance
equation for the bubble

    % from above solve for the velocity for each time step based on the results of
previous step

    solU=solve(F,uf);
    Uf=double(solU);
    u(i+1,1)=Uf;                    %Caluclate the new velocity for the bubble in each step
    dis(i+1,1)=dis(i)+(dt*Uf);      %Caluclate the new location for the bubble in each step


    % for each velocity the,Nu & hi will be calculated
    Pe(i,1)=Re(i)*Pr;

    Nu(i,1)=(0.2575*(Re(i)^0.7))*((Ja).^-0.2043)*((Pr).^-0.4564);  % Bubble Nusselt
number
```

```
    % from above the heat transfer coefficient will be calclated

    hi(i,1)= (Nu(i)*k)/(r(i)*2);

    % appling the above results in heat transfer equation to obtain the new
    % mass m(i+1)

    ht(i,1)= hi(i)*(4*pi*(r(i)^2))*(Tsat - Tl);

    solve_m=((m(i)-mf)/dt)*Hfg == ht(i);

    solmf= solve(solve_m,mf);
    mf=double(solmf);
    m(i+1,1)=mf;

    % the calculated new mass will be used to get the new radius r(i+1)

    r(i+1,1)= nthroot((mf/(rho_g*(4/3)*pi)),3);
    v(i,1)=(4/3)*pi*((r(i)*1000)^3);

    if r(i+1) <= 0
        break
    end


end
T = t(1:size(t)-1);
U = u(1:size(u)-1);
R = r(1:size(r)-1);
M = m(1:size(m)-1);
Dis = dis(1:size(dis)-1);

VarNames = {'Time_step_s', 'Velocity_meter_per_sec','Displacement_m', 'Radius_m'};
Table = table(t,u,dis,r,'VariableNames',VarNames)


Figure (1)
plot(T,v)
title('Time-dependent bubble volume')
xlabel('Time (s)')
ylabel('Bubble Vulume (mm^3)')
set(gca,'XTick',0:0.005:0.04)
set(gca,'YTick',0:10:60)
hold on
```

```
Figure (2)
plot(T,hi)
title('Time-dependent bubble heat transfer coefficient')
xlabel('Time (s)')
ylabel('heat transfer coefficient W/(m^2K)')
hold on

Figure (3)
plot(T,ht)
title('Time-dependent bubble heat transfer ')
xlabel('Time (s)')
ylabel('heat transfer')
hold on
```

%This code demonstrates the ability to calculate the bubble's condensation (velocity & radius)
%while raising in the flow field for a period of time for data T = 15

```
clear
clc


% Constants

rho_l=965.3;          %iquid density [kg/m3]
rho_g=0.5975;          %vapor density [kg/m3]
Hfg=2283*1000;          %Latent heat of vaporization [J/kg]
muo=0.0003144;          %liquid viscosity [kg/m.s]
Cp=4.204*1000;          %Liquid specific heat [J/kg.K]
Tsat= 373.2;          %Local liquid sat temperature [K]
Tl=363.2;          %Local liquid temperature [K]
k=0.6613;          %liquid thermal conductivity [W/m.K]
g=9.81;          %Gravety constant [m/s^2]
% Cd=2.6;          %drug coefficient for 10^3 < Re < 10^4

Ja=(rho_l*Cp*(Tsat-Tl))/(rho_g*Hfg);      % Jakob number
Pr=(Cp*muo)/k;                  % Constant Prandtl number


%Time duration , time steps and step size

tmax = 0.035;          % Final time (seconds)
nt = 1000;          % Number of time steps (iterations)
dt = tmax/nt          % Step Size (seconds)

%Initial conditions

t0=0;
r0=(4.86/1000)/2;          % Initial bubble radius at T=0 (m)
u0=0.0001;          % Initial bubble velocity at T=0 (m/s)
mi=rho_g*(4/3)*pi*r0^3;      % Initial bubble mass  at T=0 (kg)
dis0=0;          % Initial bubble location (m)


%Initiating the parameters radius (r),velocity(u),mass(m),time(t) &
%displacement (dis)

r(1)=r0;
u(1)=u0;
```

```
m(1)=mi;
t(1)=t0;
dis(1)=dis0;

for i=1:nt

   t(i+1,1)=t(i)+dt

   syms uf mf rf

   Re(i,1)=(rho_l*u(i)*(r(i)*2))/muo;              % Bubble Reynold number

   if (Re(i) >= 0) && (Re(i) <= 100)               % Drug coefficient
      Cd(i,1)=(24/Re(i))+(1/(5+Re(i)))+1.5;
   else
      Cd(i,1)=(240/Re(i))+((1.44*10^(-5))*(Re(i)^1.5));
   end




   Fb(i,1)=(4/3)*pi*(r(i))^3*g*(rho_l-rho_g);       % Buoyancy force (N)
   Fd(i,1)=(pi*(r(i))^2*Cd(i)*((rho_l*(u(i)^2))/2));  % Drag force (N)

   F=((4/3)*pi*r(i)^3*(rho_g+(0.5*rho_l))*((uf-u(i))/dt))-Fb(i)+Fd(i); % Force balance
equation for the bubble

   % from above solve for the velocity for each time step based on the results of
previous step

   solU=solve(F,uf);
   Uf=double(solU);
   u(i+1,1)=Uf;             %Caluclate the new velocity for the bubble in each step
   dis(i+1,1)=dis(i)+(dt*Uf);    %Caluclate the new location for the bubble in each step


   % for each velocity the,Nu & hi will be calculated
   Pe(i,1)=Re(i)*Pr;

   Nu(i,1)=(0.2575*(Re(i)^0.7))*((Ja).^-0.2043)*((Pr).^-0.4564);  % Bubble Nusselt
number


   % from above the heat transfer coefficient will be calclated

   hi(i,1)= (Nu(i)*k)/(r(i)*2);
```

```
    % appling the above results in heat transfer equation to obtain the new
    % mass m(i+1)

    ht(i,1)= hi(i)*(4*pi*(r(i)^2))*(Tsat - Tl);

    solve_m=((m(i)-mf)/dt)*Hfg == ht(i);

    solmf= solve(solve_m,mf);
    mf=double(solmf);
    m(i+1,1)=mf;

    % the calculated new mass will be used to get the new radius r(i+1)

    r(i+1,1)= nthroot((mf/(rho_g*(4/3)*pi)),3);
    v(i,1)=(4/3)*pi*((r(i)*1000)^3);

    if r(i+1) <= 0
       break
    end


end
T = t(1:size(t)-1);
U = u(1:size(u)-1);
R = r(1:size(r)-1);
M = m(1:size(m)-1);
Dis = dis(1:size(dis)-1);

VarNames = {'Time_step_s', 'Velocity_meter_per_sec','Displacement_m', 'Radius_m'};
Table = table(t,u,dis,r,'VariableNames',VarNames)


Figure (4)
plot(T,v,'--')
title('Time-dependent bubble volume')
xlabel('Time (s)')
ylabel('Bubble Vulume (mm^3)')
set(gca,'XTick',0:0.005:0.04)
set(gca,'YTick',0:10:60)
hold on

Figure (8)
plot(T,hi,'--')
title('Time-dependent bubble heat transfer coefficient')
xlabel('Time (s)')
ylabel('heat transfer coefficient W/(m^2K)')
```

```
hold on

Figure (10)
plot(T,ht,'--')
title('Time-dependent bubble heat transfer ')
xlabel('Time (s)')
ylabel('heat transfer')
hold on
```

%This code demonstrates the ability to calculate the bubble's condensation (velocity & radius)
%while raising in the flow field for a period of time for data T = 15

```
clear
clc


% Constants

rho_l=968.6;          %iquid density [kg/m3]
rho_g=0.5975;          %vapor density [kg/m3]
Hfg=2295*1000;          %Latent heat of vaporization [J/kg]
muo=0.0003333;          %liquid viscosity [kg/m.s]
Cp=4.199*1000;          %Liquid specific heat [J/kg.K]
Tsat= 373.2;          %Local liquid sat temperature [K]
Tl=358.2;          %Local liquid temperature [K]
k=0.659;          %liquid thermal conductivity [W/m.K]
g=9.81;          %Gravety constant [m/s^2]
% Cd=2.6;          %drug coefficient for 10^3 < Re < 10^4

Ja=(rho_l*Cp*(Tsat-Tl))/(rho_g*Hfg);        % Jakob number
Pr=(Cp*muo)/k;                    % Constant Prandtl number


%Time duration , time steps and step size

tmax = 0.035;          % Final time (seconds)
nt = 1000;          % Number of time steps (iterations)
dt = tmax/nt          % Step Size (seconds)

%Initial conditions

t0=0;
r0=(4.86/1000)/2;                % Initial bubble radius at T=0 (m)
u0=0.0001;                % Initial bubble velocity at T=0 (m/s)
mi=rho_g*(4/3)*pi*r0^3;        % Initial bubble mass  at T=0 (kg)
dis0=0;                % Initial bubble location (m)


%Initiating the parameters radius (r),velocity(u),mass(m),time(t) &
%displacement (dis)

r(1)=r0;
u(1)=u0;
```

```
m(1)=mi;
t(1)=t0;
dis(1)=dis0;

for i=1:nt

  t(i+1,1)=t(i)+dt

  syms uf mf rf

  Re(i,1)=(rho_l*u(i)*(r(i)*2))/muo;              % Bubble Reynold number

  if (Re(i) >= 0) && (Re(i) <= 100)              % Drug coefficient
     Cd(i,1)=(24/Re(i))+(1/(5+Re(i)))+1.5;
  else
     Cd(i,1)=(240/Re(i))+((1.44*10^(-5))*(Re(i)^1.5));
  end




  Fb(i,1)=(4/3)*pi*(r(i))^3*g*(rho_l-rho_g);      % Buoyancy force (N)
  Fd(i,1)=(pi*(r(i))^2*Cd(i)*((rho_l*(u(i)^2))/2));  % Drag force (N)

  F=((4/3)*pi*r(i)^3*(rho_g+(0.5*rho_l))*((uf-u(i))/dt))-Fb(i)+Fd(i); % Force balance
equation for the bubble

  % from above solve for the velocity for each time step based on the results of
previous step

  solU=solve(F,uf);
  Uf=double(solU);
  u(i+1,1)=Uf;               %Caluclate the new velocity for the bubble in each step
  dis(i+1,1)=dis(i)+(dt*Uf);    %Caluclate the new location for the bubble in each step


  % for each velocity the,Nu & hi will be calculated
  Pe(i,1)=Re(i)*Pr;

  Nu(i,1)=(0.2575*(Re(i)^0.7))*((Ja).^-0.2043)*((Pr).^-0.4564);  % Bubble Nusselt
number


  % from above the heat transfer coefficient will be calclated

  hi(i,1)= (Nu(i)*k)/(r(i)*2);
```

```
    % appling the above results in heat transfer equation to obtain the new
    % mass m(i+1)

    ht(i,1)= hi(i)*(4*pi*(r(i)^2))*(Tsat - Tl);

    solve_m=((m(i)-mf)/dt)*Hfg == ht(i);

    solmf= solve(solve_m,mf);
    mf=double(solmf);
    m(i+1,1)=mf;

    % the calculated new mass will be used to get the new radius r(i+1)

    r(i+1,1)= nthroot((mf/(rho_g*(4/3)*pi)),3);
    v(i,1)=(4/3)*pi*((r(i)*1000)^3);

    if r(i+1) <= 0
        break
    end


end
T = t(1:size(t)-1);
U = u(1:size(u)-1);
R = r(1:size(r)-1);
M = m(1:size(m)-1);
Dis = dis(1:size(dis)-1);

VarNames = {'Time_step_s', 'Velocity_meter_per_sec','Displacement_m', 'Radius_m'};
Table = table(t,u,dis,r,'VariableNames',VarNames)


Figure (4)
plot(T,v,':','linewidth',1.2)
title('Time-dependent bubble volume')
xlabel('Time (s)')
ylabel('Bubble Vulume (mm^3)')
set(gca,'XTick',0:0.005:0.04)
set(gca,'YTick',0:10:60)
hold on


Figure (8)
plot(T,hi,':','linewidth',1.2)
title('Time-dependent bubble heat transfer coefficient')
xlabel('Time (s)')
```

```
ylabel('heat transfer coefficient W/(m^2K)')
hold on



Figure (10)
plot(T,ht,':','linewidth',1)
title('Time-dependent bubble heat transfer ')
xlabel('Time (s)')
ylabel('heat transfer')
hold on
```

%This code demonstrates the ability to calculate the bubble's condensation (velocity & radius)
%while raising in the flow field for a period of time for bubble D = 5 mm

```
clear
clc


% Constants

rho_l=968.6;          %iquid density [kg/m3]
rho_g=0.5975;          %vapor density [kg/m3]
Hfg=2295*1000;           %Latent heat of vaporization [J/kg]
muo=0.0003333;            %liquid viscosity [kg/m.s]
Cp=4.199*1000;          %Liquid specific heat [J/kg.K]
Tsat= 373.2;          %Local liquid sat temperature [K]
Tl=358.2;              %Local liquid temperature [K]
k=0.659;            %liquid thermal conductivity [W/m.K]
g=9.81;            %Gravety constant [m/s^2]
% Cd=2.6;             %drug coefficient for 10^3 < Re < 10^4

Ja=(rho_l*Cp*(Tsat-Tl))/(rho_g*Hfg);        % Jakob number
Pr=(Cp*muo)/k;                    % Constant Prandtl number


%Time duration , time steps and step size

tmax = 0.035;            % Final time (seconds)
nt = 1000;             % Number of time steps (iterations)
dt = tmax/nt            % Step Size (seconds)

%Initial conditions

t0=0;
r0=(5/1000)/2;              % Initial bubble radius at T=0 (m)
u0=0.0001;              % Initial bubble velocity at T=0 (m/s)
mi=rho_g*(4/3)*pi*r0^3;       % Initial bubble mass  at T=0 (kg)
dis0=0;              % Initial bubble location (m)


%Initiating the parameters radius (r),velocity(u),mass(m),time(t) &
%displacement (dis)

r(1)=r0;
```

```
u(1)=u0;
m(1)=mi;
t(1)=t0;
dis(1)=dis0;

for i=1:nt

    t(i+1,1)=t(i)+dt

    syms uf mf rf

    Re(i,1)=(rho_l*u(i)*(r(i)*2))/muo;                % Bubble Reynold number

    if (Re(i) >= 0) && (Re(i) <= 100)                  % Drug coefficient
        Cd(i,1)=(24/Re(i))+(1/(5+Re(i)))+1.5;
    else
        Cd(i,1)=(240/Re(i))+((1.44*10^(-5))*(Re(i)^1.5));
    end


    Fb(i,1)=(4/3)*pi*(r(i))^3*g*(rho_l-rho_g);        % Buoyancy force (N)
    Fd(i,1)=(pi*(r(i))^2*Cd(i)*((rho_l*(u(i)^2))/2));  % Drag force (N)

    F=((4/3)*pi*r(i)^3*(rho_g+(0.5*rho_l))*((uf-u(i))/dt))-Fb(i)+Fd(i); % Force balance
equation for the bubble

    % from above solve for the velocity for each time step based on the results of
previous step

    solU=solve(F,uf);
    Uf=double(solU);
    u(i+1,1)=Uf;                   %Caluclate the new velocity for the bubble in each step
    dis(i+1,1)=dis(i)+(dt*Uf);     %Caluclate the new location for the bubble in each step


    % for each velocity the,Nu & hi will be calculated
    Pe(i,1)=Re(i)*Pr;

    Nu(i,1)=(0.2575*(Re(i)^0.7))*((Ja).^-0.2043)*((Pr).^-0.4564);  % Bubble Nusselt
number

    % from above the heat transfer coefficient will be calclated

    hi(i,1)= (Nu(i)*k)/(r(i)*2);

    % appling the above results in heat transfer equation to obtain the new
```

```
   % mass m(i+1)

   ht(i,1)= hi(i)*(4*pi*(r(i)^2))*(Tsat - Tl);

   solve_m=((m(i)-mf)/dt)*Hfg == ht(i);

   solmf= solve(solve_m,mf);
   mf=double(solmf);
   m(i+1,1)=mf;


   % the calculated new mass will be used to get the new radius r(i+1)

   r(i+1,1)= nthroot((mf/(rho_g*(4/3)*pi)),3);
   v(i,1)=(4/3)*pi*((r(i)*1000)^3);

   if r(i+1) <= 0
      break
   end


end
T = t(1:size(t)-1);
U = u(1:size(u)-1);
R = r(1:size(r)-1);
M = m(1:size(m)-1);
Dis = dis(1:size(dis)-1);

VarNames = {'Time_step_s', 'Velocity_meter_per_sec','Displacement_m', 'Radius_m'};
Table = table(t,u,dis,r,'VariableNames',VarNames)

Figure (4)
plot(T,v)
title('Time-dependent bubble volume')
xlabel('Time (s)')
ylabel('Bubble Vulume (mm^3)')
set(gca,'XTick',0:0.005:0.04)

hold on

Figure (5)
plot(T,Re)
title('Time-dependent Reynold number')
xlabel('Time (s)')
ylabel('Reynold number (Re)')
hold on
```

Figure (8)
plot(T,hi)
title('Time-dependent bubble heat transfer coefficient')
xlabel('Time (s)')
ylabel('heat transfer coefficient W/(m^2K)')
hold on

Figure (10)
plot(T,ht)
title('Time-dependent bubble heat transfer ')
xlabel('Time (s)')
ylabel('heat transfer')
hold on

```
%This code demonstrates the ability to calculate the bubble's condensation (velocity &
radius)
%while raising in the flow field for a period of time for bubble D = 6 mm

clear
clc


% Constants

rho_l=968.6;          %iquid density [kg/m3]
rho_g=0.5975;          %vapor density [kg/m3]
Hfg=2295*1000;          %Latent heat of vaporization [J/kg]
muo=0.0003333;           %liquid viscosity [kg/m.s]
Cp=4.199*1000;          %Liquid specific heat [J/kg.K]
Tsat= 373.2;         %Local liquid sat temperature [K]
Tl=358.2;            %Local liquid temperature [K]
k=0.659;           %liquid thermal conductivity [W/m.K]
g=9.81;           %Gravety constant [m/s^2]
% Cd=2.6;          %drug coefficient for 10^3 < Re < 10^4

Ja=(rho_l*Cp*(Tsat-Tl))/(rho_g*Hfg);        % Jakob number
Pr=(Cp*muo)/k;                  % Constant Prandtl number


%Time duration , time steps and step size

tmax = 0.035;          % Final time (seconds)
nt = 1000;           % Number of time steps (iterations)
dt = tmax/nt          % Step Size (seconds)

%Initial conditions

t0=0;
r0=(6/1000)/2;            % Initial bubble radius at T=0 (m)
u0=0.0001;             % Initial bubble velocity at T=0 (m/s)
mi=rho_g*(4/3)*pi*r0^3;       % Initial bubble mass  at T=0 (kg)
dis0=0;           % Initial bubble location (m)


%Initiating the parameters radius (r),velocity(u),mass(m),time(t) &
%displacement (dis)

r(1)=r0;
u(1)=u0;
```

```
m(1)=mi;
t(1)=t0;
dis(1)=dis0;

for i=1:nt

   t(i+1,1)=t(i)+dt

   syms uf mf rf

   Re(i,1)=(rho_l*u(i)*(r(i)*2))/muo;              % Bubble Reynold number

   if (Re(i) >= 0) && (Re(i) <= 100)              % Drug coefficient
      Cd(i,1)=(24/Re(i))+(1/(5+Re(i)))+1.5;
   else
      Cd(i,1)=(240/Re(i))+((1.44*10^(-5))*(Re(i)^1.5));
   end



   Fb(i,1)=(4/3)*pi*(r(i))^3*g*(rho_l-rho_g);        % Buoyancy force (N)
   Fd(i,1)=(pi*(r(i))^2*Cd(i)*((rho_l*(u(i)^2))/2));   % Drag force (N)

   F=((4/3)*pi*r(i)^3*(rho_g+(0.5*rho_l))*((uf-u(i))/dt))-Fb(i)+Fd(i); % Force balance
equation for the bubble

   % from above solve for the velocity for each time step based on the results of
previous step

   solU=solve(F,uf);
   Uf=double(solU);
   u(i+1,1)=Uf;                 %Caluclate the new velocity for the bubble in each step
   dis(i+1,1)=dis(i)+(dt*Uf);   %Caluclate the new location for the bubble in each step


   % for each velocity the,Nu & hi will be calculated
   Pe(i,1)=Re(i)*Pr;

   Nu(i,1)=(0.2575*(Re(i)^0.7))*((Ja).^-0.2043)*((Pr).^-0.4564);  % Bubble Nusselt
number


   % from above the heat transfer coefficient will be calclated

   hi(i,1)= (Nu(i)*k)/(r(i)*2);
```

```
    % appling the above results in heat transfer equation to obtain the new
    % mass m(i+1)

    ht(i,1)= hi(i)*(4*pi*(r(i)^2))*(Tsat - Tl);

    solve_m=((m(i)-mf)/dt)*Hfg == ht(i);

    solmf= solve(solve_m,mf);
    mf=double(solmf);
    m(i+1,1)=mf;

    % the calculated new mass will be used to get the new radius r(i+1)

    r(i+1,1)= nthroot((mf/(rho_g*(4/3)*pi)),3);
    v(i,1)=(4/3)*pi*((r(i)*1000)^3);

    if r(i+1) <= 0
        break
    end


end
T = t(1:size(t)-1);
U = u(1:size(u)-1);
R = r(1:size(r)-1);
M = m(1:size(m)-1);
Dis = dis(1:size(dis)-1);

VarNames = {'Time_step_s', 'Velocity_meter_per_sec','Displacement_m', 'Radius_m'};
Table = table(t,u,dis,r,'VariableNames',VarNames)


Figure (4)
plot(T,v,'--')
title('Time-dependent bubble volume')
xlabel('Time (s)')
ylabel('Bubble Vulume (mm^3)')
set(gca,'XTick',0:0.005:0.04)

hold on

Figure (5)
plot(T,Re,'--')
title('Time-dependent Reynold number')
xlabel('Time (s)')
ylabel('Reynold number (Re)')
```

```
hold on


Figure (8)
plot(T,hi,'--')
title('Time-dependent bubble heat transfer coefficient')
xlabel('Time (s)')
ylabel('heat transfer coefficient W/(m^2K)')
hold on

Figure (10)
plot(T,ht,'--')
title('Time-dependent bubble heat transfer ')
xlabel('Time (s)')
ylabel('heat transfer')
hold on
```

```
%This code demonstrates the ability to calculate the bubble's condensation (velocity &
radius)
%while raising in the flow field for a period of time  for bubble D = 5 mm

clear
clc


% Constants

rho_l=968.6;          %iquid density [kg/m3]
rho_g=0.5975;          %vapor density [kg/m3]
Hfg=2295*1000;          %Latent heat of vaporization [J/kg]
muo=0.0003333;          %liquid viscosity [kg/m.s]
Cp=4.199*1000;          %Liquid specific heat [J/kg.K]
Tsat= 373.2;          %Local liquid sat temperature [K]
Tl=358.2;          %Local liquid temperature [K]
k=0.659;          %liquid thermal conductivity [W/m.K]
g=9.81;          %Gravety constant [m/s^2]
% Cd=2.6;          %drug coefficient for 10^3 < Re < 10^4

Ja=(rho_l*Cp*(Tsat-Tl))/(rho_g*Hfg);          % Jakob number
Pr=(Cp*muo)/k;                    % Constant Prandtl number


%Time duration , time steps and step size

tmax = 0.035;          % Final time (seconds)
nt = 1000;          % Number of time steps (iterations)
dt = tmax/nt          % Step Size (seconds)

%Initial conditions

t0=0;
r0=(7/1000)/2;                % Initial bubble radius at T=0 (m)
u0=0.0001;                % Initial bubble velocity at T=0 (m/s)
mi=rho_g*(4/3)*pi*r0^3;        % Initial bubble mass  at T=0 (kg)
dis0=0;                % Initial bubble location (m)


%Initiating the parameters radius (r),velocity(u),mass(m),time(t) &
%displacement (dis)

r(1)=r0;
u(1)=u0;
```

```matlab
m(1)=mi;
t(1)=t0;
dis(1)=dis0;

for i=1:nt

    t(i+1,1)=t(i)+dt

    syms uf mf rf

    Re(i,1)=(rho_l*u(i)*(r(i)*2))/muo;              % Bubble Reynold number

    if (Re(i) >= 0) && (Re(i) <= 100)               % Drug coefficient
        Cd(i,1)=(24/Re(i))+(1/(5+Re(i)))+1.5;
    else
        Cd(i,1)=(240/Re(i))+((1.44*10^(-5))*(Re(i)^1.5));
    end




    Fb(i,1)=(4/3)*pi*(r(i))^3*g*(rho_l-rho_g);      % Buoyancy force (N)
    Fd(i,1)=(pi*(r(i))^2*Cd(i)*((rho_l*(u(i)^2))/2)); % Drag force (N)

    F=((4/3)*pi*r(i)^3*(rho_g+(0.5*rho_l))*((uf-u(i))/dt))-Fb(i)+Fd(i); % Force balance
% equation for the bubble

    % from above solve for the velocity for each time step based on the results of
% previous step

    solU=solve(F,uf);
    Uf=double(solU);
    u(i+1,1)=Uf;              %Caluclate the new velocity for the bubble in each step
    dis(i+1,1)=dis(i)+(dt*Uf);    %Caluclate the new location for the bubble in each step


    % for each velocity the,Nu & hi will be calculated
    Pe(i,1)=Re(i)*Pr;

    Nu(i,1)=(0.2575*(Re(i)^0.7))*((Ja).^-0.2043)*((Pr).^-0.4564);  % Bubble Nusselt
% number


    % from above the heat transfer coefficient will be calclated

    hi(i,1)= (Nu(i)*k)/(r(i)*2);
```

```
    % appling the above results in heat transfer equation to obtain the new
    % mass m(i+1)

    ht(i,1)= hi(i)*(4*pi*(r(i)^2))*(Tsat - Tl);

    solve_m=((m(i)-mf)/dt)*Hfg == ht(i);

    solmf= solve(solve_m,mf);
    mf=double(solmf);
    m(i+1,1)=mf;

    % the calculated new mass will be used to get the new radius r(i+1)

    r(i+1,1)= nthroot((mf/(rho_g*(4/3)*pi)),3);
    v(i,1)=(4/3)*pi*((r(i)*1000)^3);

    if r(i+1) <= 0
        break
    end


end
T = t(1:size(t)-1);
U = u(1:size(u)-1);
R = r(1:size(r)-1);
M = m(1:size(m)-1);
Dis = dis(1:size(dis)-1);

VarNames = {'Time_step_s', 'Velocity_meter_per_sec','Displacement_m', 'Radius_m'};
Table = table(t,u,dis,r,'VariableNames',VarNames)


Figure (4)
plot(T,v,':','linewidth',1.2)
title('Time-dependent bubble volume')
xlabel('Time (s)')
ylabel('Bubble Vulume (mm^3)')
set(gca,'XTick',0:0.005:0.04)

hold on

Figure (5)
plot(T,Re,':','linewidth',1.2)
title('Time-dependent Reynold number')
xlabel('Time (s)')
ylabel('Reynold number (Re)')
```

hold on

Figure (8)
plot(T,hi,':','linewidth',1.2)
title('Time-dependent bubble heat transfer coefficient')
xlabel('Time (s)')
ylabel('heat transfer coefficient W/(m^2K)')
hold on

Figure (10)
plot(T,ht,':','linewidth',1)
title('Time-dependent bubble heat transfer ')
xlabel('Time (s)')
ylabel('heat transfer')
hold on

```
%This code demonstrates the ability to calculate the bubble's condensation (velocity &
radius)
%while raising in the flow field for a period of time  for double bubbles

clear
clc


% Constants

rho_l=968.6;           %iquid density [kg/m3]
rho_g=0.5975;           %vapor density [kg/m3]
Hfg=2295*1000;            %Latent heat of vaporization [J/kg]
muo=0.0003333;             %liquid viscosity [kg/m.s]
Cp=4.199*1000;            %Liquid specific heat [J/kg.K]
Tsat= 373.2;           %Local liquid sat temperature [K]
Tl=358.2;              %Local liquid temperature [K]
k=0.659;             %liquid thermal conductivity [W/m.K]
g=9.81;             %Gravety constant [m/s^2]
% Cd=2.6;              %drug coefficient for 10^3 < Re < 10^4

Ja=(rho_l*Cp*(Tsat-Tl))/(rho_g*Hfg);       % Jakob number
Pr=(Cp*muo)/k;                   % Constant Prandtl number


%Time duration , time steps and step size

tmax = 0.05;             % Final time (seconds)
nt = 1000;              % Number of time steps (iterations)
dt = tmax/nt            % Step Size (seconds)

%Initial conditions

t0=0;
r0=(3.86/1000)/2;              % Initial bubble radius at T=0 (m)
u0=0.0001;            % Initial bubble velocity at T=0 (m/s)
mi=rho_g*(4/3)*pi*r0^3;       % Initial bubble mass  at T=0 (kg)
dis0=0;              % Initial bubble location (m)


%Initiating the parameters radius (r),velocity(u),mass(m),time(t) &
%displacement (dis)

r(1)=r0;
u(1)=u0;
```

```
m(1)=mi;
t(1)=t0;
dis(1)=dis0;

for i=1:nt

   t(i+1,1)=t(i)+dt

   syms uf mf rf

   Re(i,1)=(rho_l*u(i)*(r(i)*2))/muo;            % Bubble Reynold number

   if (Re(i) >= 0) && (Re(i) <= 100)
      Cd(i,1)=(24/Re(i))+(1/(5+Re(i)))+1.5;
   else
      Cd(i,1)=(240/Re(i))+((1.44*10^(-5))*(Re(i)^1.5));
   end


   Fb(i,1)=(4/3)*pi*(r(i))^3*g*(rho_l-rho_g);        % Buoyancy force (N)
   Fd(i,1)=(pi*(r(i))^2*Cd(i)*((rho_l*(u(i)^2))/2));  % Drag force (N)

   F=((4/3)*pi*r(i)^3*(rho_g+(0.5*rho_l))*((uf-u(i))/dt))-Fb(i)+Fd(i); % Force balance
equation for the bubble

   % from above solve for the velocity for each time step based on the results of
previous step

   solU=solve(F,uf);
   Uf=double(solU);
   u(i+1,1)=Uf;               %Caluclate the new velocity for the bubble in each step
   dis(i+1,1)=dis(i)+(dt*Uf);    %Caluclate the new location for the bubble in each step


   % for each velocity the,Nu & hi will be calculated
   Pe(i,1)=Re(i)*Pr;

   Nu(i,1)=(0.2575*(Re(i)^0.7))*((Ja).^-0.2043)*((Pr).^-0.4564);  % Bubble Nusselt
number

   % from above the heat transfer coefficient will be calclated

   hi(i,1)= ((Nu(i)*k)/(r(i)*2));

   % appling the above results in heat transfer equation to obtain the new
   % mass m(i+1)
```

```
ht(i,1)= hi(i)*(4*pi*(r(i)^2))*(Tsat - Tl);

solve_m=((m(i)-mf)/dt)*Hfg == ht(i);

solmf= solve(solve_m,mf);
mf=double(solmf);
m(i+1,1)=mf;

htt(i,1)=(ht(i))*2;

% the calculated new mass will be used to get the new radius r(i+1)

r(i+1,1)= nthroot((mf/(rho_g*(4/3)*pi)),3);
v(i,1)=(4/3)*pi*((r(i)*1000)^3);

if r(i+1) <= 0
    break
end


end
T = t(1:size(t)-1);
U = u(1:size(u)-1);
R = r(1:size(r)-1);
M = m(1:size(m)-1);
Dis = dis(1:size(dis)-1);

VarNames = {'Time_step_s', 'Velocity_meter_per_sec','Displacement_m', 'Radius_m'};
Table = table(t,u,dis,r,'VariableNames',VarNames)


Figure (4)
plot(T,v)
title('Time-dependent bubble volume')
xlabel('Time (s)')
ylabel('Bubble Vulume (mm^3)')
set(gca,'XTick',0:0.005:0.05)
set(gca,'YTick',0:10:60)
hold on




Figure (8)
plot(T,hi)
```

```
title('Time-dependent bubble heat transfer coefficient')
xlabel('Time (s)')
ylabel('heat transfer coefficient W/(m^2K)')
hold on

Figure (10)
plot(T,htt)
title('Time-dependent bubble heat transfer ')
xlabel('Time (s)')
ylabel('heat transfer')
hold on
```

```matlab
%This code demonstrates the ability to calculate the bubble's condensation (velocity &
radius)
%while raising in the flow field for a period of time   for four  bubbles


clear
clc


% Constants

rho_l=968.6;          %iquid density [kg/m3]
rho_g=0.5975;          %vapor density [kg/m3]
Hfg=2295*1000;          %Latent heat of vaporization [J/kg]
muo=0.0003333;          %liquid viscosity [kg/m.s]
Cp=4.199*1000;          %Liquid specific heat [J/kg.K]
Tsat= 373.2;          %Local liquid sat temperature [K]
Tl=358.2;              %Local liquid temperature [K]
k=0.659;            %liquid thermal conductivity [W/m.K]
g=9.81;            %Gravety constant [m/s^2]
% Cd=2.6;            %drug coefficient for 10^3 < Re < 10^4

Ja=(rho_l*Cp*(Tsat-Tl))/(rho_g*Hfg);      % Jakob number
Pr=(Cp*muo)/k;                  % Constant Prandtl number


%Time duration , time steps and step size

tmax = 0.05;          % Final time (seconds)
nt = 1000;            % Number of time steps (iterations)
dt = tmax/nt          % Step Size (seconds)

%Initial conditions

t0=0;
r0=(3.06/1000)/2;              % Initial bubble radius at T=0 (m)
u0=0.0001;              % Initial bubble velocity at T=0 (m/s)
mi=rho_g*(4/3)*pi*r0^3;      % Initial bubble mass  at T=0 (kg)
dis0=0;              % Initial bubble location (m)


%Initiating the parameters radius (r),velocity(u),mass(m),time(t) &
%displacement (dis)

r(1)=r0;
```

```
u(1)=u0;
m(1)=mi;
t(1)=t0;
dis(1)=dis0;

for i=1:nt

    t(i+1,1)=t(i)+dt

    syms uf mf rf

    Re(i,1)=(rho_l*u(i)*(r(i)*2))/muo;               % Bubble Reynold number

    if (Re(i) >= 0) && (Re(i) <= 100)
       Cd(i,1)=(24/Re(i))+(1/(5+Re(i)))+1.5;
    else
       Cd(i,1)=(240/Re(i))+((1.44*10^(-5))*(Re(i)^1.5));
    end


    Fb(i,1)=(4/3)*pi*(r(i))^3*g*(rho_l-rho_g);         % Buoyancy force (N)
    Fd(i,1)=(pi*(r(i))^2*Cd(i)*((rho_l*(u(i)^2))/2));  % Drag force (N)

    F=((4/3)*pi*r(i)^3*(rho_g+(0.5*rho_l))*((uf-u(i))/dt))-Fb(i)+Fd(i); % Force balance
equation for the bubble

    % from above solve for the velocity for each time step based on the results of
previous step

    solU=solve(F,uf);
    Uf=double(solU);
    u(i+1,1)=Uf;               %Caluclate the new velocity for the bubble in each step
    dis(i+1,1)=dis(i)+(dt*Uf);    %Caluclate the new location for the bubble in each step


    % for each velocity the,Nu & hi will be calculated
    Pe(i,1)=Re(i)*Pr;

    Nu(i,1)=(0.2575*(Re(i)^0.7))*((Ja).^-0.2043)*((Pr).^-0.4564);  % Bubble Nusselt
number


    % from above the heat transfer coefficient will be calclated

    hi(i,1)= ((Nu(i)*k)/(r(i)*2));
```

```
    % appling the above results in heat transfer equation to obtain the new
    % mass m(i+1)

    ht(i,1)= hi(i)*(4*pi*(r(i)^2))*(Tsat - Tl);

    solve_m=((m(i)-mf)/dt)*Hfg == ht(i);

    solmf= solve(solve_m,mf);
    mf=double(solmf);
    m(i+1,1)=mf;

    htt(i,1)=(ht(i))*4;

    % the calculated new mass will be used to get the new radius r(i+1)

    r(i+1,1)= nthroot((mf/(rho_g*(4/3)*pi)),3);
    v(i,1)=(4/3)*pi*((r(i)*1000)^3);

    if r(i+1) <= 0
       break
    end


end
T = t(1:size(t)-1);
U = u(1:size(u)-1);
R = r(1:size(r)-1);
M = m(1:size(m)-1);
Dis = dis(1:size(dis)-1);

VarNames = {'Time_step_s', 'Velocity_meter_per_sec','Displacement_m', 'Radius_m'};
Table = table(t,u,dis,r,'VariableNames',VarNames)


Figure (4)
plot(T,v,'--')
title('Time-dependent bubble volume')
xlabel('Time (s)')
ylabel('Bubble Vulume (mm^3)')
set(gca,'XTick',0:0.005:0.05)
set(gca,'YTick',0:10:60)
legend('Devided Bubble into 4 Bubbles')
hold on


Figure (10)
```

```
plot(T,htt,'--')
title('Time-dependent bubble heat transfer ')
xlabel('Time (s)')
ylabel('heat transfer')
legend('Single Large Bubble','Total of 4 Bubbles')
hold on
```

```
%This code demonstrates the ability to calculate the bubble's condensation (velocity &
radius)
%while raising in the flow field for a period of time   for six  bubbles


clear
clc


% Constants

rho_l=968.6;          %iquid density [kg/m3]
rho_g=0.5975;          %vapor density [kg/m3]
Hfg=2295*1000;          %Latent heat of vaporization [J/kg]
muo=0.0003333;          %liquid viscosity [kg/m.s]
Cp=4.199*1000;          %Liquid specific heat [J/kg.K]
Tsat= 373.2;          %Local liquid sat temperature [K]
Tl=358.2;          %Local liquid temperature [K]
k=0.659;          %liquid thermal conductivity [W/m.K]
g=9.81;          %Gravety constant [m/s^2]
% Cd=2.6;          %drug coefficient for 10^3 < Re < 10^4

Ja=(rho_l*Cp*(Tsat-Tl))/(rho_g*Hfg);          % Jakob number
Pr=(Cp*muo)/k;                    % Constant Prandtl number


%Time duration , time steps and step size

tmax = 0.04;              % Final time (seconds)
nt = 1000;              % Number of time steps (iterations)
dt = tmax/nt              % Step Size (seconds)

%Initial conditions

t0=0;
r0=(2.673/1000)/2;              % Initial bubble radius at T=0 (m)
u0=0.0001;              % Initial bubble velocity at T=0 (m/s)
mi=rho_g*(4/3)*pi*r0^3;          % Initial bubble mass  at T=0 (kg)
dis0=0;              % Initial bubble location (m)


%Initiating the parameters radius (r),velocity(u),mass(m),time(t) &
%displacement (dis)

r(1)=r0;
```

```
u(1)=u0;
m(1)=mi;
t(1)=t0;
dis(1)=dis0;

for i=1:nt

    t(i+1,1)=t(i)+dt

    syms uf mf rf

    Re(i,1)=(rho_l*u(i)*(r(i)*2))/muo;              % Bubble Reynold number

    if (Re(i) >= 0) && (Re(i) <= 100)
        Cd(i,1)=(24/Re(i))+(1/(5+Re(i)))+1.5;
    else
        Cd(i,1)=(240/Re(i))+((1.44*10^(-5))*(Re(i)^1.5));
    end


    Fb(i,1)=(4/3)*pi*(r(i))^3*g*(rho_l-rho_g);        % Buoyancy force (N)
    Fd(i,1)=(pi*(r(i))^2*Cd(i)*((rho_l*(u(i)^2))/2));   % Drag force (N)

    F=((4/3)*pi*r(i)^3*(rho_g+(0.5*rho_l))*((uf-u(i))/dt))-Fb(i)+Fd(i); % Force balance
equation for the bubble

    % from above solve for the velocity for each time step based on the results of
previous step

    solU=solve(F,uf);
    Uf=double(solU);
    u(i+1,1)=Uf;               %Caluclate the new velocity for the bubble in each step
    dis(i+1,1)=dis(i)+(dt*Uf);     %Caluclate the new location for the bubble in each step


    % for each velocity the,Nu & hi will be calculated
    Pe(i,1)=Re(i)*Pr;

    Nu(i,1)=(0.2575*(Re(i)^0.7))*((Ja).^-0.2043)*((Pr).^-0.4564);  % Bubble Nusselt
number


    % from above the heat transfer coefficient will be calclated

    hi(i,1)= ((Nu(i)*k)/(r(i)*2));
```

```
    % appling the above results in heat transfer equation to obtain the new
    % mass m(i+1)

    ht(i,1)= hi(i)*(4*pi*(r(i)^2))*(Tsat - Tl);

    solve_m=((m(i)-mf)/dt)*Hfg == ht(i);

    solmf= solve(solve_m,mf);
    mf=double(solmf);
    m(i+1,1)=mf;

    htt(i,1)=(ht(i))*6;

    % the calculated new mass will be used to get the new radius r(i+1)

    r(i+1,1)= nthroot((mf/(rho_g*(4/3)*pi)),3);
    v(i,1)=(4/3)*pi*((r(i)*1000)^3);

    if r(i+1) <= 0
       break
    end


end
T = t(1:size(t)-1);
U = u(1:size(u)-1);
R = r(1:size(r)-1);
M = m(1:size(m)-1);
Dis = dis(1:size(dis)-1);

VarNames = {'Time_step_s', 'Velocity_meter_per_sec','Displacement_m', 'Radius_m'};
Table = table(t,u,dis,r,'VariableNames',VarNames)


Figure (4)
plot(T,v,':')
title('Time-dependent bubble volume')
xlabel('Time (s)')
ylabel('Bubble Vulume (mm^3)')
set(gca,'XTick',0:0.005:0.05)
set(gca,'YTick',0:10:60)
legend('Single Large Bubble','Devided Bubble into 6 Bubbles')
hold on


Figure (10)
```

```
plot(T,htt,':')
title('Time-dependent bubble heat transfer ')
xlabel('Time (s)')
ylabel('heat transfer')
legend('Single Large Bubble','Total of 6 Bubbles')
hold on
```

Appendix B

This section provides the details of UDF (User defined function) used in the ANSYS Fluent in Chapter 5.

```c
#include "udf.h"
#include "sg.h"
#include "sg_mphase.h"
#include "flow.h"
#define PI 3.141592654
DEFINE_PROFILE(membrane_speed,        /* function name   */
          th   ,            /* thread          */
          nv)                /* variable number */
{
 face_t f;
 real x[ND_ND];
 real f_time = RP_Get_Real("flow-time");
 begin_f_loop (f,th)
  {
   F_CENTROID(x,f,th);
   if (f_time<=8e-3)
   {F_PROFILE(f,th,nv) = 3;
   }
   else
   F_PROFILE(f,th,nv) = 0;
  }
 end_f_loop (f,th)
}
```